Macroscopic Magnetic Self-assembly

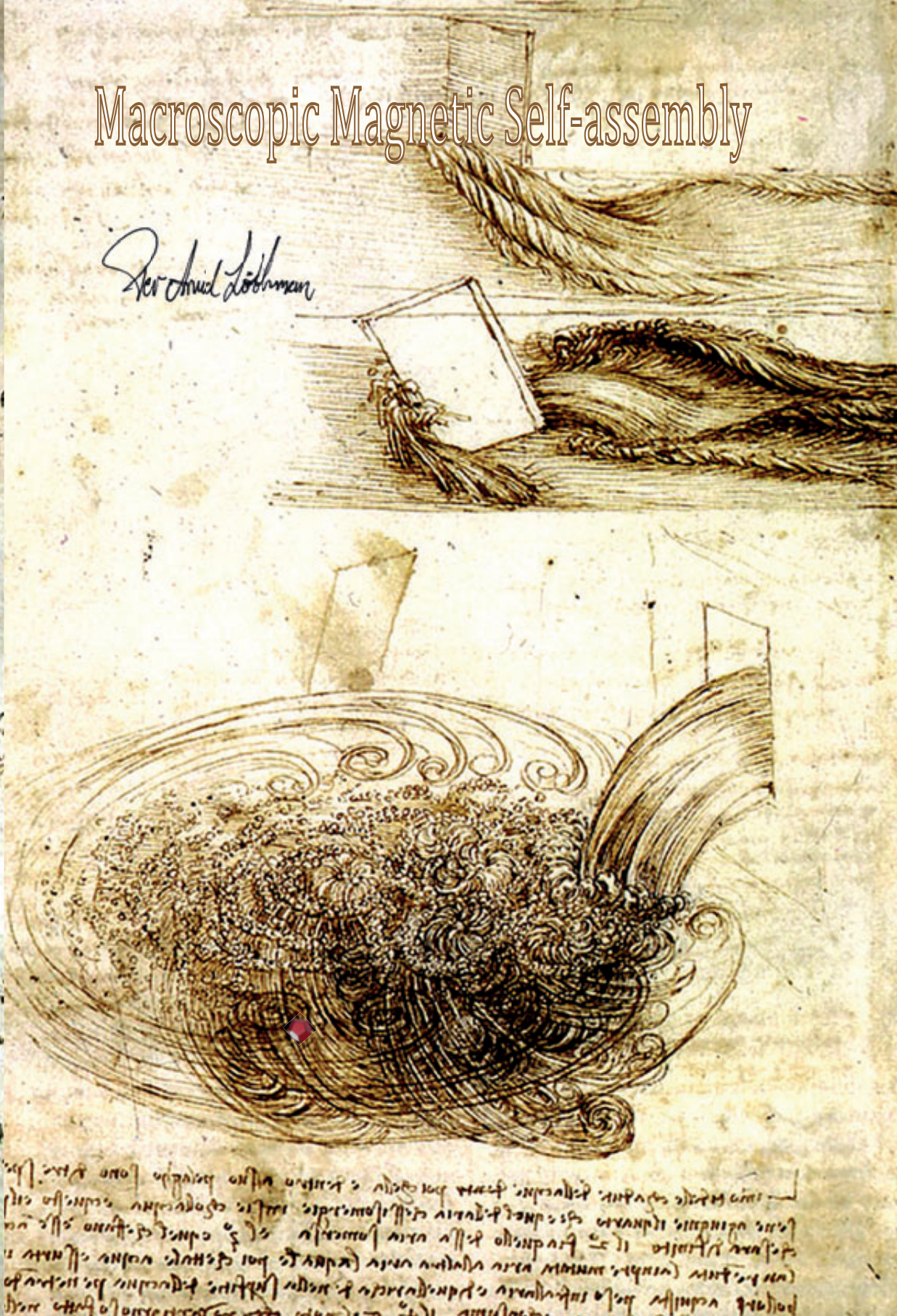

Macroscopic Magnetic Self Assembly

Graduation committee

prof. dr. J.N. Kok	University of Twente (chairman and secretary)
prof. dr. ir. L. Abelmann	Saarland University (supervisor)
prof. dr. ir. G. Krijnen	University of Twente (supervisor)
prof. dr. U. Hartmann	Saarland University
prof. dr.-Ing. M. Vielhaber	Saarland University
prof. dr. H. Broersma	University of Twente
prof. dr. J.J.L.M. Cornelissen	University of Twente
dr. M. Mastrangeli	Delft University of Technology

Deans

prof. dr. J.N. Kok	University of Twente, faculty of Electrical Engineering, Mathematics and Computer Science
prof. dr. G. Kickelbick	Saarland University, faculty of Natural Sciences and Technology

UNIVERSITY OF TWENTE.

KIST Europe

UNIVERSITÄT DES SAARLANDES

The research described in this dissertation was funded by KIST Europe.

Cover design by Per Löthman

Printed by RIDDERPRINT www.ridderprint.nl
© Per Arvid Löthman, Saarbrücken, Germany, 2018.
Electronic mail address: p.a.lothman@alumnus.utwente.nl
ISBN 978-90-365-4512-9
DOI 10.3990/1.9789036545129

Macroscopic Magnetic Self Assembly

DISSERTATION

to obtain the degree of doctor at the University of Twente,
on the authority of the rector magnificus, prof. dr. T.T.M. Palstra,

and to obtain the degree of doctor at Saarland University,
on the autority of the president, prof. dr. M.J. Schmitt,

on account of the decision of the graduation committee,
to be publicly defended
on Wednesday, 11 April 2018 at 16:45

by

Per Arvid Löthman

born on 13 November 1965,
in Enköping, Sweden

This dissertation is approved by

prof. dr. ir. L. Abelmann Saarland University (supervisor)
prof. dr. ir. G.J.M. Krijnen University of Twente (supervisor)

Contents

Chapter 1

Introduction

Autonomous processes that result in patterns and structures, without external influence such as direction or intervention by humans or robots are referred to as *self-assembly*. It is a spontaneous, often aesthetical, process as order appears from dissorder, influenced by the properties of the individual components such as shape, mass, charge or surface roughness. In contrast to *self-organisation*, a non-equilibrium process, self-assembly is concerned with the development of thermodynamical *energy minimum structures*. A combination of the two mechanisms can occur especially in biological systems and may play a role in natural selection and form one theory of pattern formation in nature. Both processes belong to *complex system* science and explain how collective order develops. Self-assembly is not necessarily bound to one scale but can act *hierarchially*, simultaneously or sequentially on multiple scales. An intriguing example is the growth of snowflakes, where the interplay between air-humidity, temperature, water droplets and ice-crystallites leads to various fascinating shapes such as stellar crystals, needles, columns and dendritic plates (Magono, 1966; Nakamura and Cartwright, 2016). This example elegantly shows how self-assembly is responsible for generation of order in nature.

Crystallization, protein folding, assembly of cells, nanoparticles or weather systems are examples of self-assembly which illustrate its scale-independence. The result of self-assembly is the structure that is formed, which is encoded in the *particles*, the smallest individual entity in the structure. Apart from particles, *assembling* and *disturbing* energies are essential ingredients for the self-assembly process. The term “particle" is usually applied to small quantities of matter, large enough to be assigned macroscopic properties such as volume, density, pressure, and temperature [*]. The *role* of the particles in self-assembly is to carry the encoded information which manifests itself in the resulting structure and pattern and in the *local interaction* between the particles. The local interactions includes the attractive assembling energy and the *geometry* of the particles which may hinder or enhance connection in one or several directions. The *driving force* of self-assembly is the

[*] http://glossary.ametsoc.org/wiki/Particle

interplay between the assembling and disturbing energies. In micro- or nanoscopic self-assembly the disturbing energy is mostly the thermal energy which makes the particle conduct a random walk designated *Brownian motion*. The assembling energies are frequently surface energy, magnetic or electric interactions. At the macroscopic scale, the assembling energy is often of magnetic origin (Gross and Dorigo, 2008), or mechanical connections (Penrose, 1959; Penrose and Penrose, 1957) and the source of disturbing energy can be tumbling (Boncheva et al., 2002; Gracias et al., 2000), shaking (Jacobs et al., 2002), stirring (Bowden et al., 1997; Terfort et al., 1997) or turbulent flow (Ilievski et al., 2011b; Murugesan et al., 2015; Roland et al., 1992; Zheng et al., 2004). Particles encounter each other in the provided *energy landscape* in order to self-assemble. The energy landscape for any solid state system regulates the observed structure, thermodynamics, and dynamics. Knowledge about the energy landscape can therefore provide valuable insight and predict likely properties of the final product. The task of the self-assembly process is to find the global energy minimum of the particles as they explore the energy landscape. Particles of various sizes (nano-, micro-, meso- and macroscopic) can self-assemble into 1-, 2- and 3-dimensional structures or patterns. Self-assembly is not limited by scale (Whitesides and Grzybowski, 2002). However, *microscopic self-assembly* has been investigated to a greater extent (Elwenspoek et al., 2010) than macroscopic self-assembly. Magnetically folded millimeter-sized structures (Iwase and Shimoyama, 2005) or DNA origami (Mastrangeli et al., 2009; Rothemund, 2006) or self-assembly of nanoparticles are typical examples for small scale self-assembly.

Why is it important to study self-assembly, and why on the macroscopic scale? The importance of enhanced knowledge in self-assembly is that it answers relevant fundamental questions in physics, and, if controllable, it can fundamentally change several fields of science and technology. The popular anecdote of how cars may be made in future - add individual parts (doors, wheels, roof, engine etc.), shake - and - voilà! - through the interaction of the parts, a car has been made - may serve as a thought provoking illustration of the future role that self-assembly may play. Investigations where the ingredients of self-assembly (particles, assembling and disturbing energies, environment etc.) are systematically altered and the result is unambigously detectable and thereby will contribute to the advancement of science and technology. Some of the anticipated outcomes are large-scale patterning obtained by spontaneous structuring and position control; understanding of the formation, evolution, and organization of nanoscale systems; new approaches in nucleation, crystal growth, surface and interface mechanisms; novel optical, electrical, magnetic, and mechanical properties of self-assembled systems. It is a promising alternative to assembly in the *manufacturing industry*. In the semiconductor industry manufacturing based on self-assembly is believed to play an important role. The continous requirement of down-scaling in order to produce smaller and more efficient devices and computers will at some point be limited by the existing manufacturing technology. Storing and processing bits of information using only a few atoms (Bennewitz et al., 2002) may be achievable in the future but higher data densities requires true three dimensional materials in which both the

resolution and extent of features is identical in all directions (Abelmann et al., 2010). Self-assembly is a favorable method to realize true three-dimensional data storage. In *Materials science* self-assembly resembles a novel manufacturing or synthesis technique which may be important for especially nanostructured materials. The classical question in materials development "How can the relationships between structures and compositions, matrices, and their interfaces control the properties of the materials?" or "materials by design" becomes relevant when implementing self-assembly into *Materials science*.

There are two concepts of making functional materials; *Top-down* and *Bottom-up*. A top-down approach is essentially the breaking down or decomposition of a bulk or raw material to gain a smaller and functional material. Various methods such as lithography can be used to pattern materials. The maximum resolution of these patterns is significantly lower than the dimensions of structures formed using bottom-up methods. A bottom-up approach is the piecing together of smaller components to give rise to more complex system. Molecular synthesis, organic chemistry, colloid chemistry, polymer science make materials starting from the smallest building blocks. Often there is a lack of long-range order in extended materials made via the bottom-up approach. Materials science needs an accessible strategy to bridge these two concepts, and self-assembly lends itself perfectly as a bridge between the two concepts: bottom-up to allow particles to organize themselves into regular patterns or structures by using local forces to find the lowest-energy configuration or to use top-down fabricated entities and let them explore the energy landscape to reach a thermodynamical minimum energy structure. Self-assembly allows for the fabrication of materials with the high resolution of bottom-up methods and the longer-range structure of the top-down approach. Self-assembly is also useful in *micro- and nanotechnology* since it allows for the organisation of structures too small to be manipulated individually into the ordered patterns and structures that often give function to the material. Hierarchically ordered materials may also be achieved since self-assembly works at multiple scales. As with any system, self-assembled devices or materials are unlikely to be useful on a larger scale until they can be produced reproducibly in large quantities. Here, self-assembly has the advantage in that it is a *parallel* process and involves a large number of particles (crystallization might involve 10^{27} molecules) in contrast to robotic pick-and-place assembly methods which are *serial*. Architecture, construction and design are other fields that will likely experience a positive influence of detailed knowledge of self-assembly.

We can increase our knowledge by studying microscopic self-assembly but the momentary state of the self-assembly process, captured via scanning or transmission electron microscopy or other microscopy-techniques, describes a "frozen-in" condition. It does not reveal the process and dynamics behind the self-assembled structure. We cannot "see how" the structure is formed or which pathways were taken. The dynamics of self-assembly remains a challenge due to the small size and time constants involved. Some approaches have been applied to model and simulate such processes (Grant et al., 2011; Whitelam and Jack, 2015; Zhang et al., 2005). Such Monte-carlo simulations are comprehensive but scale unfavorably

with the number of particles.

The lack of a comprehensive understanding of the underlying mechanisms (involving thermodynamics, kinetics, scaling laws etc.) of self-assembly represents a challenge and limits its usage. Knowledge concerning rational design of particles that would self-assemble into specific material geometries and structures is needed for successful implementation of self-assembly in science and engineering. Reproducibility and control of the basic mechanisms in order to predict and produce patterns and structures with tunable size, periodicity and position and novel physical properties are further challenges.

We decided to contribute to a future vision of self-assembly by slowing down the process by using macroscopic particles, vessels, volumes and, as a consequence, longer time scales which makes self-assembly readily observable. The process can be recorded and evaluated using horizontally and vertically mounted cameras. Our self-assembly reactor can be seen as an analog simulator of the microscale. By using macroscopic self-assembly we may learn about the microscale. “What can we learn from the macroscopic scale about the microscale" is the overarching question of this thesis.

It is well known that micro- and macroscopic studies complement each other in the sense that they study various manifestations of the same phenomena. By using the ideal gas law, the thermal energy of a gas molecules can be described macroscopically via pressure, volume, temperature and the number of molecules. The kinetic theory of gases delivers the microscopic representation of the thermal energy of the same gas as the kinetic energy, and velocity of gas molecules can be calculated. The strength of materials can be described macroscopically by their elongation behaviour (Young’s modulus) and microscopically by their crystal lattice. Macroscopic and microscopic studies are often complementary, and just two sides of the same coin. We think of macroscopic self-assembly as a *representative* study and not as investigations of manifestations of the same phenomena at different scales. We *magnify and represent* the microscopic scale by using *analog* macroscopic particles, energies and vessels. We elucidate how macroscopic studies can represent microscopic phenomena and how the macroscopic self-assembly reactor is an analogous representation of the microscopic scale. We use the following representations; centimeter sized spherical particles represent microsized particles, the millimeter sized magnets in the particles represent van der Waal’s interaction which, similar to the magnetic dipoles, decrease to the sixth power of the distance; turbulent flow represents thermal energy (similar chaotic nature and randomness); Fluid flow can be described by the dimensionless Reynolds number which is the ratio between inertial and viscous forces. Viscous forces are frictional shear forces due to the relative motion of layers in the flowing fluid resulting in different degree of friction, thus, different viscosity values. Inertial forces are due to the momentum, mass times velocity, of the fluid. The inertial forces dominate in turbulent flow. There is a similarity between mass, momentum and heat transfer. For example one-dimensional diffusion transport of mass, momentum and thermal energy has been expressed in Fick’s, Newton and Fourier’s laws in terms of the products of gradients of mass concentration, momentum and temperature and

the proportionality constants, which are the mass diffusion coefficient, kinematic viscosity and thermal diffusion coefficient and all are in units of cm^2/s. Since transport of mass, heat and momentum follow the same laws, turbulence can be said to represent the thermal energy. The momentum of the turbulent flow is used to move the macrocscopic particles similar to how water molecules move with increasing temperature. A precise scaling between turbulence and thermal energy so that a certain Reynolds number corresponds to a temperature value, is a matter of future research.

Macroscopic experiments can deepen our understanding of self-assembly at the nano- and microscale and mimic natural phenomena. The design and identification of a macroscopic analogon to the micro-/nanoscopic particles and environment can be challenging but rewarding in terms of expected outcomes and gain of knowledge and insight. To which extent macroscopic self-assembly can contribute to the general theory of self-assembly depends on the *similarity* between the self-assembly at the macro- and microscale.

Analog experimentation has been applied for earthquakes (slider-block, Burridge-Knopoff model (Mora et al., 2013)) genetic mutations, self-replication and mechanical crystallization (Penrose, 1959; Penrose and Penrose, 1957). Olson and Tibbits *et al.* self-assembled magnetic, polymeric, centimeter sized analogons of spherical viruses and enzymes by shaking the pentagonal particles in a glas bottle which serves as a template for the self-assembly (Olson, 2015; Olson et al., 2007; Tibbits, 2011; Tibbits and Tomas, 2013). Analog experimentation is a useful albeit not a standard method in science and technology.

In Figure 1.1 the dynamics of the self-assembly process of twelve magnetic polymer spheres are shown. Higher turbulence leads to a more chaotic behaviour, similar to how molecules move in a gas or liquid. The minimum energy structure (ring) is formed at low turbulence. This sequence nicely demonstrates the pathway of self-assembly as particles explore the *energy landscape* provided. The twelve spheres explore the energy landscape (or potential energy surface PES) provided by turbulence which include energy spectra which contributes to the self-assembly process in various ways such as motion, separation, vibration, acceleration, rotation etc. of the particles and intermediate structures.

1.1 Research question and contents of this thesis

In this thesis an experimental setup, designated ”macroscopic self-assembly reactor", was introduced as a simulator for microscopic self-assembly. With its help the question *what can I learn about the microscopic scale by studying the macroscopic scale* has been elucidated. Particles with permanent magnets were subject to a downward gravitational force and a drag force induced by an upward water flow.

A single particle was used in order to characterize the particle kinetics and disturbing energy and how it changes with the degree of turbulent flow (Chapter 2 and 3). Two particles were used in order to characterize the disturbing energy based

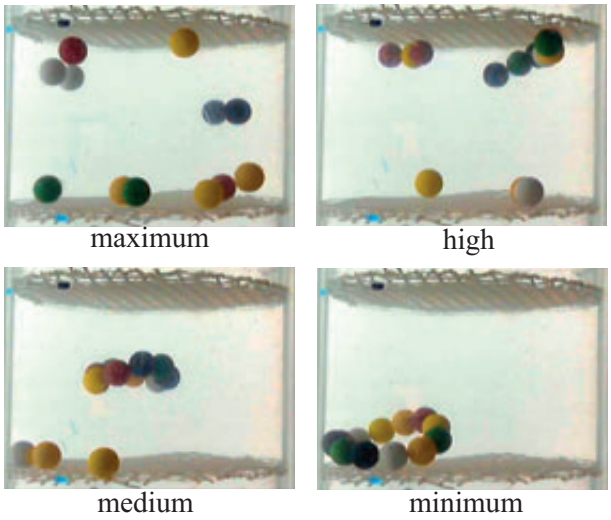

FIGURE 1.1 – *The effect of degree of turbulence on the structure-formation of 12 magnetic polymer spheres. Decreasing turbulence leads to increased structure formation (lines and rings of different lengths and shapes). At maximum turbulence only single spheres appears whereas at minimum turbulence, a low energy structure (a 12-sphere-ring) appears. (Click onto or scan the QR code for the accompanying movie)*

upon sphere interaction and distance. Multiple particles (three to six spheres) characterize and explore the energy landscape of the reactor by the structures they form at various degree of turbulence (Chapter 4). Lastly, self-assembly of twelve magnetic pentagons into a dodecahedral virus was investigated as an elegant example for how macroscopic self-assembly can be used in the study of a microscopic biological phenomena; the self-assembly of a spherical virus (Chapter 5).

Chapter 2

Characterization of a macroscopic self-assembly reactor

Abstract

We built and characterised a macroscopic self-assembly reactor which agitates magnetic, centimeter-sized particles by a turbulent water flow. By scaling up self-assembly processes to centimeter-sized objects characteristic time constants also scale drastically. This makes the system a physical simulator of microscopic self-assembly, where the interaction of inserted particles are easily observable. Trajectory analysis of single particles reveal their velocity to be Maxwell-Boltzmann distributed and show that their average squared displacement over time can be modeled by a confined random walk model, demonstrating a high level of similarity to Brownian motion. The interaction of double particles has been modeled and verified experimentally by observing the distance between two particles over time. The disturbing energy (analogous to temperature) obtained experimentally increased with sphere size, and differed by an order of magnitude between single- and double sphere systems (approximately 80 µJ versus 6.5 µJ respectively).

The work in this chapter was a team effort. The design of the self-assembly reactor and the initial realization were done by Remco Sanders and Léon Woldering. My contribution includes particle design, conduction of experiments and modification of the reactor. Building, programming and calibrating the dual-camera system as well as performing the data analysis was carried out by Tijmen Hageman who also wrote the software for particle detection, 3D-reconstruction, particle tracking and trajectory analysis.

2.1 Introduction

Self-assembly is the process in which a disorganised system assembles into a specific product without external interference. The final properties of the assembly are determined by the properties of the individual parts. Self-assembly is used extensively by nature; for example, in crystal growth, protein folding, the assembly

of molecules into larger compounds, and the creation of complex organs such as the human brain.

Self-assembly is a prospective candidate for use in areas where conventional production and assembly methods are problematic. Although it is not limited to specific dimensions (Whitesides and Grzybowski, 2002), self-assembly is especially applicable to small scales (Elwenspoek et al., 2010); for example, because conventional machining tools for three-dimensional construction are limited to larger feature sizes, while photo-lithography processes are two-dimensional in nature. Mastrangeli *et al.'s* (Mastrangeli et al., 2009) review gives an excellent summary of this area, ranging from nanosized DNA origami (Rothemund, 2006) to magnetically folded milli-scale structures (Iwase and Shimoyama, 2005).

Arguably, one of the most promising applications will arise in the semiconductor industry. As a result of the continuous downscaling of fabrication processes, non-volatile data storage systems will at some point run into their limits to store and process bits of information using only a few atoms (Bennewitz et al., 2002). To achieve higher data densities, it is necessary to move to the third dimension. The first steps in this direction have been taken by stacking wafers (Dellutri et al., 2006) or layers (Tanaka et al., 2007). However, the stacking approach is not suitable to achieve truly three-dimensional structures, in which both the resolution and extent of the features is identical in all directions (Abelmann et al., 2010). We believe that the most promising production method is three-dimensional self-assembly.

Not only is three-dimensional self-assembly a prospective candidate for highly repetitive memory structures, it will also open a path for more complex electronics, such as processors. For instance, Gracias *et al.* (Gracias et al., 2000) have designed millimeter-sized polyhedra with integrated electronics. By self-assembling these into crystals, functional electrical circuits have been demonstrated on a centimeter-scale. Scaling down the building blocks is a crucial step towards scalability of the system as a whole.

It has been demonstrated that microscopic spherical particles can form regular structures up to centimeter-sized dimensions (Philipse, 1989). By tuning the particle properties and/or the driving force of self-assembly, one can control the size and dimensions of the resulting structures (Manoharan et al., 2003; Rycenga et al., 2008).

Although major progress has been made in three-dimensional microscopic self-assembly, observing the dynamic behaviour during the assembly process remains a challenge due to the small size and time constants involved. Several approaches have been explored to model and simulate these processes (Grant et al., 2011; Whitelam and Jack, 2015; Zhang et al., 2005). However, these approaches rely on exhaustive Monte-Carlo simulations, scaling unfavourably with the number of particles involved.

Magnetic forces have been used extensively as driving forces in self-assembly on all scales, together with various sources of agitating energy.

When exposed to an external magnetic field, it has been demonstrated that nanoscopic magnetic rods form bundles (Love et al., 2003) or multimers when driven by ultrasound (Tanaka et al., 2007). Although paramagnetic spheres form

chains, they will form ribbon structures (connected, parallel chains) for chains exceeding 30 particles (Darras et al., 2016; Messina and Stankovic, 2017) and flower-like patterns result when magnetic and non-magnetic beads are mixed with ferrofluids (Erb et al., 2009). In the absence of an external magnetic field, a theoretical study of off-centred magnetic dipoles in spherical particles (Yener and Klapp, 2016) shows that lateral displacement of the dipoles results in structures that are more compact than chains. On millimetre-scales, magnetic forces and vibrations have been used to quickly and efficiently assemble particles with correct orientation on a template (Shetye et al., 2008, 2010). Templated self-assembly has further been studied by agitating particles levitated in a paramagnetic fluid (Ilievski et al., 2011a; Woldering et al., 2016). Also on centimetre-scales, magnetic forces have been used to form particles rather than structures, such as the spontaneously folding elastomeric sheets with embedded electronics; as demonstrated in (Boncheva et al., 2005). Lash *et al* (Lash et al., 2015) showed that polystyrene beads self-assemble into HCP packed structures by solvent evaporation. Larger polystyrene particles (>18 μm) required additional disturbing energy (ultrasonic energy) to self-assemble. Macroscopic self-assembly processes on a centimetre scale are dominated by two-dimensional structures, where mechanical shaking is the most widely used source of disturbing energy.

Hacohen et al. (Hacohen et al., 2015) demonstrated DNA-inspired patterned bricks with embedded magnets, self-assembling into a programmed structure, but report gravity bias. Stambaugh *et al.* (Stambaugh et al., 2003) reported self-assembled 2D structures of centimetre-sized spherical particles with internal magnets that were shaken vertically, and observed different resulting structures that were based on particle concentration and magnet shape. Ilievsky *et al.* (Ilievski et al., 2011b) demonstrated self-assembly of centimetre-sized magnetic cubes into chains in a turbulent flow by submerging them in a rotating reactor filled with water, this way introducing eddy flows as a disturbing energy. They also introduced the concept of effective temperature, describing the motion of particles as if Brownian by nature. Even though the assembly process is three-dimensional, the resulting structures are limited to a single dimension and the dynamics involved have not been studied.

To build upon this work, we introduce an experimental setup, which is designated as a "macroscopic self-assembly reactor", as a simulator for microscopic self-assembly. In this reactor, we study the motion and interaction of centimetre-sized objects. Particles are subject to a downward gravitational force and a drag force that is created by an upward water flow. We chose the particle density to balance these forces, causing them to appear weightless. Following Ilievski (Ilievski et al., 2011b), we use a turbulent water flow as an agitating source, simulating the Brownian motion on a microscopic scale. We employ permanent magnets, resulting in attraction forces between the particles.

By increasing particle size from micrometers to centimetres, not only the ease of observation but also the characteristic time constants increase decidedly. This makes the self-assembly process visible using conventional cameras. As a result of scaling up the system, the environment also changes; laminar flows become

turbulent while inertia effects become dominant. At the same time, Brownian motion becomes negligible. Therefore, it is crucial to study to what extent the macroscopic system is a good simulator for microscopic environments, which is the main topic of this publication.

In this chapter we characterise the motion and dynamics of particles in a macroscopic self-assembly reactor. By observing the trajectories of a single particle in the reactor, we quantify the similarity between Brownian motion of said dynamics. By observing the interaction of two particles in the reactor, we can characterise the most fundamental building block of the self-assembly process, which is the interaction of magnetic spheres in a turbulent environment.

2.2 Theory

Brownian motion is the apparent motion of microscopic particles suspended in a fluid or gas, resulting from collisions with their surrounding molecules, and it can be characterised by a three-dimensional random walk. The nature of the environment in terms of flow patterns (laminar, turbulent) is characterised by the Reynolds number: (Landau and Lifshitz, 1987)

$$\mathrm{Re} = \frac{\rho v L}{\mu}, \tag{2.1}$$

where ρ [$\mathrm{kg\,m^{-3}}$] is the density of the fluid/gas, v [$\mathrm{m\,s^{-1}}$] the velocity of the fluid/gas with respect to the object, L [m] a characteristic diameter and μ [$\mathrm{kg\,m^{-1}\,s^{-1}}$] the dynamic viscosity of the fluid/gas. Low and high numbers (loosely speaking $\mathrm{Re} < 1$ and $\mathrm{Re} > 5000$) correspond to respectively laminar and turbulent flow.

2.2.1 Diffusion

A random walk has an average square displacement that increases linearly as time increases. We can define a diffusion constant D [$\mathrm{m^2\,s^{-1}}$], which in a system with three degrees of freedom links average displacement $\langle x^2 \rangle$ [$\mathrm{m^2}$] to time t [s] according to

$$\langle x^2 \rangle = 6Dt. \tag{2.2}$$

This model holds only if the average distance travelled is much smaller than the size of the container in which the particles move. In our experiment this is not the case and, therefore, container geometry needs to be taken into account.

To account for the confined space, we first consider a particle performing a random walk along a single dimension. The particle displacement with respect to its starting location after t seconds is normally distributed with variance $\sigma_x^2 = 2Dt$. Hence, the average squared displacement $\langle x^2 \rangle$ is equal to the variance of the distribution. The probability of the particle being outside of the confined space is

zero. To account for this effect, we replace the normal distribution by a truncated normal distribution. If the truncation is symmetrical on both tails of the normal distribution, x_t [m], then the truncated distribution is given by

$$n_t(x,\sigma,x_t) = \begin{cases} \frac{n(x,\sigma)}{N(x_t,\sigma)-N(-x_t,\sigma)} & -x_t \le x \le x_t \\ 0 & \text{otherwise,} \end{cases} \tag{2.3}$$

where $n(x,\sigma)$ is the normal distribution and $N(x,\sigma)$ is the cumulative normal distribution. The average squared displacement of a confined particle is the variance of this distribution:

$$\langle x^2 \rangle = \sigma^2 \left(1 - \frac{x_t n(x_t,\sigma)}{N(x_t,\sigma) - \frac{1}{2}} \right). \tag{2.4}$$

For $x_t/\sigma \gg 1$, the particle does not yet experience the confinement. In this situation $n(x_t,\sigma) \approx 0$ and $\langle x^2 \rangle = \sigma^2$. For $x_t/\sigma \ll 1$ the chance of finding the particle in the container is uniformly distributed ($n_t = 1/2x_t$), and $\langle x^2 \rangle$ saturates at $x_t^2/3$.

When moving to three dimensions, the average squared displacement of the separate dimensions can be simply summed because they are orthogonal.

The diffusion coefficient can only be determined if there has been a sufficient amount of collisions. In between the collisions, particles have constant velocity and direction. Due to the stochastic nature of the collision events, the velocity autocorrelation decays exponentially with time constant (Langevin, 1908; Lemons and Gythiel, 1997)

$$\tau_v = \frac{m^*}{f}, \tag{2.5}$$

where f [kgs^{-1}] is the drag coefficient and m^* [kg] is the effective mass.

The situation for $t \ll \tau_v$ is referred to as the ballistic regime. Here, the average squared distance travelled $\langle x^2 \rangle$ is quadratic rather than linear in time. The transition from the (quadratic) ballistic regime to the (linear) diffusion regime (eq. 2.2) is modelled phenomenologically by:

$$\sigma^2 = 6D \frac{t^2}{t + \tau_v}. \tag{2.6}$$

Note that both the effective mass m^* and the drag coefficient f depend on the environment. The effective mass takes into account the fact that when the particle is accelerated, the surrounding water mass is also accelerated. For incompressible fluids with either zero viscosity or infinite viscosity (Stokes flow), the added mass is 50 % of the mass of the water displaced by the sphere (Landau and Lifshitz, 1987). For turbulent flow, both experimental (Pantaleone and Messer, 2011) as well as numerical simulations (Chang and Maxey, 1994, 1995) show that the added mass is also to a good approximation 50 %, irrespective of the Reynolds number or acceleration. There are reports that the added mass might be bigger in cases where the sphere is traveling through its own wake (Odar and Hamilton, 1964), which is

rare in our experimental setup. Therefore, we have suggested a simple estimate of the added mass (Landau and Lifshitz, 1987),

$$m^* = m + \tfrac{2}{3}\pi r^3 \rho_{\text{fluid}}, \tag{2.7}$$

for a particle with radius r [m] and mass m [kg] surrounded by a fluid with density ρ_{fluid} [kg m^{-3}].

2.2.2 Velocity distribution

Li *et al.* (Li et al., 2010) have experimentally proven that the velocity of particles performing a Brownian motion is M-B distributed. This distribution of velocity v [m s^{-1}] is determined by its mode v_{p},

$$p(v) = \frac{4v^2}{\sqrt{\pi} v_{\text{p}}^3} e^{-\left(\frac{v}{v_{\text{p}}}\right)^2}. \tag{2.8}$$

At the mode, the distribution reaches its maximum; thus v_{p} is the most probable velocity. For completeness, we note that the average squared velocity is $\langle v^2 \rangle = \frac{3}{2} v_{\text{p}}^2$.

2.2.3 Drag coefficient

Brownian motion is primarily studied on the microscopic scale, where the Reynolds number is much smaller than unity. In this case, the drag force is linear in velocity and the relevant drag coefficient f is equal to the Stokes drag coefficient. However, on a macroscopic scale, we deal with turbulent flow and a high Reynolds number, where the drag force F_{d} [N] is quadratic in velocity (Landau and Lifshitz, 1987),

$$F_{\text{d}} = \tfrac{1}{2} \rho_{\text{fluid}} C_{\text{d}} A v^2, \tag{2.9}$$

where C_{d} is the drag coefficient and A [m^2] is the cross sectional area of the object in the direction of motion.

In our experiment, the particles are continuously "falling" through the upward water flow. This upward flow is set to the terminal velocity v_{t} of the particles, so that they levitate in front of the camera. Assuming that the changes in the velocity of the particle caused by turbulence are much smaller than the terminal velocity, we can obtain an effective drag coefficient by linearising around the terminal velocity

$$f = \left.\frac{\mathrm{d}F_{\text{d}}}{\mathrm{d}v}\right|_{v=v_{\text{t}}} = \rho_{\text{fluid}} C_{\text{d}} A v_{\text{t}}. \tag{2.10}$$

2.2.4 Disturbing energy

On the micro-scale, the diffusion coefficient and velocity distribution of particles in the fluid can be linked to the temperature. This concept can be extrapolated to macro-scale systems where disorder is achieved by shaking rather than by temperature. In that case, one speaks about effective temperature (Ilievski et al.,

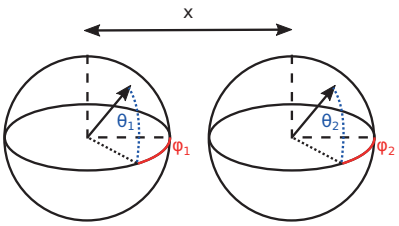

FIGURE 2.1 – *The interaction between two spheres modelled by magnetic dipoles at distance x with orientation vector* $\boldsymbol{\theta} = [\theta_1\ \phi_1\ \theta_2\ \phi_2]$.

2011b; Wang and Wolynes, 2011), which is usually significantly higher than the environmental temperature. Since shaking can be highly directional, we prefer to characterize the shaking action by energy (kT [J]) rather than temperature to avoid confusion.

Starting from the velocity distribution (eq. 2.8), and considering that $\langle v^2 \rangle = {}^{3kT}/_{m}$ for three-dimensional random walks, the most probable velocity is related to the kinetic energy through:

$$kT = \tfrac{1}{2} m^* v_{\mathrm{p}}^2. \tag{2.11}$$

The Einstein relation also relates the diffusion constant and viscous drag coefficient of a particle to the thermal energy kT:

$$kT = fD. \tag{2.12}$$

If particles in a self-assembly reactor behave according to Brownian motion, both relation (2.11) and (2.12) can be used to obtain the disturbing energy and should give identical results.

In addition to measuring the disturbing energy kT from Brownian motion, we can also estimate it from the interaction between two attracting magnetic objects. In this situation, we use the fact that the probability of the system being in a state is governed by M-B statistics. (Feynman et al., 1970) Consider a system of two spherical magnetic particles in a confined space (Figure 2.1). The chance that the distance of those particles measured from center-to-center is smaller than x_0 is:

$$p(x \le x_0) = \frac{1}{Z} \int_d^{x_0} \int_{\boldsymbol{\theta}} g_\mathrm{r}(x) e^{-\frac{E_\mathrm{m}(\boldsymbol{\theta},x)}{kT}} d\boldsymbol{\theta} dx \tag{2.13}$$

$$Z = \int_d^{D} \int_{\boldsymbol{\theta}} g_\mathrm{r}(x) e^{-\frac{E_\mathrm{m}(\boldsymbol{\theta},x)}{kT}} d\boldsymbol{\theta} dx$$

$$\boldsymbol{\theta} = \left[\theta_1\ \phi_1\ \theta_2\ \phi_2\right].$$

Here $g_\mathrm{r}(x)$ is the probability density function of a sphere pair with distance x between their centres, unaffected by magnetic forces, which models the influence of the geometry of the reactor.

The distance between the cylindrical magnets is at all times at least a factor of four of the magnet height h ($h \le d/4$). At this point, we approximate their magnetic field as well as their magnetic moments by point dipoles. This approximation is accurate within 1.3 % for our magnet geometry. In that case, the magnetic energy of particle 1 with magnetic moment $\boldsymbol{m}(\theta_1, \phi_1)$ [Am^2] in a field $\boldsymbol{B}(\theta_2, \phi_2, x)$ [T] generated by particle 2 reduces to

$$E_\mathrm{m}(\boldsymbol{\theta}, x) = -\boldsymbol{m}(\theta_1, \phi_1) \cdot \boldsymbol{B}(\theta_2, \phi_2, x). \tag{2.14}$$

Equation (2.13) can be approximated numerically by a Monte-Carlo approach in which a large number of random combinations of sphere locations and orientations are selected, yielding different values for E_m. The geometry factor g_r is approximated by repeated random sampling of two point locations in a confined geometry and then gathering statistics about their distance.

2.3 Materials and methods

2.3.1 Reactor

The experimental setup consists of a transparent cylinder with an inner diameter of 17.3(1) cm containing the particles of interest (Figure 2.2). Gravity is counteracted by pumping water from the bottom to the top via four 4.0(1) cm diameter inlet holes using a MAXI.240T pump (PSH pools). The water exiting the cylinder is collected in an open container connected to the pump inlet. The water flow entering the pump is monitored using an altometer (IFS 4000, Krohne Messtechnik GmbH).

Meshes spaced at 17 cm prevent the particles from moving outside the field of view of cameras placed around the reactor. The dynamics of the particle-fluid system are determined by the particle density and geometry, as well as water flow speed and its degree of turbulence.

At flow speeds of approximately 30 $\mathrm{cm\,s^{-1}}$ and a water temperature of 20 °C the system is characterised by Reynolds numbers of 57 000 and 61 000 for respectively the reactor cylinder and the inlet tubes. This is more than an order of magnitude

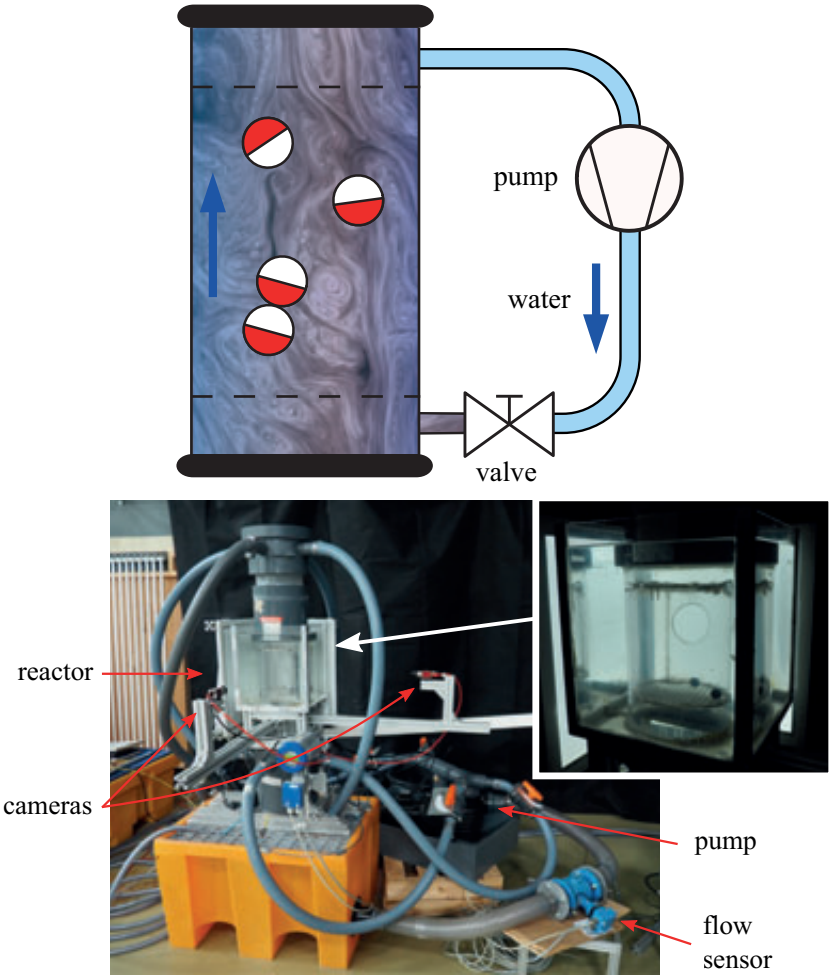

FIGURE 2.2 – *Schematic (top) and experimental (bottom) setup of the macroscopic self-assembly reactor. Water is pumped from the bottom to the top of the reactor, counteracting gravity and supplying energy to the particles via turbulent flow. Meshes prevent the particles from moving outside of the field of view of cameras placed around the reactor.*

larger than 2040, the lowest number which can support turbulence in a tube. (Avila et al., 2011) The turbulence generated by the tubing, the disruptive nature of the inlet area and the meshes is supported by this environment.

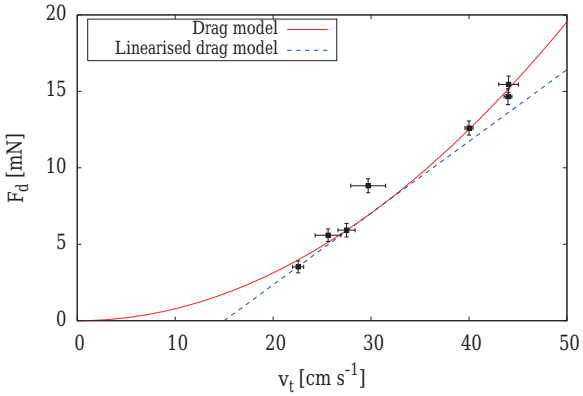

FIGURE 2.3 – *Calculated drag force versus measured terminal velocity for spheres with equal diameter but varying densities. The effective drag coefficient is obtained by linearisation around the terminal velocity (eq. 2.10), illustrated by the blue dashed line for* v_t=30 cm s^{-1}.

2.3.2 Particles

The particles used in the experiments are 3D-printed polymeric (ABS) spheres with a diameter of 1.67(1) cm to 2.02(2) cm and a corresponding density of 1.33(2) g cm^{-3} to 1.25(4) g cm^{-3} (larger particles have lower density). The core of the spheres consist of cylindrical, axially magnetised NdFeB magnets with a length of 3.80(5) mm and a diameter of 3.80(5) mm (Supermagnete, grade N42, Webcraft GmbH). The dipole moment (50.8(1) mA m^2) was determined by measuring the force between two magnets using a balance.

The drag coefficient of the particles was estimated from their terminal drop velocity. For this, particles with a range of densities but identical diameter of 1.85 cm were released at the top of a 2 m high cylinder filled with water. Once an equilibrium between drag- and gravitational force had been established (approximately 0.5 m after release), the velocity of the particles was measured with a video camera over a distance of 1.0 m. Figure 2.3 shows the measured relation between drag force and terminal velocity. From fitting equation 2.9, we obtain $\frac{1}{2}\rho_{\text{fluid}} C_{\text{d}} A$ = 78(3) g m^{-1}. Assuming the density of water to be 1000 kg m^{-3}, we obtain C_{d}=0.58(2). Spheres of this diameter and velocity in water have a Reynolds number of approximately 5500. At this value, Brown *et al.* (Brown and Lawler, 2003) predict C_{d}=0.39, which is substantially lower. The reason for the discrepancy is unknown to us. The measured drag coefficient is used in the remainder of this paper.

2.3.3 Reconstruction

Two calibrated, synchronised cameras (Mako G-131, Allied Vision) were placed around the reactor at an angle of approximately 90° and they recorded datasets at 30 fps at a resolution of 640×512. The reactor is surrounded by a square, water-filled aquarium to prevent refraction due to its cylindrical nature. Back-light panels were used to enhance contrast. Single spheres were observed for 15 min and two spheres for 30 min. Offline, the location of the spheres was automatically detected using a custom written MATLAB script. A method based on the direct linear transform algorithm (Hartley and Zisserman, 2004) was used for 3D reconstruction, giving an average reconstruction error of 0.16 cm. Trajectories closer than 1.5 cm to the meshes were discarded to rule out the significant effect of the altered hydrodynamic interaction at these interfaces. The velocity vector of the particle is obtained by $\mathbf{v} = \Delta\mathbf{x} f_{\text{cam}}$, the product of the particle displacement between two frames, and the camera frame rate.

2.4 Results

2.4.1 Single particles

Figure 2.4 shows a set of reconstructed trajectories of a 1.85 cm sphere in the reactor. Each trajectory starts and ends when exiting and entering the areas within 1.5 cm of the meshes, and is indicated by a different color.

Figure 2.5 shows the velocity calculated from these trajectories. The histogram is obtained from the absolute velocity (10 600 data points) of a 1.80 cm sphere. A M-B distribution was fitted to the data by minimising the maximum distance $E_{\max}$ between the cumulative empirical and cumulative M-B distribution, yielding fitting parameter v_{p}. A Kolmogorov-Smirnoff (K-S) test was used to quantify the quality of fit and to obtain a significance level Q to disproof the null hypothesis that the two distributions are the same. (Press et al., 1992) With a $E_{\max}$ of 0.0073 and a Q of 0.70, we have good reason to assume that the velocity is MB-distributed.

Figure 2.6 displays the resulting v_{p} for spheres of various diameters, for which we find a range from 15.92 $\text{cm}\,\text{s}^{-1}$ to 17.54 $\text{cm}\,\text{s}^{-1}$. The fit to the M-B distribution has a Q-value above 0.05 for five out of the seven measurements. Even though the data suggests a slight decrease of velocity with increasing sphere size, the particle velocity fits very well to a model assuming constant velocity, with an average of 16.6(2) $\text{cm}\,\text{s}^{-1}$. This analysis was carried out using a chi-square fitting routing, yielding the reduced χ^2 error metric (ideally being around 1) and the corresponding Q-value (the probability that a χ^2 equal or greater than the observed value is caused by chance). (Press et al., 1992) The reduced χ^2 of this fit is close to unity (0.68) with a very high Q-value of 0.67.

Figure 2.7 shows the normalised distribution of the particle at several z-slices across the reactor. It can be seen that the particle has a preference for the bottom area, especially near the reactor walls of the positive x-coordinate. We believe that this phenomenon is caused by a non-uniform flow pattern of water that results from

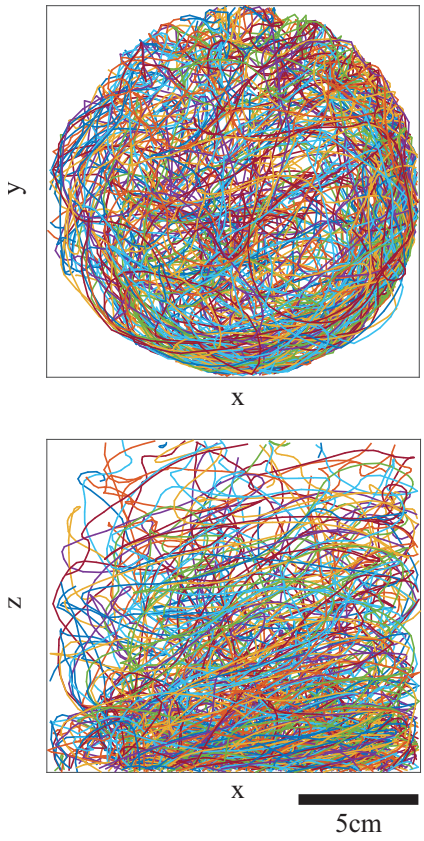

FIGURE 2.4 – ***Top:*** *upper and* ***bottom:*** *side views of the reconstructed trajectories of a single sphere (diameter* 1.85 cm*) moving through the reactor. Coordinates less than* 1.5 cm *close to the top- and bottom meshes are removed to rule out significant influence of the meshes. In this way, the single trajectory is cut into many smaller ones, which are each assigned a different color.*

the specific valve settings. These observations are analogous to a multi-temperature environment in a system of micro-particles; as particles are biased towards a state of minimum energy, they are more likely to be in areas with lower thermal energy.

The average squared displacement was calculated from the longest trajectories; that is, those with a minimum duration of 2.0 s. Figure 2.8 shows the resulting curve for a sphere with a diameter of 1.90 cm. The curve shows a quadratic regime below 0.3 s, shortly entering an approximate linear regime before slowly converging to a horizontal asymptote.

The movement of the sphere is in the quadratic, or ballistic, regime when the measurement time is shorter than the average time between directional changes

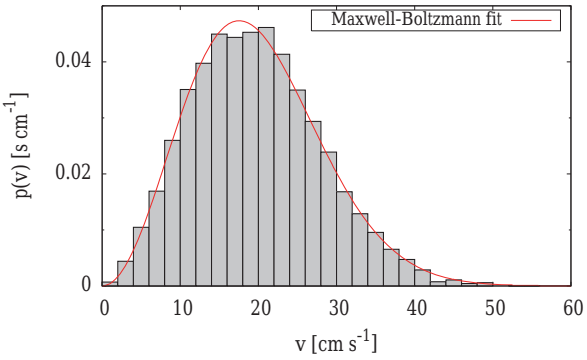

FIGURE 2.5 – *Maxwell-Boltzmann (M-B) distribution fitted to the measured velocity distribution of a particle with a diameter of* 1.80 cm. *The Kolmogorov-Smirnov (K-S) test quantifies a maximum distance between the theoretical and experimental cumulative distributions of* 0.0073 w*ith a Q value of* 0.70 *, indicating a high probability that the velocity is indeed M-B distributed.*

("collisions"), τ_v. Using measured values for the drag coefficient and effective mass in equation 2.5, we obtain values for τ_v ranging from 134 ms to 149(10) ms. The saturation measured for longer observations is caused by the confined geometry of the reactor and it will change as the reactor is changed in shape and size.

The model described by equations 2.4 and 2.6 was fitted to the measurements, yielding values for diffusion coefficient D and average reactor size x_t.

We have to take into account that the model has its limitations. First of all it is based on a symmetrical truncated normal distribution. This would require the particle to always start in the center of the reactor. In contrast, all of the measured trajectories start at a random place at the top or bottom of the reactor due to the method that we used to obtain separate trajectories.

Secondly, the cylindrical geometry of the reactor is not included in the model. These two issues mainly affect the estimation of the reactor size.

Finally, the ballistic regime was phenomenologically modelled without physical background. This region, which has a high weight factor during fitting the model to the data (due to the small error bars in the data), can result in a significant fitting error.

Given that only the latter aspect could give errors in the estimation of D, we consider the obtained values for D to be quite reasonable, with values between 17 and 23 $cm^2\,s^{-1}$ (see figure 2.6). The average diffusion coefficient for all of the measured diameters is 20(1) $cm^2\,s^{-1}$. Judging from the graph, there seems to be no reason to assume that the diffusion coefficient has a strong dependence on sphere diameter. It should be noted, however, that this assumption leads to a very highly

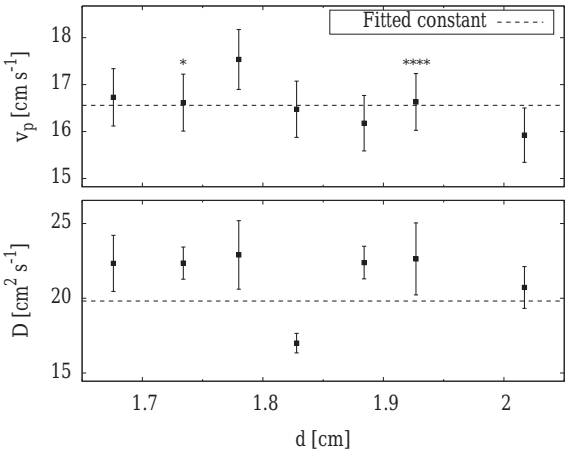

FIGURE 2.6 – ***Top:*** *Mode of the M-B distribution obtained by fitting to the measured velocity distribution of particles of various diameters (reduced* $\chi^2 = 0.68$*,* $Q = 0.67$*). Stars indicate the quality of fit (Q-value) of the K-S test (*$* < 0.05$*,* $**** < 0.0001$*).* ***Bottom:*** *Diffusion coefficient obtained by fitting the diffusion model to the average square displacement (reduced* $\chi^2 = 5.85$*,* $Q = 4 \cdot 10^{-6}$*).*

reduced χ^2 (5.85) and low quality of fit Q ($4 \cdot 10^{-6}$). However, due to the previously mentioned model inaccuracies, we think that we may have underestimated the errors in the estimation of D.

2.4.2 Two-sphere results

From the two-sphere experiments, the distance x between the particles was tracked over time. Figure 2.9 shows the cumulative probability of sphere distance $p(x \leq x_0)$ for spheres of various diameters. Spheres with smaller diameters have a lower magnetic energy in the connected state and, therefore, a higher probability of being connected. In other words, $p(x \leq d)$ becomes larger for smaller d. All of our measurements follow a similar profile: they consist of a curved regime for $x \leq 3\,\text{cm}$ followed by an approximately linear region for $x > 3\,\text{cm}$. The linear regime indicates that magnetic forces are no longer significant for particle interaction. For $x > 13\,\text{cm}$ there is a saturation effect caused by the reactor geometry. The model of equation 2.13 has been fitted to the curves by minimising the maximum distance between the curves (based on the Kolmogorov-Smirnoff method (Press et al., 1992)). Although this is not an exact fit, it manages to capture the shape with a maximum error of 5 % of the full range.

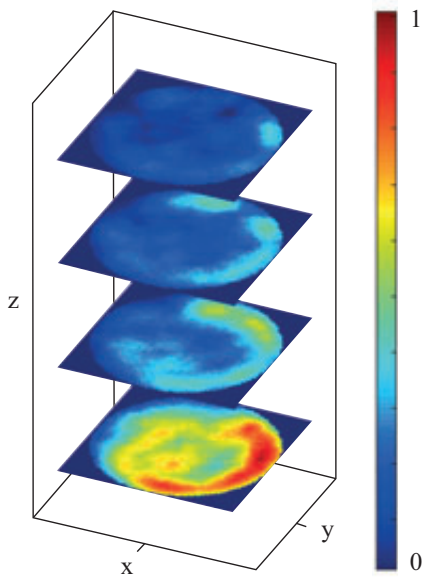

FIGURE 2.7 – *Normalised probability distribution of a single sphere (diameter* 1.85 cm*) in the reactor, displayed in slices along the reactor tube. The particle has a clear preference for the bottom region as well as the edge regions. Quantised, the particle has a chance of* 62 %*,* 48 % *and* 26 % *to be in, respectively, the right (positive x-coordinate), back (positive y-coordinate) and top (positive z-coordinate) halves of the reactor.*

2.4.3 Disturbing energy

The experiments provide three methods for the characterisation of the equivalent thermal energy of the system. Numerical values for the kinetic energy were calculated from the measured velocity and added mass according to equation 2.11. The measured diffusion coefficient and drag coefficient at the set water flow speed (equation 2.10) were used to calculate the energy using the Einstein relation (equation 2.12). Additionally, two-particle experiments provide numerical values for the equivalent energy as a result of fitting equation 2.13 to the measured data, as depicted in figure 2.9.

The resulting values for all of the spheres are summarised in figure 2.10. A first observation is that the results obtained via single sphere experiments (velocity, diffusion) are in the same order of magnitude, and differ by approximately 20 µJ. They span a range from approximately 60 µJ to 120 µJ. These values are, however, more than a factor of ten higher than the results obtained via the two sphere experiments, which range from approximately 6 µJ to 7 µJ. The possible origin for this discrepancy is discussed in the following section.

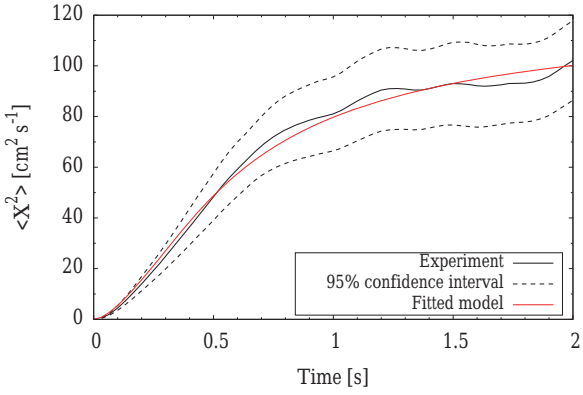

FIGURE 2.8 – *Average squared displacement as a function of time for a sphere with diameter* 1.90 cm*, calculated from* 65 *trajectories. The model fits within the* 95 % *confidence interval.*

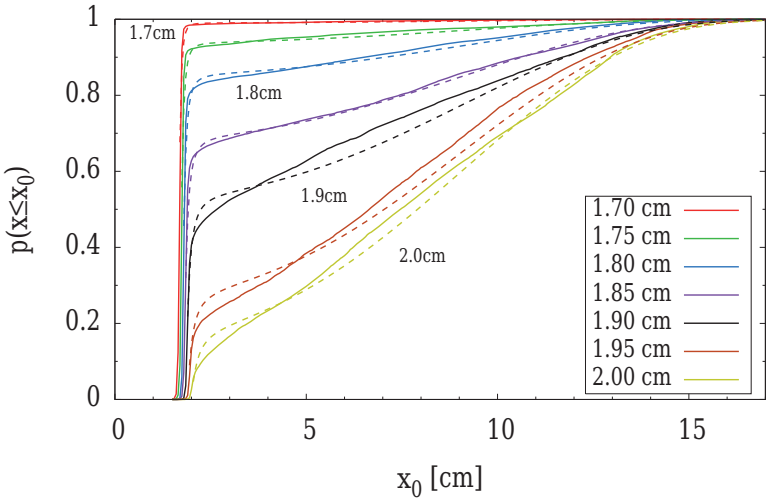

FIGURE 2.9 – *Measured probability (cumulative) of the distance between the centres of two magnetic spheres (x) for various sphere diameters. A model based on M-B statistics captures the shapes of the curves with a maximum error of* 5 % *of the full range. As the spheres decrease in size, they are more likely to be in a connected state.*

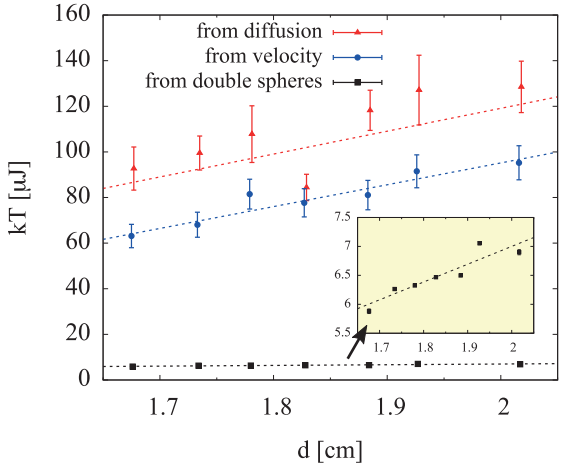

FIGURE 2.10 – *Disturbing energy of the turbulent field calculated from the diffusion coefficient, the velocity distribution and double sphere experiments. The disturbing energy estimated from the single sphere experiments (diffusion, velocity) are approximately a factor 10 higher than that estimated from double sphere experiments. The dashed lines are guides to the eye. There is an increase in energy with an increase in sphere diameter, which is proportional with the increase in mass and friction coefficient.*

In all cases, the energy increases as the sphere size increases, by approximately 17 %, 41 %, and 46 % for, respectively, two-sphere experiments, diffusion, and velocity. As we concluded previously, the diffusion coefficient and average sphere velocity do not depend on the sphere size (figure 2.6). The increase of energy is caused by an increase in mass and friction coefficient, and both are dependent on sphere radius.

2.5 Discussion

From the trajectory analysis of single particles, we were able to determine that their velocity distribution closely follows a M-B distribution. Additionally, we have seen that the average squared displacement as a function of time follows a shape that was predicted by a confined random walk model. These conclusions strongly support the hypothesis that particles in the reactor perform a random walk.

When increasing the particle size, the observed disturbing energy kT also increases. However, there is no observable increase in velocity or diffusion coefficient. For the energy calculated via velocity and diffusion, this means that this increase in energy is caused by an increase in, respectively, effective particle mass

and drag coefficient. The corresponding curves, as shown in figure 2.10, are very similar due to the fact that the particle mass and drag force are coupled. With an increase in particle radius, both the mass and surface area are increased. The increase in energy occurs without physically changing the nature of the disturbing energy; that is, the speed and turbulence of the water flow is unaltered. This means that the amount of energy that is transferred from the environment to the particle is dependent on the particle geometry.

An explanation for this effect might be found in the wavelength dependence of the turbulence. Turbulence is introduced as a large wavelength disturbance at the bottom of the cylinder, after which it propagates upwards in an energy cascade that transfers the energy to smaller wavelengths. This process is dissipative (Richardson cascade (Richardson, 1922)). The resulting energy spectrum drops off at increasing wave numbers. (Kolmogorov, 1941) Therefore, we can assume that the disturbing energy as experienced by the particles is not, like in Brownian motion, characterised by a flat spatial frequency spectrum (white noise) but instead drops off at shorter wavelengths. So, effectively, the bandwidth of the energy transfer increases for larger particles.

The assumption of a dissipative energy cascade could also explain why the energy obtained from two-sphere experiments is lower compared to single sphere experiments. While all of the spatial frequency components in the turbulent flow drive an object around the system in a random walk, wavelengths in order of the particle diameter contribute most effectively to separation of connected particles. The disturbing energy dropping with decreasing wavelength would explain why the disturbing energy estimated from the two particle experiment is smaller than that obtained from the random walk.

It is perhaps in the spatial frequency spectrum where the analogy between turbulent flow and true Brownian motion breaks down. Therefore, we will need to characterise the effective energy of the system separately for particles of different size. Special care needs to be taken for large clusters of particles because they are effectively a large particle and, therefore, subject to a higher energy portion. At the same time, particle-particle interaction is subject to a lesser amount of disturbing energy. Consequently, such systems will have a bias towards the occurrence of smaller particle clusters.

2.6 Conclusions

We have constructed an experimental setup that allows us to study the connection dynamics of centimeter-scale objects by analysing the interaction of magnetic attraction forces and disturbing turbulent forces. This “macroscopic self-assembly reactor” serves as a physical simulator of self-assembly processes on the microscale and nanoscale, allowing easy observation by drastically increasing both the length and time scales.

Trajectory analysis of single spherical particles shows that they perform a random walk, which analogous to Brownian motion. Spheres with diameters

ranging from 1.7 cm to 2.0 cm have a range of velocities that are M-B distributed. The most probable velocity (mode) is independent of sphere size and has a value of 16.6(2) $\mathrm{cm\,s^{-1}}$. The average square displacement over time, or the 'diffusion profile,' fits to a confined random walk model. The diffusion coefficient appears to be independent of sphere size, with an average value of 20(1) $\mathrm{cm^2\,s^{-1}}$. Although statistical analysis disproves this statement, we believe that the measurement error has been underestimated.

The particle distribution is non-uniform over the reactor. The particle is, for instance, three times as often in the bottom half of the reaction compared to the top half. Although this non-uniform distribution does not affect the Brownian motion behaviour, it reduces the virtual reactor size.

In two-particles systems, we observe self-assembly dynamics; that is, the particles occasionally connect and disconnect. The cumulative distribution of the distance between the centers of the particles fits with a maximum error of 5 % of the full range of the distribution to a model based on M-B statistics.

The disturbing energy (analogue to temperature) of the reactor was estimated from the velocity distribution and diffusion (single particle experiments), as well as from the dynamic interaction of two-particle systems. The estimates of the disturbing energy determined from single sphere experiments are in the same order of magnitude. However, the disturbing energy obtained from two-sphere experiments is at least one order of magnitude lower (approximately 6.5 µJ compared to 80 µJ). From this we can conclude that for self-assembly studies, the disturbing energy of the system cannot be calibrated from single sphere experiments alone.

The disturbing energy increases with increasing sphere diameter, from 1.7 cm to 2.0 cm. For the single sphere experiment, this increase is more prominent (41 % via diffusion analysis, 46 % via velocity analysis) than for the two-sphere experiment (17 %). We reason that the energy transfer from the turbulent environment to the particles is dependent on particle size and geometry.

In addition to the two-sphere experiment, periodic connection and disconnection events have also been observed for a six-sphere system, forming ring- and line-based structures. This demonstrates that the reactor can be successfully applied to study self-assembly processes at convenient length and time scales, and it may be a good simulator for microscopic environments.

Chapter 3

Self-assembly via turbulent flow and magnetic interaction

Abstract

Turbulence can be used as a source of disturbing energy in macroscopic self-assembly. It is a macroscopic equivalent to thermal energy kT on the microscale. The amount of turbulence can be adjusted by changing the input flow into the reaction chamber. We measured the effect of an increase in turbulence on particle diffusion, velocity and disturbing energy. In our experimental setup, we can vary the disturbing energy by a factor of eight. Since we use upward flow to avoid sedimentation, there is a directional dependency in the motion of the particles. A region exists in which this asymmetry is minimal. This study shows that one can tune the disturbing energy analogous to a temperature change at the microscale, which increases the relevance of macroscale self-assembly studies for the self-assembly processes of micro- and nano-particles.

The work in this chapter was a team effort. The reactor was initially designed and constructed by Remco Sanders and Léon Woldering. My contribution included modification of the reactor (especially providing tunable turbulent flow), design of the particles and conduction of the experiments. Tijmen Hageman composed the theoretical background, built and wrote the software for particle detection, 3D-reconstruction, particle tracking and trajectory analysis.

3.1 Introduction

In a self-assembly process, order seems to appear from disorder spontaneously. Particles self-assemble due to their mutual attraction and the disturbing energy in the environment. In macroscopic self-assembly the mutual attraction or assembling energy is frequently magnetic (Gross and Dorigo, 2008), and the disturbing energy turbulent flow (Ilievski et al., 2011b; Murugesan et al., 2015; Roland et al., 1992; Zheng et al., 2004). Turbulence is inherently random and chaotic and

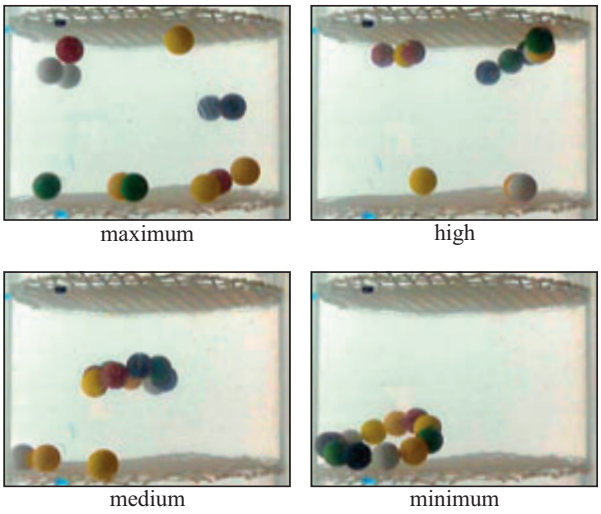

FIGURE 3.1 – *The effect of degree of turbulence on the structure-formation of twelve magnetic polymer spheres that self-assemble in a vertical turbulent water flow. Decreasing turbulence leads to increased structure formation (lines and rings of different lengths and shapes). At maximum turbulence only single spheres appear whereas at minimum turbulence, the lowest energy structure (a 12-sphere-ring) appears. The local magnetic forces of each individual sphere interacts as the spheres explore the energy landscape in order to find the lowest-energy configuration. A video of the process can be found on the website using the QR code in the margin*

resembles microscopic thermal motion. Thermal operations such as slow or rapid cooling or heating of liquids, solids or gases can be realized analogously by rapid regulation of the turbulent flow. Figure 3.1 shows excerpts of a video recording of macroscopic self-assembly of twelve polymer spheres of 2 cm diameter with embedded permanent magnets. The structure formation is clearly dependent on the degree of turbulence; at maximum turbulence the spheres are disconnected and only start to form structures as turbulence decreases. At low turbulence the minimum energy structure (ring) is formed. This is a macroscopic representation of a microscopic quenching or cooling sequence and nicely demonstrates the paths of self-assembly. In this chapter we desribe a method to adjust turbulence, and we systematically characterize the effect of turbulence on velocity distributions and diffusion of particles in the turbulent flow. To the best of our knowledge, this is the first time systematic investigations of turbulence as a disturbing energy have been made.

3.2 Theory

The analysis of particle trajectories and two particle interaction were introduced in chapter 2. Here, we also analyse the diffusion coefficient and velocity distribution for the projection of the particle movement on the vertical axis (z), along the main direction of the flow, and in the horizontal plane perpendicular to the flow (x, y). The diffusion of a particle in a confined space was described in chapter 2for one dimensional movement along a line segment. If the particle motion along the three projections is uncorrelated, we can apply the same expression for the average squared displacement,

$$\langle x^2 \rangle = \sigma_x^2 \left(1 - \frac{x_t n(x_t, \sigma_x)}{N(x_t, \sigma_x) - \frac{1}{2}} \right). \tag{3.1}$$

where $n(x, \sigma_x)$ is the normal distribution and $N(x, \sigma_x)$ is the cumulative normal distribution. For x, we can substitute the y or z coordinate. σ_x is the standard deviation of the displacement and the variance σ_x^2 can be related to the diffusion coefficient along a coordinate in one dimension by

$$\sigma_x^2 = 2D_x t \tag{3.2}$$

In chapter 2, we used the Maxwell-Boltzmann distribution to the describe the distribution of the vectorial velocity, using a most probable velocity v_p. The distribution of the velocity of the individual components is Gaussian distributed, described by the standard deviation ϕ of the velocity distribution.

$$p(v_x) = \frac{1}{\sqrt{2\pi\phi_x^2}} e^{-\frac{v_x^2}{2\phi_x^2}} \tag{3.3}$$

where again x can be substituted with y or z.

3.3 Methods

The self-assembly reactor has been introduced in chapter 2. The system has four inlet ports on the bottom of the cylinder and the inlet ports were equipped with valves. This allowed us to inject the water flow asymmetrically and increase the turbulence by increasingly closing the valves. The valves are 2-way PVC ball valves (Type S6 DN40-14, 50 mm diameter, Praher Plastics Austria GmbH).

A schematic front- and top-view of the reactor is shown in figure 3.2. The valves can be set between 0° (fully closed) and 90° (fully open). Maximum flow turbulence and asymmetry between the four valves can be achieved by opening one valve only (right position, indicated by 0°). The remaining three valve were set identically, where 90° represents minimal asymmetry since all four valves are open to the same maximum degree.

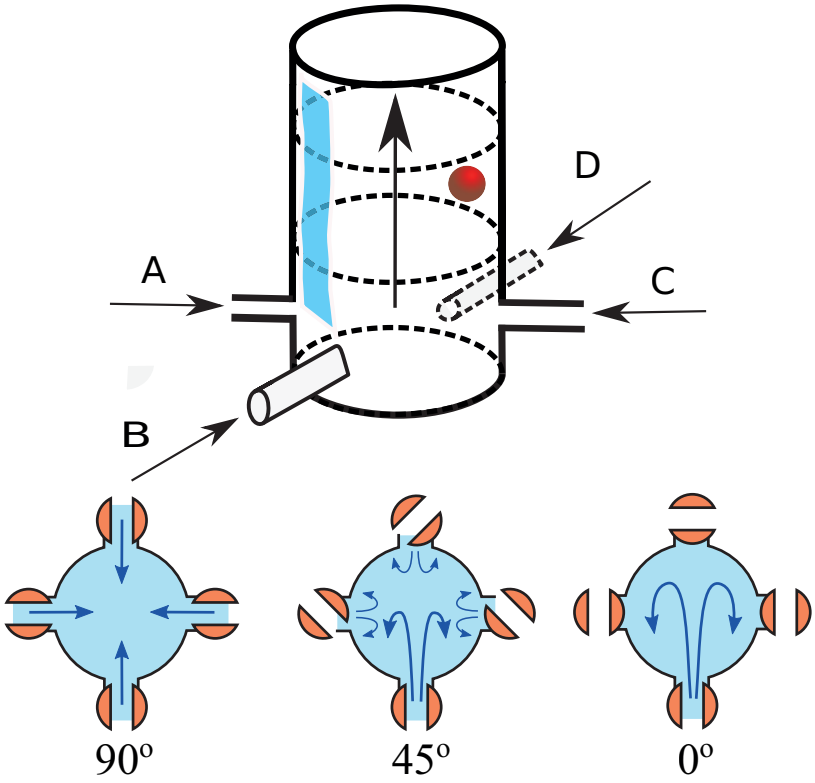

FIGURE 3.2 – *Schematic front- and top-view of the self-assembly reactor. Four water inlets (A,B,C and D), a particle (red) and flow direction are shown in the front-view. The dotted circles in the middle of the reactor indicate the position of the nets that are used as placeholders for the particle(s). In the bottom-view, three valve settings are shown; minimum (left,* 90° *valve opening), medium (*45° *valve-opening) and maximum (right,* 0° *valve-opening) which corresponds to 52.48; 41.9 and 0 cm/sec flow speed according to figure 3.4. One of the valves is kept open for all three settings which, in addition to the turbulent flow from the three closed valves, provides an asymmetry to the flow field.*

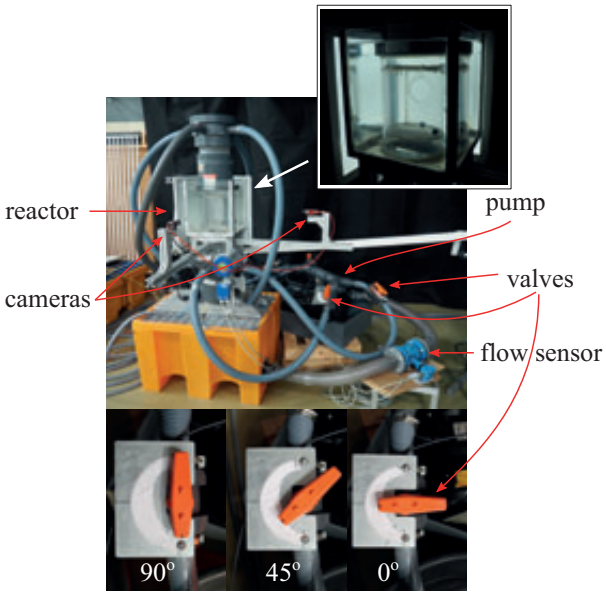

FIGURE 3.3 – *Front-view of the self-assembly reactor. Four bottom-inlet tubes, valves, pump, cameras are shown. The inset shows a magnification of the actual reaction chamber. Below, three pictures of one of the three valves at different valve-opening, as in figure 3.2, corresponding to increasing degree of turbulence in the incoming water flow.*

The self-assembly reactor and three representative valve settings (bottom) are displayed in figure 3.3. The valve settings in the bottom row correspond to the bottom schematic image in figure 3.2.

3.3.1 Flow calibration

We expected the turbulence in the cylinder to be proportional to the valve opening of the three valves. Since we used ball-valves, the flow through the valves however has a non-linear relationship with the valve angle. Therefore we chose to convert valve angle to flow by measuring the flow through the cylinder as function of the valve opening, see figure 3.4. For this measurement, three valves were closed and one valve was opened over an angle θ. We used maximum pump power.

From this measurement we derived a dimensionless measure for the asymmetry of the flow:

$$\text{flow asymmetry} = 1 - \frac{f(\theta)}{f(90°)}, \tag{3.4}$$

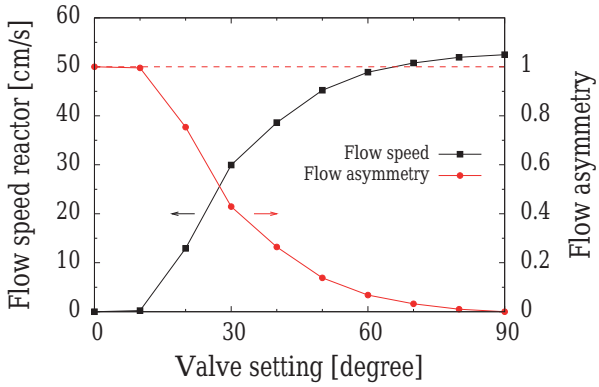

FIGURE 3.4 – *Flow speed through the reactor versus valve setting at maximum pump power (left axis). Due to the nature of the valve, the flow varies highly non-linear with valve opening. Using equation 3.4, a flow asymmetry factor can be defined (right axis) that has a more linear relationship with turbulence.*

where $f(\theta)$ is the water flow speed through the valves controlled during the experiments at opening angle θ. At minimum turbulence, when all valves are fully open, the flow asymmetry is defined as 0 and at maximum turbulence, when three valves are closed, the flow asymmetry is 1. The asymmetry and turbulence increase with decreased valve opening of the three valves. In addition to turbulence increasing asymmetry cause a lower flow speed in the reactor and probably larger vortices in the tank which is due to the asymmetry only.

3.3.2 Particles

The particles were identical as described in chapter 2. They are 18.80(7) mm diameter polymer (ABS) spheres with a 3.80×3.80(5) mm cylindrical NdFeB permanent magnet placed in the center of each sphere.

3.3.3 Reconstruction

Two synchronized cameras were used for video recordings as described in chapter chapter 2. Particles were observed at different degrees of turbulence. For each setting, videos were recorded for 15 min for single sphere experiments and 30 min for two sphere experiments. Both the 3D trajectories of a single sphere and the 3D distance between two spheres were reconstructed via custom written Matlab scripts.

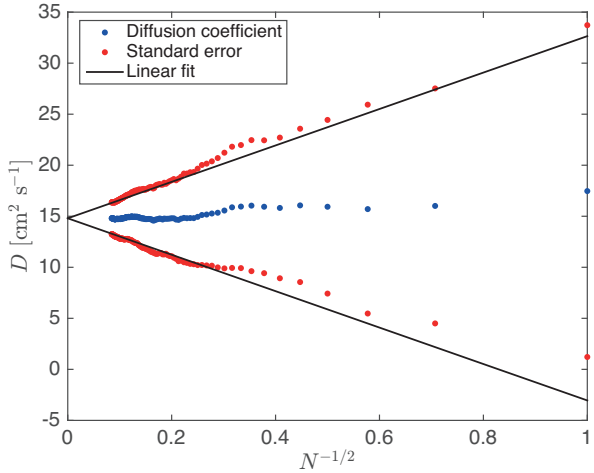

FIGURE 3.5 – *The estimated diffusion coefficient (blue dots) and 1σ confidence interval as a function of the inverse square root of the number of trajectories (N).*

3.3.4 Measurement precision

To determine the diffusion constant, the trajectory of the particle in the turbulent flow was observed as described in chapter 2. Each trajectory longer than 0.5 s was fitted to the diffusion model described in chapter 2. These values are averaged for a large number of trajectories to obtain an estimate of the diffusion coefficient. The precision of the estimate increases with the number of measurements, which is expressed by the standard error (the standard deviation of the fit divided by the square of the number of fits).

To validate this process, we determined the diffusion coefficient for sets of data with varying number of trajectories. The result is shown in figure 3.5, where the blue dots represent the estimate of the diffusion coefficient as function of the number of trajectories N. As expected, the estimated value converges (to about 15 cm^2 s^{-1}) with increasing number of measurements. The red dots indicate the 1σ confidence limit on the estimate (we are 68 % confident that the diffusion coefficient lies between the red dots). By plotting the confidence interval as a function of $N^{-1/2}$, figure 3.5 shows that indeed the precision of the estimate increases with the square root of the number of trajectories.

From this measurement, we conclude that for a 1σ confidence limit of 5 % of the estimated value, we need at least 570 trajectories. We obtain approximately 80 trajectories of 0.5 s duration per minute. The total measurement time per experiment should therefore be at least 7 min. To be on the safe side, the duration of the experiments in this study was 15 min.

3.4 Results

We observed the movement of a single sphere and the interaction between two spheres in the reactor, and first determined the disturbing energy as a function of the flow asymmetry, applying the methods introduced in chapter 2. We also investigated the directional dependence in the velocity distribution, which will be discussed in section 3.4.2.

3.4.1 Relation between flow asymmetry, turbulence and disturbing energy

We observed the influence of turbulence on the kinetic behaviour of a single particle in terms of the most probable speed v_p and its diffusion coefficient, as well as the interaction between two particles. From these observations, we could determine the relation between the flow asymmetry and the disturbing energy kT.

Influence of flow asymmetry and turbulence on velocity

Figure 3.6 shows the velocity distribution of a particle in a turbulent flow for various settings of flow asymmetry. The graphs were obtained by a kernel density estimation using a Gaussian kernel with a standard deviation of $1\,\mathrm{cm\,s^{-1}}$. With increasing flow asymmetry there is an increase in particle velocity.

The velocity data was fitted to a Maxwell-Boltzmann distribution, as described in chapter 2, with only the most probable speed v_p as fitting parameter. In figure 3.7 this most probably speed is shown as a function of flow asymmetry. This relation is approximately linear. Over the full range of available flow asymmetry, the velocity varies by a factor of three from approximately $10\,\mathrm{cm\,s^{-1}}$ to $30\,\mathrm{cm\,s^{-1}}$.

Influence of flow asymmetry on diffusion coefficient

The diffusion coefficient was estimated by fitting a confined random walk model to the measured average squared displacement, as in chapter 2. The latter was obtained by averaging the squared displacement of trajectories with a duration of 2 s. Figure 3.8 shows the diffusion coefficient as a function of flow asymmetry. As in the case of velocity, the diffusion increases roughly linear with flow asymmetry, now by a factor of six from approximately $7\,\mathrm{cm^2\,s^{-1}}$ to $44\,\mathrm{cm^2\,s^{-1}}$.

Influence of flow asymmetry on disturbing energy kT

As described in chapter 2, the velocity distribution as well as the diffusion coefficient of a single sphere can be related to disturbing energy, using the kinetic energy $kT = {}^1\!/_2 m^* v_\mathrm{p}^2$ and the Einstein relation $kT = fD$ respectively.

A third method for obtaining the disturbing energy can be obtained from particle interaction. When two particles are inserted in the reactor, they connect and disconnect intermittently. The ratio between the time they are connected and disconnected depends on their magnetic interaction energy and the disturbing

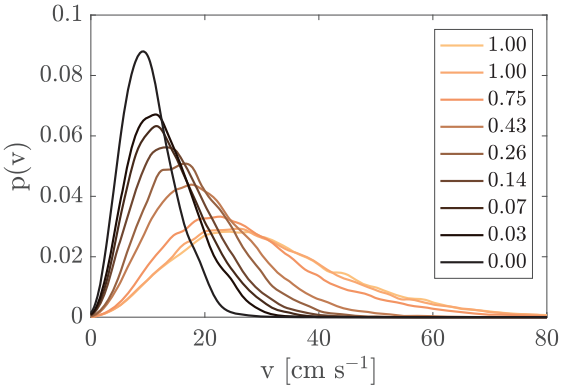

FIGURE 3.6 – *Velocity distributions of a single particle for different flow asymmetry settings (legend) in the reactor show a Maxwell-Boltzmann-like distribution. The distribution was obtained via a kernel density estimation using a Gaussian kernel with* $\sigma = 1\,\mathrm{cm\,s^{-1}}$. *Increased turbulence leads to a higher average velocity.*

energy in the system. In chapter 2a method is described to extract this disturbing energy from the distribution of observed particle distances. This method is more precise and fundamentally more correct than the method based on the connection-disconnection duration.

In figure 3.9, all estimates for the disturbing energy are plotted together. The relationship between kT and flow asymmetry fit well to a linear function in all three cases. The estimates of the disturbing energy from the single sphere experiments are very similar, certainly considering the measurement error. However, like in chapter 2, these values are an order of magnitude higher than the values obtained from the two-sphere experiments. For both single and two sphere experiments the disturbing energy increases with increasing flow asymmetry. The increase is a approximately a factor two higher for the single sphere experiment (for the two single sphere experiment the increase $(a+b)/b = 6(1)$, and for the double sphere, $(a+b)/b$=3.1(7)).

3.4.2 Directional dependency of disturbing energy

The water flow is directed from the bottom to the top in the reactor in order to counteract gravity acting on the particles. It is therefore expected that the vertical (z) component of the particles motion deviates from the horizontal (x and y) components. Additionally, there might be an asymmetry in the xy-plane as well, since the flow is injected asymmetrically at high turbulence. These effects are present both in the velocity distribution as well as in the diffusion coefficient.

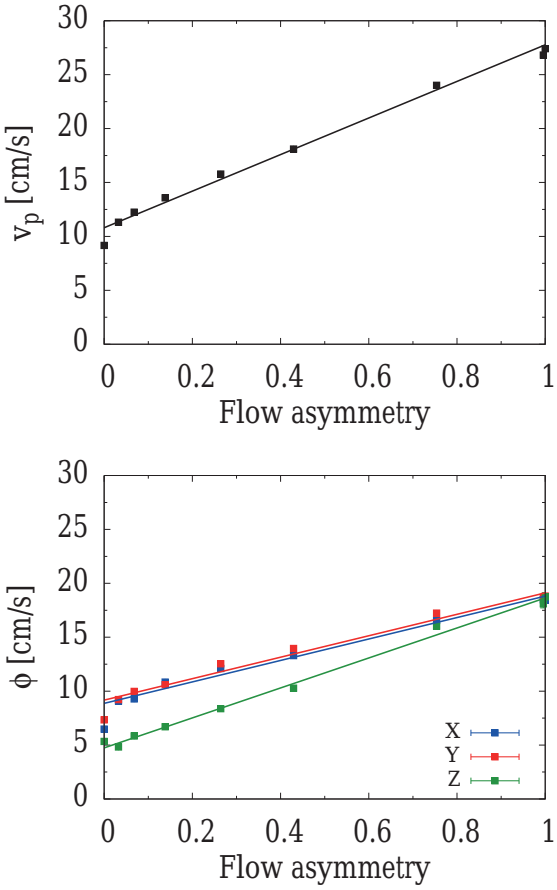

FIGURE 3.7 – ***Top:*** *the most probable speed v_p of the Maxwell-Boltzmann distributed particle velocity as a function of flow asymmetry. The relation is approximately linear. The velocity increases by almost a factor of three, indicating that the turbulence is increased.* ***Bottom:*** *the standard deviation of the horizontal $(x,\ y)$ and vertical (z) components of the particle velocities as a function of flow asymmetry. The velocity in the vertical direction is significantly lower than in the horizontal direction for a flow asymmetry below* 0.5

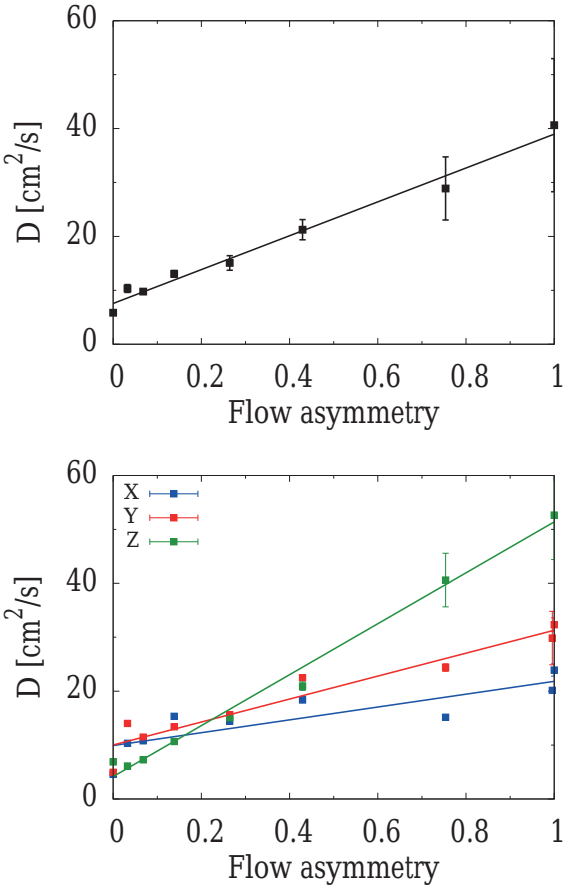

FIGURE 3.8 – ***Top:*** *the diffusion coefficient of the motion of a single particle as a function of flow asymmetry. The diffusion coefficient increased approximately a factor six from minimum to maximum turbulence. The relation is roughly linear.* ***Bottom:*** *the diffusion coefficient per dimension as a function of flow asymmetry. Above a symmetry of* 0.5*, the difference between the components is fairly large, but reduces significantly for lower turbulence. The estimation of D underestimates its error bars, which for that purpose have been ignored for the fit.*

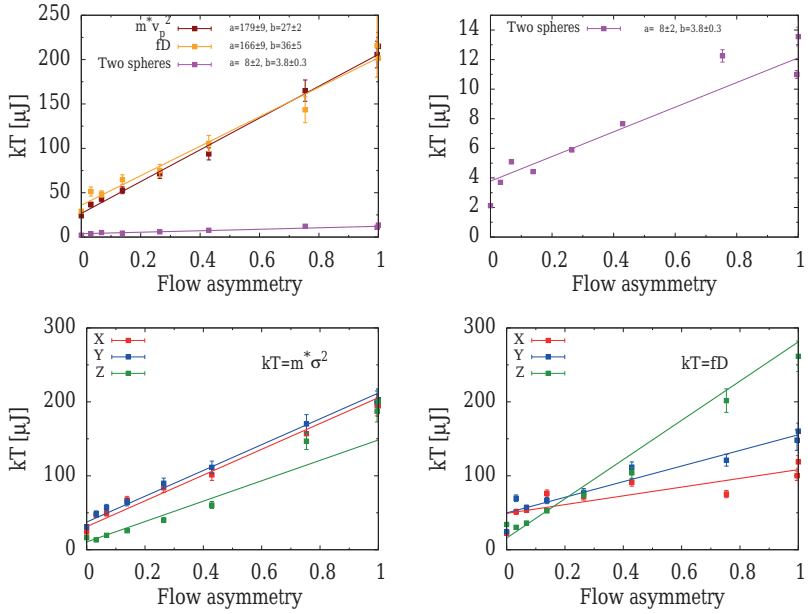

FIGURE 3.9 – *The disturbing energy (kT) increases approximately linear with flow asymmetry.* ***Top left:*** *determined from single sphere experiments, using the diffusion coefficient (Einstein relation fD) and most probable velocity ($m^* v_p^2$) and from the interaction between two spheres. The disturbing energy determined from the velocity distribution agrees very well with that obtained from the diffusion coefficient. The values obtained from this single sphere experiments however are an order of magnitude higher than that of the two sphere experiment.* ***Top right:*** *Enlarged view of the energy determined via the interaction between two spheres.* ***Bottom left:*** *The directional dependence of the disturbing energy derived from the velocity.* ***Bottom right:*** *The directional dependence of the disturbing energy derived from the diffusion coefficient. Due to the fact that we underestimate the error on the diffusion coefficient, it is ignored by the linear fits for the Einstein relation.*

Directional dependence velocity

Figure 3.10 shows the velocity distribution of a particle in a turbulent flow for various settings of flow asymmetry. The graphs were obtained by a kernel density estimation using a Gaussian kernel with a standard deviation of $1\,\mathrm{cm\,s^{-1}}$. With increasing flow asymmetry, the velocity distribution becomes wider, such that the average absolute velocity increases. The velocity in the horizontal dimensions are similar, but the vertical velocity is significantly lower for low asymmetry settings. According to the theory a normal distribution (equation 3.3) was fitted to the measurements. The standard deviation ϕ is plotted in figure 3.7. There is no significant difference in the horizontal direction (x and y components), and there seems to be no correlation of the difference with flow asymmetry. For flow asymmetry below 0.5 the velocity in the z-direction is significantly lower, up to a factor of two.

Directional dependence diffusion coefficient

Figure 3.8 shows the diffusion coefficients along the three different directions. Even though the data is scattered, the values for the horizontal dimensions only differ moderately. The diffusion coefficient in the z-dimension, however, shows a much stronger dependence on flow asymmetry, diving below the horizontal components for low flow asymmetry and vice versa.

Directional dependency of disturbing energy kT

As before, the disturbing energy can be derived from the velocity and diffusion coefficients, but now for the individual x-, y- and z-components ($kT = m^*\phi^2$ and $kT = fD$, respectively) Figure 3.9 (bottom) shows the estimated values of the disturbing energy. For clarity, two graphs are plotted, one of the estimate based on kinetic energy (bottom left) and one for the estimate based on the Einstein relation (bottom right). Of course these graphs show similar trends as figures 3.7 and 3.8, as the particle mass and friction coefficient do not change between the measurements; the velocity and diffusion coefficient fully determine the shape of these curves.

Like with the velocity analysis, there is no significant difference in kinetic energy per dimension for higher flow asymmetries. For asymmetries below 0.5, however, the energy in the vertical component is much lower than that of the horizontal components with approximately a factor of factor two.

The results from the Einstein relation are significantly different; the energy scales different for the separate dimensions; the horizontal components are close but the vertical component has almost a factor of two more energy for high flow asymmetry settings.

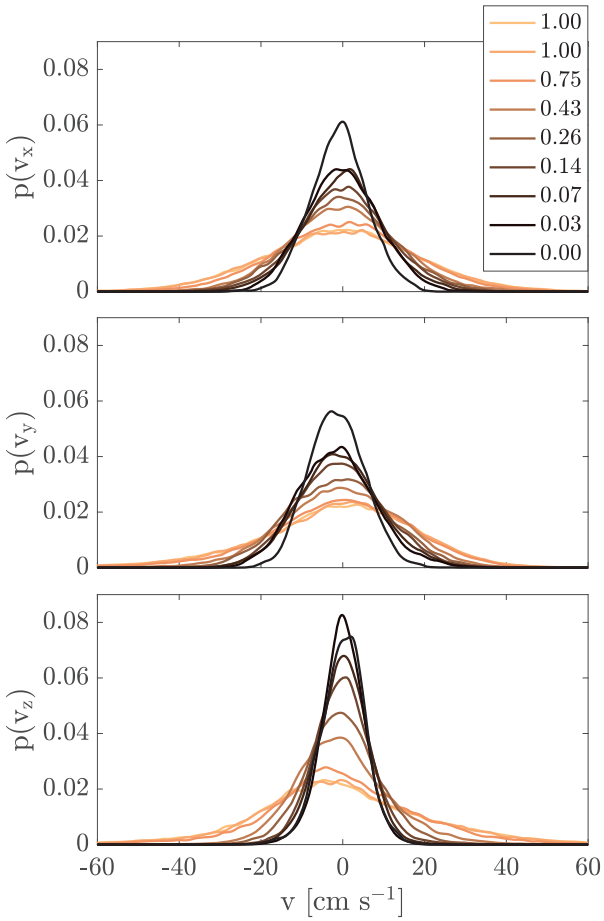

FIGURE 3.10 – *The x, y and z components of the velocity of a single particle for different flow asymmetry settings (legend) in the reactor show a Gaussian-like distribution. The distribution was obtained via a kernel density estimation using a Gaussian kernel with* $\sigma = 1\,\mathrm{cm\,s^{-1}}$. *Increased turbulence leads to a higher average velocity. The z component velocity is significantly lower than that of the other dimensions.*

3.5 Discussion

The experiments clearly show that the particle velocity, diffusion coefficient as well as the disturbing energy increase with turbulence. When three of the four inlet valves are gradually closed, the inflow becomes more asymmetric and turbulence increases. This process adds to the turbulence created by the reactor geometry.

Creating asymmetry in the inlet flow is a practical way to change turbulence and mimic temperature changes on the micro- and nano-scale. The analogy between turbulent motion and thermal fluctuation is quite intriguing. There are however at least two areas where the analogy between turbulence and thermal fluctuation does not hold: directionality and spatial frequency power density.

3.5.1 Directionality in turbulent flow

The experiments show that one cannot ignore the directionality of the turbulent flow field. In analogy with temperature fluctuation, we would have to conclude that the temperature in the system is directionally dependent.

Judging from the observations on directional dependence, increase in turbulence has a more pronounced influence on the vertical direction. The difference of velocity, diffusion coefficient and disturbing energy between the x- and y dimensions are minor, especially compared to that of the z dimension. The latter also has a higher range between minimum and maximum value at the flow asymmetry extrema.

The directionality of disturbing energy is more pronounced when derived from the Einstein relation compared to the derivation from velocity. This might have to do with the nature of the velocity; the theory of diffusion assumes a purely random process. A bias might affect how this velocity contributes to the observed displacement over time, and this way to the validity of equation 3.2.

A region exists around a flow asymmetry of 0.5 around which the directional dependence is minimal. We are confident that the directional differences between variables can be minimized by proper technical reconstruction of the self-assembly reactor. Altering the number and location of inlet tubes and valves might be one possible option to create a more homogeneous three-dimensional flow-field in which multi-particle self-assembly can be realized.

3.5.2 Richardson cascade and disturbing energy

The value of the disturbing energy (kT) determined via the two-particle experiments is an order of magnitude lower than that obtained form the diffusion or velocity of a single particle. We speculate that this is because a greater part of the provided energy contributes rather to the motion of single particles than to their close interaction. This speculation is based on the existence of a vortex hierarchy in turbulent flow (Richardson cascade (Richardson, 1926)). The asymmetrical introduction of the turbulent flow might cause a macroscopic swirl with a diameter

close to the tank diameter at the bottom of the cylinder. This swirl moves upward in a screw-like manner.

With a strong dominance of inertial forces over viscous forces in turbulence, the largest eddies are undamped. Large vortices break up into smaller vortices by a process of cascading until viscous forces are significant and will dissipate the energy.

Due to this Richardson cascade, there is an energy transfer from the larger vortices to the smaller ones. The energy is not uniformly distributed over the different lengthscales, but drops off at shorter lengthscales (Hwang and Irons, 2012). So in contrast to thermal fluctuation, the equipartition theorem does not hold for the energy spectrum (turbulence "noise" is not white).

When we consider velocity or diffusion, we take into account vortices of all size. For the two particle experiment, predominantely vortices with length scales in the order of the particle dimensions contribute to their separation. It is not surprising that the disturbing energy from the two-sphere experiment is lower than from the single sphere experiments since only a part of the vortice size spectrum contributes its determination.

In addition, the macroscopic swirl may counteract the dominating z-direction and strengthen the influence of the x- and y-directions on variables. This would explain why the x- and y-components are mostly relatively similar.

3.6 Conclusions

We created an asymmetric inlet flow into a macroscopic self-assembly reactor. Three of four bottom inlet valves were step-wise closed to the same degree, while the fourth was kept open. This results in a more asymmetric inflow, amplifying the turbulence already created by the reactor geometry. An increase of the turbulence led to an increase in the disturbing energy (analogue to thermal energy kT). We quantified the effect of an increase in turbulence on the motion of spherical centimetre-sized particles in the reactor, characterized by the velocity distribution, diffusion coefficient and disturbing energy.

When tracking the motion of a single sphere, we observed that its most probable velocity as well as the diffusion coefficient obtained from its random walk increases with higher flow asymmetry. From this we conclude that the turbulence in the system is at its lowest value when the water is injected symmetrically (i.e. all four valves are fully open).

Using thermodynamic theory, the velocity distribution and observed diffusion coefficient can be translated to an effective disturbing energy. The estimates for the disturbing energy from the velocity and diffusion are identical within measurement error. In our system, the disturbing energy can be increased from approximately 30 to 200 μJ (i.e. by a factor around six) by increasing turbulence.

In addition to the experiment with a single sphere, the disturbing energy was obtained from observation of the interaction between two spheres with embedded magnets. This experiment is more relevant for self-assembly studies. With increased

flow asymmetry, the disturbing energy is amplified with approximately a factor of three, but the absolute values are an order of magnitude lower than for the single sphere experiment (4 up to 12 µJ compared to 30 to 200 µJ).

Since the main flow in the reactor is in the vertical direction, there is a directional dependency of the movement of a single sphere. The standard deviation of the velocity distribution in in the vertical (z) direction is significantly lower than the planar (xy) direction, especially for low turbulende where the difference increases up to a factor of two.

There is a clear directional dependence of the diffusion coefficient as well. The difference between the horizontal (xy) dimensions are minor. The vertical dimension shows a much stronger dependence of energy on flow asymmetry.

We calculated the directional dependency of the disturbing energy from the velocity distributions as well as the diffusion coefficients. The energy for the x and y dimensions are similar. The energy in the z dimension is more distinct. The derivation from velocity shows similar energy for high flow asymmetry for all three dimensions, but the vertical component is up to a factor two lower for low asymmetry. The derivation from diffusion coefficient shows that the vertical component is much stronger affected by the flow asymmetry.

The thermodynamical conclusions achieved in this investigation have consequences for the study of microscale self-assembly. Our results indicate that macroscale self-assembly can be used as an analogous system in order to study microscale self-assembly since we can change turbulence and the disturbing energy in a similar manner as we can change temperature for microscale systems. Processes such as crystallization or quenching are likely to be studied analogously at the macroscopic scale provided that an ideally directional homogeneous turbulent flow field can be decreased rapidly in order to achieve quenching. One can take advantage of the possibility of inhomogeneous design which may open up novel venues of investigation. An inhomogeneous turbulent flow field may be interpreted as a temperature gradient. A precisely designed three-dimensional inhomogeneous turbulent flow field may be used for macroscopic mimicking of several processes in for example microscopic mammal or bacterial cells, organelles or organs. For the moment this resembles solely a future vision, but at the same time an achievable target.

Chapter 4

Formation of magnetic dipoles rings and lines

Abstract

Multimember rings and lines of centimeter sized magnetic polymer spheres form as a result of turbulence in a macroscopic self-assembly reactor. Structure formation of three, four, five and six spheres at increasing turbulence was evaluated with respect to ring and line occurance. A line-ring transition was observed for four spheres with equal occurance of chains and lines. Less than four spheres resulted in line formation and exceeding four spheres in predominantely rings. By altering turbulence we provide an adjustable and broad-range energy landscape for the magnetic polymer spheres to explore. Decreasing high turbulence lead to structure formation similar to solidification and sublimation. The structure formation was recorded with two horizontally mounted and perpendicular video cameras. The recordings were evaluated by observation of the video images by eight persons.

This chapter is a team effort. My contribution was the construction of the experiment, data collection, organisation of the observation by the eight observers and analysis of the observations. Tijmen Hageman wrote the program to assist in the observation.

4.1 Introduction

As macro- or microscopic particles explore the energy landscape they naturally tend to form low energy structures, sometimes via one or several intermediates. The final thermodynamic global energy minimum may be reached only after extensive structural reorganisation and the result depends on the reorganisational pathway taken by the particle collective.

The energy landscape is the environment in which both macroscopic or microscopic scale self-assembly takes place. Knowledge about the energy landscape and its relation to the self-assembled structures is a prerequisite for implementation of self-assembly into several fields of science and technology. Self-assembled

structures of dipolar particles (i.e., with electric or magnetic dipoles) are of great interest for several applications. Novel optical and stimuli-responsive materials are based on self assembly of magnetic particles (Messina and Stankovic, 2017). In the absence of an external magnetic field structure formation of magnetic spheres was investigated by Guo et al. (2005). Magnetic spheres of several tens of micrometers diameter where placed on a thin silicon wafer and self-assembled due to applied vibrations. Twenty spheres were used and the number of N-member rings were counted in each of the 500 self-assembly trials. There was no ring formation observed for $N < 3$ or $N > 20$ magnetic spheres but there was a ring formation peak at $N = 9$. The probability of ring appearance vs. number of spheres in each ring was Poisson distributed.

According to Wen et al. (1999) magnetic spheres form stable rings in the absence of a magnetic field, since the ring leads to magnetic flux closure and represents the most stable configuration (Wen et al., 1999). At high bead concentrations, all structures such as rings, lines, and clusters join together to form a lattice-like structure. A computer simulation of the dipole-dipole interaction carried out by the same authors was in agreement with the experimental observations. Messina et al. (2014) show that lines are stable as the number of magnetic spheres $N \leqslant 3$ (dimers and trimers) and that for $4 \leqslant N \leqslant 13$ rings are the predominant structure At $N \geqslant 14$ rings start to stack upon eachother and form tubular structures. At $N = 14$ there is a clear transition between a single ring and a double ring where two seven-member rings that stack upon each other. A transition from lines to rings was observed at $N = 4$ where the two structures are equally stable whereas rings are more stable at $N \geqslant 4$. All dimensions in space (1D, 2D and 3D) are represented in the study. The dipoles vectors of the magnets in the ring are tangential to the circle and constitute a vortex like configuration ("curling dipole vectors") and represents the minimal energy structure. Simple experiments with magnetic spheres confirmed the results of the simulations.

Two dimensional self-assembly of five millimeter magnetic spheres was studied theoretically and experimentally by the same authors. A small number of magnets leads to the stable configuration of rings at $4 \leqslant N \leqslant 18$. At $N \geqslant 17$ so called onion shaped structures (smaller rings inside the larger) start to form. For $N = 18$ there is a six-member ring inside of the outer twelve-member ring, both are shaped as hexagons. The onion shaped multiple rings are local energy minima whereas structures with“buckling” i.e. the outer ring is about one member too big in order to surround the inner ring so the outer ring has a “bump” in its structure. The “buckled structures” represent structures with somewhat higher energy compared to the other onion structures resulting in a rough energy landscape starting at $N = 19$ (“buckled” and “unbuckled” structures alternate which causes the roughness). In the presence of a strong magnetic field two dimensional self-assembly of spherical magnets was investigated theoretically. Energy minima structures are identified through numerical optimization procedures. For $N = 26$ magnets, a single straight line is found to be the ground state but in the regime of larger $N \geq 27$ the spherical magnets assemble into two touching lines (ribbon). A transition from two to three touching lines occur at $N = 129$. Self-assembly of parallel magnetic lines

is thought of as the result of an interplay between dipole-dipole interactions and short ranged excluded volume correlations. Similar results has been obtained for colloidal ribbon formation (Messina and Stankovic, 2017).

Magnetic nano cubes in the sub 15 nm range were shown to self-assemble in solution and in external magnetic fields into highly ordered lines, sheets, and cuboids. The structures remain stable after the external magnetic field was removed (Taheri et al., 2015).

Particles have to encounter each other in the provided energy landscape (potential energy surface, PES) in order to connect, rearrange, and self-assemble. Contributing to the energy landscape are the disturbing energy and the attractive interaction between the magnetic particles. The potential energy surface for any solid state system regulates the observed structure, thermodynamics, and dynamics.

The task of the self-assembly process is to find the global minimum on the PES which particles during self-assembly conduct as they explore the energy landscape. Using multiple spherical, magnetic centimeter sized particles and letting them explore different energy landscapes i.e. different degree of turbulence, provides valuable insights of multiple member self-assembly. Figure 3.1 in chapter 3 shows for instance the self-assembly of 12 identical magnetic spheres, and how the minimum energy state is reached after slowly reducing turbulence.

In this chapter we investigate systematically how a magnetic centimeter sized polymer spheres with embedded magnets explore the energy landscape provided by turbulent flow. The occurance of structures at various levels of disturbing energy and at varying number of spheres was evaluated. Different people in our lab were asked to analyse snapshots of the videos of the experiment and register their decision (line, ring, non-determined) with respect to what they observe in each image. In this way we could evaluate the prevalence of each structured at each level of turbulence in question. To the best of our knowledge this is the first time that structure formation of multiple magnetic spheres has been systematically investigated a the macroscopic scale.

4.2 Theory

The analysis of the structure formation of magnetic dipoles is an interesting fundamental problem in physics and materials science. A particular interesting question is whether dipoles lend themselves for the study of how novel materials can be build via individual dipolar sub units. There is a large body of theoretical analysis of dipole interaction (Friedrich et al., 2015), (Messina et al., 2014), (Messina and Stankovic, 2017).

Below we give a short summary of the theory relevant for our work.

4.2.1 Energy of Rings and Lines

As two magnetic dipoles approach each other a potential energy $U(\boldsymbol{r_{12}})$ of interaction develops according to equation 4.1, where C is a constant which depends on

the surrounding medium ($\mu_0/4\pi$ in vacuum), $\boldsymbol{r}_{12}$ is the distance between the two magnetic objects and $\boldsymbol{m_i}$ is the dipole strength.

$$U(\boldsymbol{r_{12}}) = C\frac{1}{r_{12}^3}\left[\boldsymbol{m}_1\boldsymbol{m}_2 - 3\frac{(\boldsymbol{m}_1\boldsymbol{r}_{12})(\boldsymbol{m}_2\boldsymbol{r}_{12})}{r_{12}^2}\right] \tag{4.1}$$

Like (Messina et al., 2014), we normalize the energy to the potential energy of two parallel dipoles at distance d ($\boldsymbol{m}_1 \parallel \boldsymbol{m}_2$, $\boldsymbol{m}_{1,2} \perp \boldsymbol{r_{12}}$).

$$U_{\uparrow\uparrow} \equiv \frac{Cm^2}{d^3} \tag{4.2}$$

For N interacting magnets, we can calculate the normalized potential energy of interaction per magnet by

$$u_N = \frac{1}{N}\sum_{i=1}^{N-1}\sum_{j=i+1}^{N}\frac{U(\boldsymbol{r}_{ij})}{U_{\uparrow\uparrow}}r_{ij} \geqslant d \tag{4.3}$$

Using this method, we obtain for a straight line of N dipoles

$$u_N^{\text{line}} = -\frac{2}{\mathrm{N}}\sum_{i=1}^{N-1}\sum_{j=i+1}^{N}\frac{1}{(j-i)^3} \tag{4.4}$$

Note that U_2^{line}=$-U_{\uparrow\uparrow}$.

Correspondingly, for the ring structure, the reduced energy for $N > 2$ is

$$u_N^{\text{ring}} = -\frac{1}{4}\sin^3\left(\frac{\pi}{N}\right)\sum_{k=1}^{N-1}\frac{3+\cos(2\pi k/N)}{\sin^3(\pi k/N)} \tag{4.5}$$

The energy for rings and lines of 3 to 6 members is displayed in figure 4.1. The energy normalized to U_2^{line}, as well as the absolute energy for the spheres used in the experiments is shown. The energy difference between ring and line structures is shown amplified in figure 4.2. There is a clear transition point just below four spheres above which the energy for ring structures is lower than for lines.

4.2.2 Chance of occurence

In the case of a constant supply of energy from the environment, for example a turbulent flow, which contributes to motion as well as separation and rearrangement of the magnetic spheres, the occurance of rings and lines has to be studied by observations over time. The free three-dimensional mobility of particles and structures leads to a constant structural rearrangement. For a given experimental duration it is convenient to use the notion of probability of a certain structure in a particular experiment. The probability P of finding a structure in state i is;

$$P_{\text{state},i} = \frac{\mathrm{e}^{-U_m(\text{state},i)/kT}}{\sum \text{all possible states}} \tag{4.6}$$

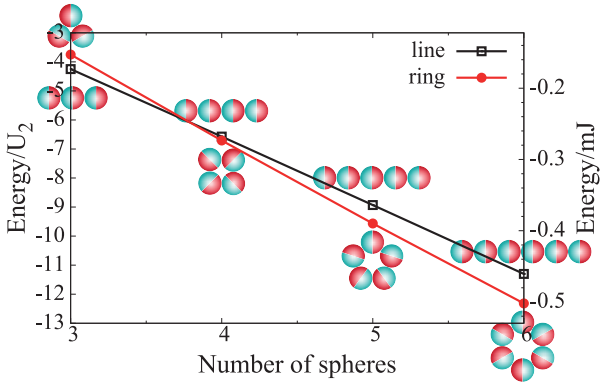

FIGURE 4.1 – *The reduced potential energy U_2 and the energy in mJ for rings and lines of different number of spheres.*

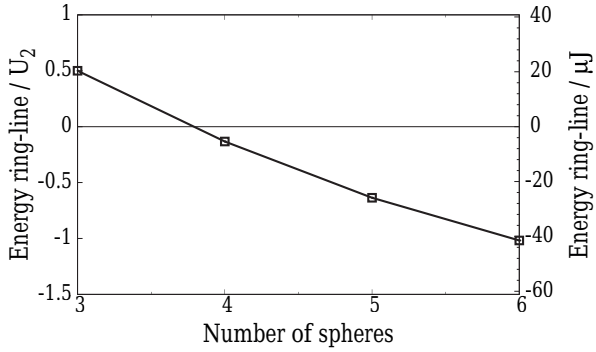

FIGURE 4.2 – *The energy difference between ring and line as a function of the number of spheres.*

Which leads to the chance of occurence of a line over the chance of occurence of a ring of

$$P_{\text{line/ring}}(kT,N) = \exp\left(-N\frac{U_{\uparrow\uparrow}}{kT}(u_N^{\text{line}} - u_N^{\text{ring}})\right) \tag{4.7}$$

Which we can recalculate into the chance of occurence of line over the sum of the chance of occurence of ring plus a line.

$$P_{\text{line/(line+ring)}}(kT,N) = \frac{P_{\text{line/ring}}}{P_{\text{line/ring}}+1} \tag{4.8}$$

4.3 Methods

4.3.1 Self-assembly Reactor

We performed self-assembly experiments in a macroscopic self-assembly reactor with centimeter sized particles in an upward directed turbulent water flow. The reactor and how turbulence and asymmetry of the flow can be varied was described in previous chapters 2 and 3. The disturbing energy kT was determined via both single and two-sphere experiments. In this chapter we use the kT values from the two-sphere experiments since they rather resemble the actual self-assembly process (connections, disconnections, distance-interaction) than single sphere experiments.

4.3.2 Particles

In our experiments we use spherical polymer-particles of 18.5 mm diameter. Cylindrical NdFeB magnets with a magnetic moment m of 50.8(1) mAm^2 were inserted in the center of the spheres as described in previous chapters 2 and 3.

4.3.3 Video analysis - human observation

All the experiments were recorded using two synchronized cameras, mounted horizontally and perpendicular to each other as described in previous chapters. The two cameras are precisely synchronized so that indvidual frames could be compared pairwise, which helps in interpreting the structure in the image. Data sets were recorded at a resolution of 640×512 and a frame rate of 10 fps for 15 min per experiment.

A subset of 900 frames were chosen for analysis of each dataset. Eight lab members evaluated the occurance of structures. The evaluation was conducted by using a MATLAB script where the occurance of "ring", "line" and "other" (neither rings or lines) in each dataset was registered for each image. "Rings" and "lines" were defined in the following way; rings or lines must consist of the maximum number of spheres present in each experiments. In other words a five-member ring will be excluded ("none") if the total number of particles in the experiment is six. Neither "rings" nor "lines" have to be perfectly round or straight but the individual members must be connected. For each frame the observer can choose one of the three alternatives which is then registered automatically for further statistical analysis.

4.4 Results

The probability of line-occurance with respect to the total number of rings and lines (neglecting "other") as a function of the disturbing energy kT is shown in figure 4.3. Included in the graph are the theoretical predictions, based on equation 4.8.

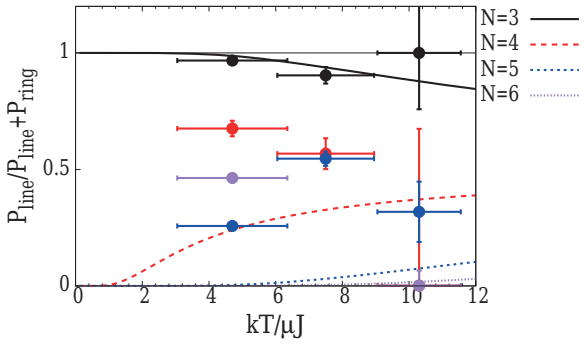

FIGURE 4.3 – *The probability of occurance of lines with respect to the total number of lines and rings as a function of disturbing energy kT for 3, 4, 5 and 6 spheres. The continuous and dotted colored lines are the predictions by the model (equation 4.8). The disturbing energy kT is determined via the two-sphere connectivity and distance-interaction experiments described in chapter 3.*

Three spheres show almost only lines. For four, five and six spheres the observations scattered, so a clear interpretation is difficult. The general trend seems to be that the fraction of rings observed increases with the number of spheres as well as with an increase in kT.

The chance of occurance of a line for the three spheres experiment is in agreement with theory, within error margins. The error margin for the highest kT value is large because only very few lines and rings (less than 3 %) were observed

The observations of all other cases (four to six spheres) reveal a higher occurance than theory. The four spheres experiment even shows the opposit trend in comparison to theory. The experimental data of five and six spheres is so scattered that a clear interpretation is difficult.

The occurance of undetermined structures seem to be largely independent of the number of spheres i.e. there is a steady increase in the probability of undetermined structures at increasing disturbing energy for all number of spheres as shown in figure 4.4. It is similar at high turbulence for all cases, but starts to increasingly split up in two groups (3, 4 and 4, 5) at lower turbulence. There is no clear physical interpretation for the spliting-up in two groups.

The occurance of undetermined structures increase with disturbing energy (kT). Increased disturbing energy leads to higher energy and chaotic motion of the particles which make them move rapidly at random and not connect. At high turbulence there are almost only individual spheres present.

As expected, the ring- and line-configuration tendencies increase with decreasing turbulence and number of spheres. Four spheres represents a transition between ring- and line-formation, energy as well as occurence are essentially identical for

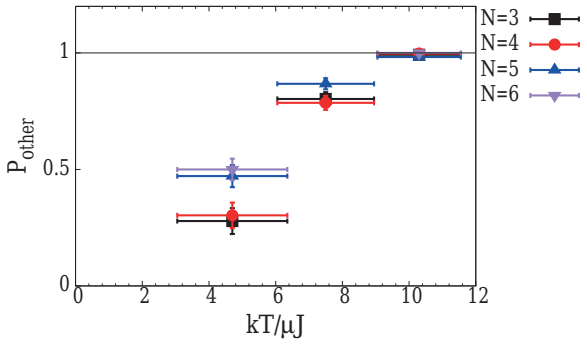

FIGURE 4.4 – *The occurance of "other" i.e. not rings nore lines, as a function of increasing disturbing energy, for 3 to 6 spheres. The occurance of undetermined structures increase with distrubing energy (kT). Also here the disturbing energy was determined via two-sphere connectivity and distance-interaction.*

both cases. The undetermined structures (“none” or “other”) increase with turbulence. Self-assembly of three spheres result in predominantely lines whereas 4, 5 and 6 spheres result essentially in ring formation. The occurence of lines tend to decrease rather than increase with turbulence.

4.5 Discussion

As predicted by theory, self-assembly of three spheres predominantely results in lines whereas five and six spheres result essentially in ring formation. Four spheres represents a transition between ring- and line-formation.

Since the “other” states necessarily have higher energy, the occurance of “other” states increases with turbulence. The chance of occurence seems to be independent of the number of spheres. We were not able to give a theoretical expression for the chance of occurence of “other” states, since we would have to calculate the energy of all possible “other” structures, which are simply too numerous.

Breaking up into “other” structures often occurs from the “line” state. In a line there are dangling sphere at each end. They can move freely in a snakelike fashion and the rotation of the spheres can make them shear-off from the line at high turbulence.

At maximum turbulence there are almost only individual spheres. This highest energy state resembles a gaseous or liquid state. At the highest level of disturbing energy kT the occurence of “other” (figure 4.4) is so high that the interpretation in terms of “rings” and “lines” (figure 4.3) is not meaningful.

The data in figure 4.3 is scattered and deviates from the theoretical model which makes the interpretation very difficult. For both “lines” and “other” an increase in

turbulence seems to reduce scattering in the data to some extent (“lines”) or to a greater extent (“other”). We do not fully understand why this is the case.

We suggest subjectivity when it comes to interpreting the images of the multiple sphere structures plays a role. In some images, even though evaluated from two horizontal views of the same structure, it might be hard to distinguish between a “ring”, “line” or “other” for the observer.

This subjectivity of image interpretation can possibly be solved by letting a larger number of people evaluate the same data set. Here we only had one person per dataset which may not be sufficient. There were two horizontal views of the same event. A third camera providing a top-view would add a third view and enhance the accuracy of structural interpretation. Increasing the time of each experiment would also lead to a higher number of images i.e. more data to evaluate and consequently a higher degree of accuracy.

4.6 Conclusions

We studied the structure formation of centimeter sized magnetic polymer spheres in a macroscopic self-assembly reactor in an upward directed turbulent water flow, at three levels of turbulence. The observed structures could be categorized as “chains”, “rings” and “others”, where “others” included bend chains, single spheres, short chains or rings and combinations thereof. In short, everything that is not either a ring or a chain consisting of the number of spheres used in each individual experiment.

Three spheres mostly form a line, which is in agreement with the theoretical estimate that the energy of a three-sphere line is lower than of a three-sphere ring structure. For four spheres, the two energy states are almost equal and for larger systems the ring structure clearly is the minimum energy state. Indeed, our observation shows that the occurance of rings dominates for systems of four spheres and more, also at high turbulence.

Even though the general behaviour of the system is in agreement with thermodynamic theory, the observed occurences of states deviate considerably from the theoretical values. The measured data scatter greatly and the chance of finding a line amongst the connected structures is much higher than what theory predicts.

The occurence of rings and chains decreases with increasing turbulence, leading to a multitude of “other” structures. The chance of finding these “other” structures does not scatter to the same degree as with the chance of finding a line with respect to rings. At maximum turbulence, predominantly single spheres are present.

4.7 Outlook

The insights gained in this initial study are the first steps towards macroscopic self-assembly design, for instance of the development of novel materials and microfabrication. Macroscopic self-assembly of spherical magnetic particles may be an ideal model system to mimic and understand phase behaviour, structure

formation and energetic landscape paths in molecular or microscopic systems. The study show clearly that multiple macroscopic magnetic spheres seek to form the minimum energy structure, just as is the case at the microscopic scale. The individual spheres present at high disturbing energy resembles a gaseous or liquid state. This macroscopic system lends itselve for the study of phase transitions. In melting or evaporation ordered structures, a solid or a liquid, disintegrate as temperature increase and the individual molecules or atoms move chaotically and rapidly, analogously represented by increase in kT and chaotic motions of the single spheres. Equally, quenching and rapid cooling can be represented by a rapid decrease in turbulence (kT).

Chapter 5

Macroscopic self-assembly of a spherical virus analog

Abstract

We investigated the analogous self-assembly of a spherical virus in a macroscopic self-assembly reactor. The experiments were recorded via three cameras, mounted horizontally and vertically to the self-assembly reactor. The self-assembly process mimics the self-assembly of spherical viruses with dodecahedral geometry. Twelve, centimeter-sized, polymeric magnetic pentagons self-assembled in the energy landscape provided by turbulent flow and magnetic interaction. Several primary (dimers, trimers, tetramers) and secondary structures were formed. The degree of turbulence influence the structure formation of both types; significantly less secondary structures were formed at high turbulence and complexity of the primary structures decreased. For the first time, we could directly observe the different steps in a macroscopic self-assembly process; a dimer structural correction process and the stepwhise process of trimer structure formation.

The work in this chapter is a team effort. The initial design and realisation of the reactor was done Remco Sanders and Léon Woldering. I modified the reactor by implementing novel light illumination and a conical insert in order to create a gradient in the flow. Tijmen Hageman mounted and programmed the three-camera imaging system. I designed and realized the particles and executed and analyzed the experiments.

5.1 Introduction

Self-assembly is an ubiquitous phenomena that occurs in nature as well as in technology. Self-assembled structures exist in abundance in biology. The proteins on the surface of bacteria (Whitelam, 2010), the filaments that constitutes the cytoskeleton of a cell (Yang et al., 2010) or the capsid (outer proteinaceous envelope) of viruses (Mateu, 2013) are all examples of self-assembly in biology.

Virus family	Type specie	Pathology	Diameter
Circoviridae	Porcine circovirus	PMWS	17 nm
Parvoviridae	Parvovirus B19	Erythema infectiosum, fifth disease	23-29 nm
Anelloviridae	Torque Teno Virus	hepatitis	30-32 nm
Geminiviridae	Maize streak virus	Maize streak disease	22 nm
Nanoviridae	Subterranean clover stunt virus	plant death	17 nm
Microviridae	Enthero-bacteria phage phiX174	Lysis of enthero-bacteria	30 nm
Chrysoviridae	Penicillium chrysogenum virus	fungicidal	35-40 nm
Hepeviridae	Orthohepe-virus A	hepatitis	27-34 nm
Barnaviridae	Mushroom bacilliform virus	La France disease	50 nm
Ourmiavirus	Ourmia melon virus	plant diseases	18 nm

Table 5.1 – *Virus families and type species of dodecahedral viruses. Pathology of type viruses and their size. PMWS stands for Post-weaning multisystemic wasting syndrome, a mortal disease in young pigs.*

About half of all known viruses, and most viruses that infect animals and humans, are spherical (Katen and Zlotnick, 2009; Mateu, 2013; Zlotnick, 2005).

The simplest spherical virus consist of twelve pentagonal protein subunits (or "monomers") forming a dodecahedron (Caspar D.L., 1962). A dodecahedron is any polyhedron with twelve flat faces. The best-known dodecahedron is the regular dodecahedron, which consist of twelve regular pentagonal faces with angles of equal size. Upon infection proteins form pentagon shaped clusters that self-assemble into novel viral dodecahedral capsids in the cell. Dodecahedral viruses are the smallest viruses known, ranging from 17 to 50 nm diameter (Dimitrov, 2004). Table 5.1 display an overview of dodecahedral viruses. When a virus infects its host organism (human, animal etc.) it uses the cell genetical machinery in order to reproduce and produce more viruses which are then released from the cell. Self-assembly of pentagonal protein clusters is a part of the reproduction and has not been investigated to any greater extent. A thorough understanding of viral self-assembly is important for several possible applications of spherical viral capsids. Novel concepts for antiviral therapies which may include prevention of the self-assembly of viral capsids or the de-assembly of already fully assembled capsids require knowledge about the underlying self-assembly process (Endres et al., 2005; de la Escosura et al., 2009; Kostiainen et al., 2010).

Macroscopic self-assembly has been used as an analogon in order to study the biological viral self-assembly. Olson (2015); Olson et al. (2007) and Tibbits and Tomas (2013) self-assembled twelve magnetic polymeric pentagons into a dodecahedron, representing a spherical virus, by mechanical shaking in a glass jar. The glass serves as a template for the self-assembly which is not representative for

the situation inside the cell where the actual self-assembly takes place. The energy input was not quantified in their study since the shaking was done randomly by hand. Instead of shaking we use turbulent water flow in a custom-made macroscopic self-assembly reactor including a conical, transparent insert. It creates a flow velocity and turbulence gradient in the water flow. The objective of our study is to identify which geometrical structures twelve magnetic pentagons, representing pentagonal subunit protein clusters, form at various degrees of turbulent flow. By comparison of video recordings taken simultaneously horizontally and vertically we can identify structures and processes between the pentagonal platelets. To the best of our knowledge, the dynamics of the 3D-self-assembly process at the macroscale has not been visualized before. Complex hollow geometrical structures (such as a dodecahedron) have not been self-assembled under controlled conditions before, i.e. at different levels of disturbing energy. There are several reasons to study analog dodecahedral viruses via macroscopic self-assembly investigations. Pathogenic viruses that cause disease to humans, plants, fungi, bacteria and animals are often dodecahedral. The size of dodecahedral viruses is very small which makes it hard to observe at the microscopic scale but simple at the macroscopic. Since time constants scale favorable when scaling up, the smallest representative virus geometry lends itself perfectly for analogous macroscopic studies. Self-assembly processes at the microscale takes presumably around only a few nanoseconds. Up-scaling by using a physical simulator (centimeter-sized particles and a macroscopic self-assembly reactor) of microscopic self-assembly events makes the processes and underlying dynamics visible and possible to investigate.

If we insert magnets into each edge of macroscopic plastic pentagonal plates we can influence connections between them by altering the magnetic polarities. The pentagon design used in this study is shown to the right in figure 5.1. The geometry-net show two white and ten white/grey pentagons. The magnetic polarity of the outward facing circular part of the magnets shown to right in figure 5.2 correspond to the white and white/grey sections (north or south poles) in the geometry-net. Two of the twelve pentagons have identical polarity at each edge (white), and ten pentagons have altering polarity (white/grey) so that white and grey edges connect to each other. Apart from the already connected pentagons, dotted lines indicate how the pentagons connect leading to a dodecahedron. This design has proved to function in the study by (Olson, 2015), as can be seen in figure 5.3 and the accompanying video.

The number of possible intermediate structures for a given set of particles can be considerable high. The total number of intermediates grows exponentially with capside size and self-assembly would require a very long time if the self-assembly pathway takes place via numerous intermediate structures. In a sail-shaped reaction landscape defined by the number of subunits in each intermediate structure, the predicted prevalence of each specie is displayed in figure 5.4.

Only a small fraction of intermediates needs to be considered when studying capsid self-assembly (Endres et al., 2005). Energy landscape approaches have shown that proteins will follow energetically preferred paths leading to smaller and faster search of conformational space (Dinner et al., 2000). The pentagonal

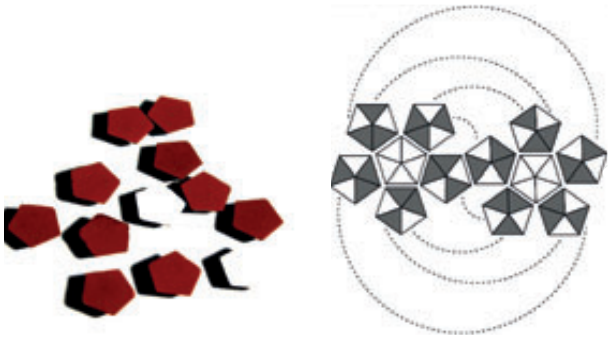

Figure 5.1 – *Twelve single plastic pentagonal monomers are shown to the left. The red pentagons correspond to pentagons with white/dark-grey triangles, and the white pentagons correspond to the white-triangle pentagons in the schematic drawing of the dodecahedral geometry-net to the right. The magnetic polarity of the outward facing part of the magnets inserted into each of the pentagon edges (shown to the right in figure 5.2) are indicated by the dark-grey or white triangles (north and/or south poles). Two of the twelve pentagons have identical polarity at each edge (white-triangle pentagons), and ten pentagons have altering polarity (white/dark-grey). Dotted lines of the geometry-net to the right indicate how the pentagons connect leading to a dodecahedron. The geometry-net was taken from (Tibbits and Tomas, 2013).*

structures with the highest number of connections of each individual pentagonal plate are the most favourable in dodecahedron self-assembly and are energetically preferred (Endres et al., 2005). A branched or linear structure would be less favourable compared to a more compact with the same number of pentagonal plates.

Some intermediate structures can break out of local energy minima, due to the applied disturbing energy. It competes with bond formation, are those systems are self-assembling systems whereas intermediate structures remaining in a local energy minima are referred to as assembling systems (Ipparthi et al., 2017).

In this chapter, we continue on the work of Olson by studying the self-assembly process of pentagons into a dodecahedron without the presence of a container, so without a template that guides the self-assembly process. The analysis by Enders will be used to catergorize the observed structures.

FIGURE 5.2 – *Complete assembled dodecahedral macroscopic virus (left). Virus and two deassembled pentagonal plates with two visible cylindrical magnets at each edge (right).*

FIGURE 5.3 – *Self-assembly of a model of a spherical virus in a bottle as demonstrated by Olson (2015). The video of the experiment is available on youtube (Click on or scan QRcode).*

5.2 Methods

5.2.1 Self-assembly Reactor

We use a custom-built macroscopic self-assembly reactor described in chapter 2 and 3. The self-assembly reactor is schematically displayed in figure 5.5 where the red and white pentagons represent the particles used in this study.

In contrast to the experiments in the previous chapters, we use a conical instead of a cylindrical insert. In the cylindrical insert, the flow velocity is constant, so there is in principle no stable position for the objects "falling" in the flow. As a result the objects are often caught at the top or bottom net. The conical insert results in a flow pattern in which the velocity decreases from bottom to top. The flow velocity is inversely proporional to the projected cone surface area, which is approximately a factor four between entry and exit. As a result, the objects have a

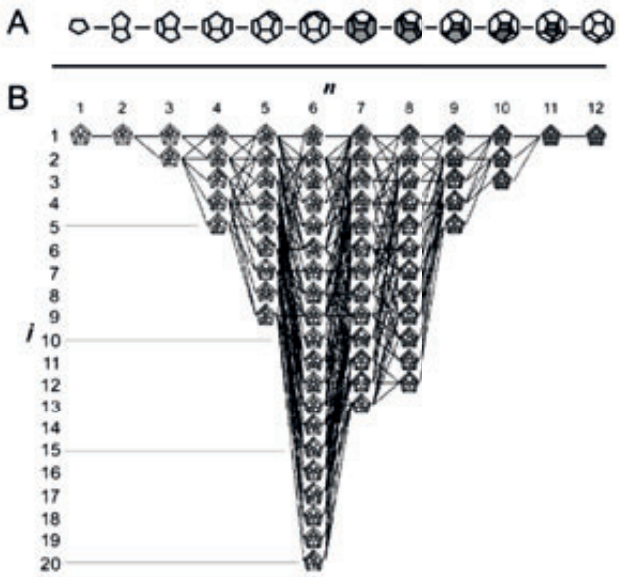

FIGURE 5.4 – *Paths and intermediate structures for self-assembly of a dodecahedron. The horizontal axis shows the number of assembled pentagons n and the the vertical axis j denotes the type of structure according to an enumeration algorithm (Endres et al., 2005). One path (A) of an array of the diagram (B) which shows paths (i.e. dynamical processes) and intermediate structures of the self-assembly of a dodecahedron composed of twelve pentagons. The intermediates are generated by algorithms of step-wise connection between twelve pentagons in the self-assembly system. A minimal assembly model was used which incorporates the most stable intermediates (B). The intermediate structures are build up by adding one pentagon at a time to each site and subsequently deleting duplicates. There are 73 stable intermediates and 263 line segments (reaction paths) between the intermediate structures). The twelve most stable intermediates (A) are those with the largest number of inter-pentagon contacts (Endres et al., 2005). This means that for a structure consisting of say three pentagons, the less branching structure is the most stable one, since it has a lower number of inter-subunit contacts. One can compare the third structure from the left shown in (A) with a linear structure consisting of three pentagons in a row. For the row-like structure the number of edge connections for each pentagon is 1-2-1 and for the more compact structure 2-2-2.*

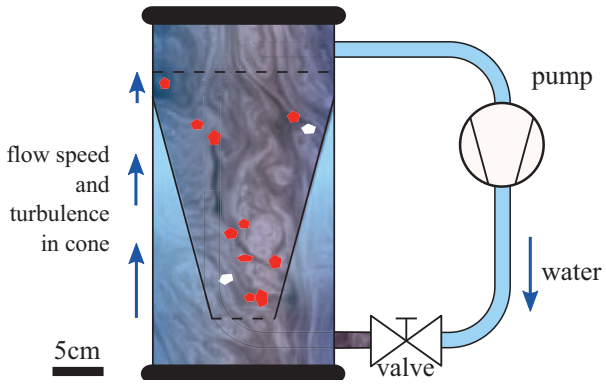

FIGURE 5.5 – *The principal operating mode of the self-assembly reactor with conical transparent cylinder. The height of the cone is* 60 cm *and the upper and lower diameter is* 19 *and* 8.5 cm *respectively. The inflow of water is regulated via four inlet valves at the bottom of the reactor. The cone creates a flow and turbulence gradient which is about four times higher at the cone inlet than at its outlet. The particles (red and white flat magnetic plastic pentagons) drop in the water flow at settle at the point where the upward water flow matches their terminal drop velocity. By adjusting the four inlet valves, the turbulence in the water can be adjusted.*

stable position where the flow matches the terminal drop velocity of the object.

The gradient in flow velocity also causes a gradient in turbulence. This of great advantage for the self-assembly process since the weight and projected area of the self-assembled structure change over time as particles de- or attach to an existing structure or start to form a structure by addition of monomers. The gradient can make the structure dynamically grow at the "right" position in the cylinder i.e. the position with "correct" velocity which is identical to the terminal velocity of the particle or structure. This makes particles move up- and downwards and tilt in the flow, or de- or attach one or several monomers to a structure and so present a smaller/bigger surface area to the flow. The weight and the drag coefficient (the projected area increases) of the structure change as the number of pentagonal monomers added throughout the self-assembly process increase and thereby the terminal velocity of the object change over time. The self-assembled object moves within the cone to a position where the flow velocity is similar or equal to the "new" terminal velocity and the self- assembly process continues.

In addition to the two horizontally mounted cameras used in the previous chapters, a third camera was vertically inserted through the top lid. This allows us to evaluate the formation of structures using three views.

We can increase the turbulence by introducing asymmetry in the flow, as

described in chapter 3. Figure 3.9 on page 38 shows the relation between flow asymmetry and disturbing energy for the cylindrical insert. The turbulence increases with increasing flow asymmetry. Since the conical insert has a turbulence gradient, we will only mention the asymmetry in this chapter as a qualitative measure for turbulence. Figure 3.4 in chapter 3 shows the relation between valve setting and flow speed through the reactor.

5.2.2 Pentagonal Particles & Dodecahedron

Twelve polymeric (ABS) flat pentagons were 3D printed and two cylindrical 1 mm × 1 mm NdFeB magnets (Supermagnete, grade N42, Webcraft GmbG, Gottmadingen, Germany) were inserted into holes in each edge and glued (figure 5.1 left and figure 5.2 right). The longitudinal, axis of the cylindrical magnet points towards the center of the pentagon so that one end of the magnet (circular face) points outwards visible in the two pentagons to the right in figure 5.2. The chosen polarities of the outwards pointing magnets are described in figure 5.1. The side length of the pentagon platelet was 1 cm and its thickness 5.7 mm. The pentagons are "regular pentagons" i.e. the interior angles between two edges are identical and equal to 108°.

5.2.3 Reconstruction and structural evaluation of recorded videos

The self-assembly was evaluated by observing how structures form in the three videos recorded for each experiment. We used three synchronized cameras (Allied Vision Mako G-131), one positioned in a tube with transparent lid, extending into the water flow at the top of the reactor. Two cameras positioned horizontally, perpendicular to each other, recording two side views. The three cameras were synchronized so that a comparison was possible. The reconstruction of videos and further details are described in chapter 2and 3.

The evaluation and identification of structures was carried out by observation and comparison of the three recorded views. Also the motion of platelets and structures as well as their connection or disconnection could be evaluated and reconstructed by comparing the images of the three views. The three images was used to unambigously identify a structure or process and they are complementary.

5.3 Results

5.3.1 Structure formation as a function of turbulence

As the pentagons self-assemble at various degrees of turbulence in the self-assembly reactor, the structures formed during each experiment can be classified according to the interaction responsible for their formation. *Primary* (stronger) and *secondary* (weaker) interactions cause formation of primary and secondary structures. The direct attachment between magnets mounted into the five edges of each pentagon (visible in figure 5.2) is referred to as primary interaction, whereas attachment

between the large flat surfaces of at least two pentagons ("stacking") is called secondary interaction. Structures between the edge and the large surface or other mixed primary/secondary interactions are *intermediates* between the primary and secondary structures. *Conglomerates* may be a mixture of all three. The number of pentagons in a structure is expressed as monomer, dimer, trimer, tetramer corresponding to 1, 2, 3 and 4 pentagons. Structures higher than dimer can be "linear" or "triangular" i.e. compact.

At minimum turbulence (no flow asymmetry) stable primary structures such as a trimer form, see figure 5.6. Secondary structures along with large conglomerates and secondary structure including face-to-edge attachment form and seem to be stable and do not rearrange within the given time of experiment. The turbulence seems to be too low, and time too short for any considerable rearrangement of primary structures, or detachment and rearrangement of secondary structures and conglomerates to occur. In general, there is a clear prevalence of secondary over primary structures with decreasing turbulence.

At moderate flow asymmetry (0.07) two trimers with/without three secondary attached monomers were observed (Figure 5.7). A stacking of white and red monomers as well as a secondary attachment to a dimer was seen but they were rather short-lived. There was not enough time to observe a possible release of the monomer attached to the trimer and subsequent progression of self-assembly.

When increasing turbulence further to 0.26 flow asymmetry, a tetramer with a secondary monomer attached can be seen (Figure 5.8). At this medium level turbulence, this is the most complex geometry found in this study, however, the degree of turbulence seem to be too low and/or time too short to remove the attached monomer which may prevent primary attachment of further monomers i.e. continued self-assembly. Also conglomerates and secondary structures are visible at this level of turbulence.

At 0.75 flow asymmetry, next to two dimers, also a trimer is formed (Figure 5.9). No secondary structures can be observed but several individual monomers which indicates that the turbulence can break up the unwanted secondary structures (higher degree of turbulence make losely attached single monomers detach). This can be compared to the monomers attached to the tri- and tetramers at 0.07 and 0.26 flow asymmetry, which could not detach at that low degree of turbulence.

At maximum turbulence only dimers and single monomers were visible (Figure 5.10). The high disturbing energy provided by the turbulence prevents not only secondary structures from forming but also the formation of more complex primary structures than dimers.

Comparing the top and bottom parts of figure 5.10, the umbrella-like structures in the side views could not have been clearly identified as di-, tri- or tetramers without the top-views. The side views appear to be very similar. The dimers in the side-views can be mistaken for tri- or tetramers and vice versa, unless they can be identified by a third topview which was done unambigously. This clearly demonstrates that the three views are beneficial and complementary in identification of structures and processes.

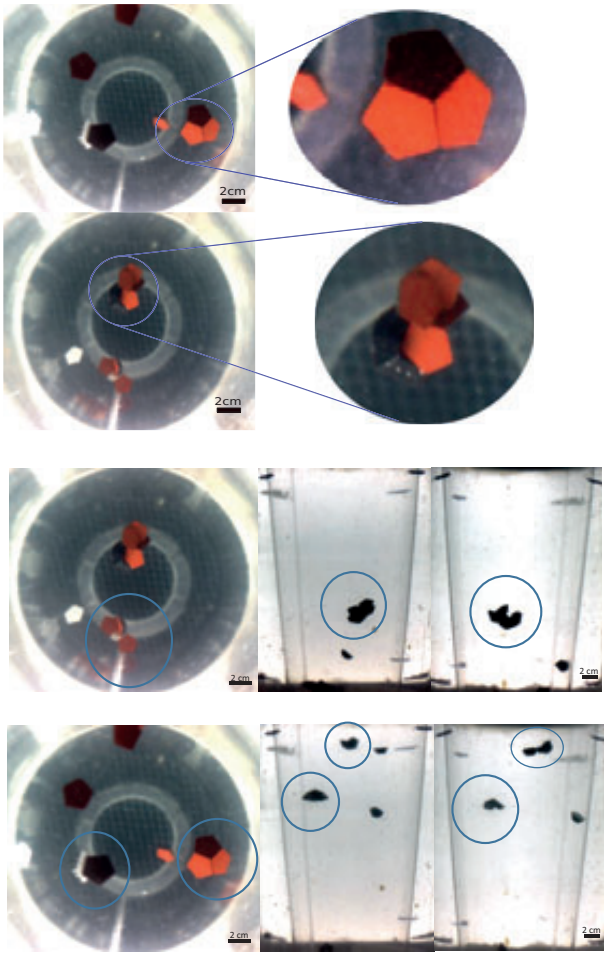

FIGURE 5.6 – *Top view (above) and side view (below) of self-assembly of twelve magnetic pentagons in the cone at lowest turbulence. Structures are highlighted by magnified excerpts. Trimer and conglomerates (blue circles) were observed.*

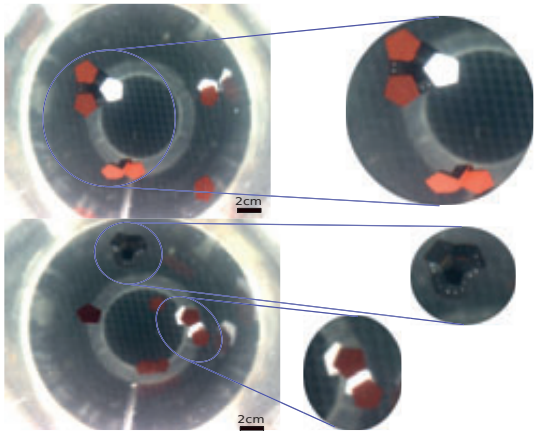

FIGURE 5.7 – *At low flow asymmetry (*0.07*) trimers can be observed, to which sometimes monomers attach.*

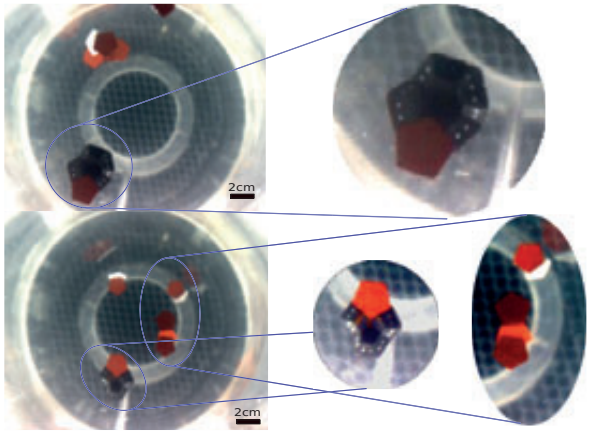

FIGURE 5.8 – *At medium flow asymmetry (*0.26*) the most complex structure in this study (a tetramer) was identified.*

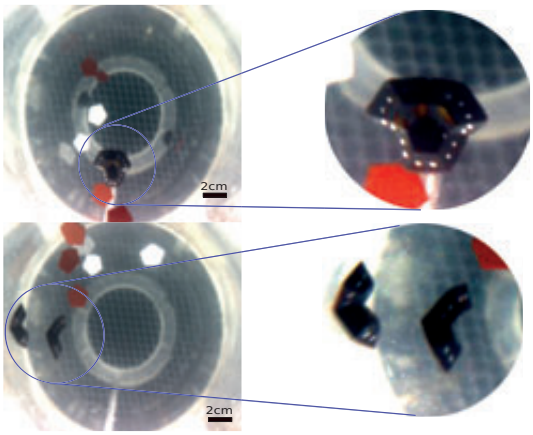

FIGURE 5.9 – *At high asymmetry (0.75) dimers and trimes are formed, but no secondary structures could be observed.*

5.3.2 Structure formation - Self-assembly dynamics

By using two horizontal and one vertical camera, the recordings of the self-assembly experiments allow for distinction of structures as mentioned above but also for analysis of the underlying process that leads to their formation. We observed a rearrangement of a dimer as well as the formation of a trimer.

Figure 5.11 shows how a dimer reassembles from a straight planar connection into the desired tilted structure at high turbulence (0.75 flow asymmetry). The two monomers do not disconnect, at least not for a long period of time, but twist with respect to eachother and remain connected. It was observed that they re-assemble as they sink or rise in the cone, which suggests that the different degree of turbulence at different heights in the cone influence the connection in various ways.

The edges of each pentagon were designed so that pentahedral connections lead to a hollow dodecahedral structure. Each edge of the pentagonal platelets is skewed to that degree that two connected pentagons are tilted and will have a dihedral angle of 116.56° when connected correctly. The dimer will appear straight if the same edges connect after one of the pentagons has been turned upside down. Since there was no clear disconnection between the two monomers this can be seen as a *correction process* which is a natural part of self-assembly. There is also an additional dimer present in the cone which does not deassemble even at this high degree of turbulent flow. This indicates that the degree of turbulence is suitable for a reassembly process to take place but not high enough for total separation of two connected pentagons. This example shows the importance of tunability of the disturbing energy (in this case: turbulence) for succesful self-assembly. It seems that the more precise one can tune the turbulence i.e. the more precisely the individual self-assembly processes can be influenced, controlled, observed and

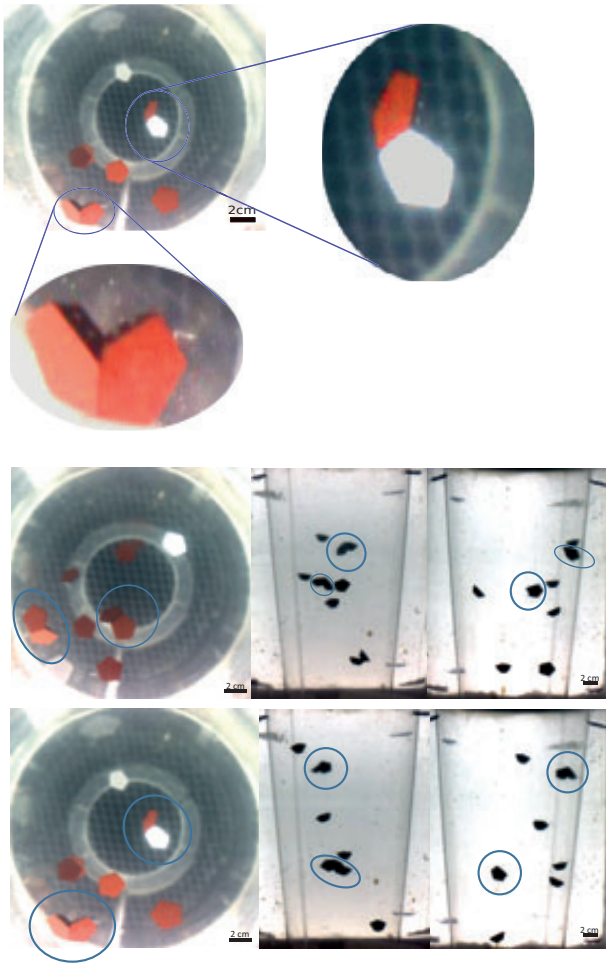

FIGURE 5.10 – *Observation at maximum turbulence. The blue circles indicate structures; a red and a white monomer as well as two red monomers form two dimers. The top and side views show that they complementarily contribrute to the identification of self-assembled structures. The umbrella-like structures in the side views could have easily been mistaken for tri- or tetramers*

studied. If the disturbing energy can only be altered in big steps and no fine tuning is possible, some self-assembly processes may never occure since the disturbing energy might be either too low or too high for a particular process to take place.

The formation of a tetramer is shown in figure 5.12 at maximum turbulence. A direct stepwhise self-assembly starting form single subunits was not seen but rather a connection between monomer and dimer and retention of the trimer at different heights in the cone i.e. at various degree of flow velocity and turbulence. The trimer withstands the high flow velocitites and turbulence even at the bottom of the cone which indicates its high stability. There are as good as no secondary structures present due to the high degree of turbulence.

In figure 5.13 the blue circles indicate the trimer as well as monomers. The trimer formation supports the idea of single subsequent monomer addition since dimers are formed prior to trimers.

5.4 Discussion

Investigations of the behaviour of single spheres and multiple magnetic polymeric spheres in a turbulent flow field has been described in the first three chapters. One cylindrical magnet is inserted into each sphere and consequently there are two ways for an approaching sphere to connect to a second sphere (to the north or south pole). In the case of pentagon self-assembly the situation is much more complex.

If we consider the ten identical pentagons in figure 5.1 there are two or three edges to which an approaching identical pentagon can connect. Five of the edges of one of the identical top or bottom pentagons (white in figure 5.1 and 5.2) can connect to one of the three edges of the ten identical pentagons. Once connected there is only limited rotational freedom.

The several shell-like intermediate structures and the final hollow dodecahedron structure behave differently in an upward directed turbulent waterflow compared to multiple connected single magnetic spheres. When a ring or chain of magnetic spheres move in the flow the individual parts can rotate to some degree without breaking the structure. There is a small freedom of rotation for each individual sphere. The dodecahedron and its intermediate structures are rather rigid and the subunits, once connected cannot rotate (with the exception of dimer-rearrangement described earlier).

The projected area increases with each added subunit so the drag force will increase accordingly and the structure moves upwards where the upward flow velocity and turbulence is lower. The structure will then "fall" down to regions of higher turbulence. Single pentagons can add to the structure or the already assembled pentagons rearrange to some extent. The cone seemingly "circulates" structures and single subunits which accounts for that the cone design rather supports the single subunit-addition model according to Endres et al. (2005); preferably single subunits rather than multimers are added to an existing structure during growth. There are several dimers observed in the cone which might contradict a strict single

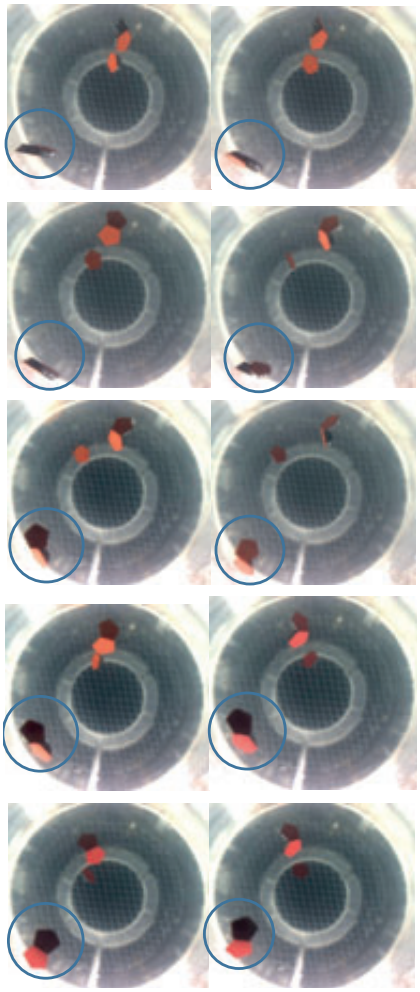

FIGURE 5.11 – *A dimer reassembles from a straight planar connection into the desired tilted structure at high turbulence* (0.75 *flow asymmetry). Starting form the top left image, continuing to the right and then to the left image below and so on, one can follow the process of dimer re-assembly over time. The blue circles indicate the dimer in question. The monomers do not disconnect during the reassembly process but twist and rearrange into the desired tilted structure.*

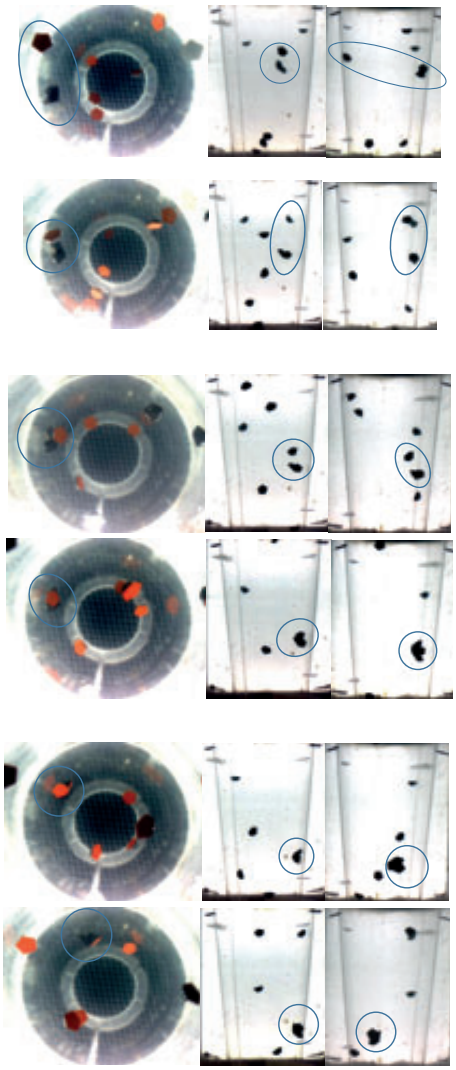

FIGURE 5.12 – *Top and side views of trimer formation at maximum turbulence. Starting at the image-triplets at the top, following images show how self-assembly proceeds over time. A monomer connects to a dimer and forms a trimer. The trimer withstands the high flow velocitites and turbulence at the bottom of the cone which indicates its stability. Due to the high turbulence there were no secondary structures observed.*

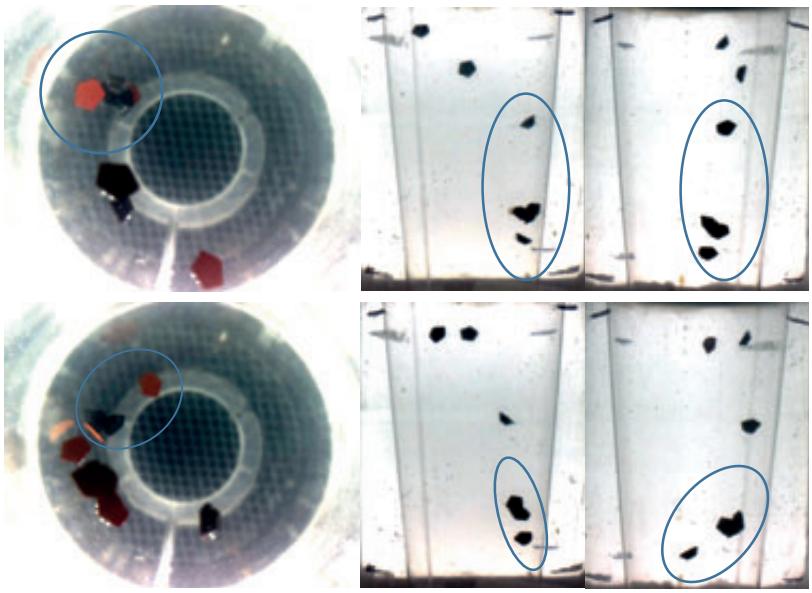

FIGURE 5.13 – *Trimers as well as monomers can be observed.*

subunit-addition model. However, direct addition of multimers to an existing structure was never observed whereas monomer addition was.

Eventhough simple primary structures such as the dimer can rearrange at high turbulence there were no primary structures of higher complexity observed. This indicates that there might not be one distinct level of disturbing energy necessary for succesful self-assembly but rather a range or a regime of changing disturbing energy.

There are 73 possible intermediate structures in the complete configuration space (Endres et al., 2005). In this study we observed four (monomer, dimer, trimer and tetramer), which means that only a little more than 5 % of the possible intermediate structures were realized. We should however realize that out of the 73 structures, there are ten intermediate states with the largest number of pentagon contacts.

5.5 Conclusions

In this study we evaluated three-dimensional self-assembly of twelve, centimeter-sized pentagonal polymer platelets with embedded magnets in an upward directed turbulent water flow. The platelets represent pentagonal protein clusters that self-assemble into a dodecahedral virus capsid inside an infected cell. The self-assembly experiments were carried out in a macroscopic self-assembly reactor.

A conical insert was introduced to introduce a gradient in flow velocity. As a result, the platelets remained in the field of view, balancing around the point where the upward flow velocity matches the terminal drop velocity.

The conical insert also caused a gradient in the amount of turbulence in the system, decreasing from bottom to top of the cone. Structures of two or more pentagon platelets were preferably observed in the upper two third of the cone, suggesting that turbulence is too high in the lower part of the cone for pentagons to attach or structures to stay intact.

The degree of turbulence was altered systematically by adjusting the symmetry at which the flow was introduced into the system. We observed that the self-assembly of twelve platelets at different degrees of turbulence included primary structures (dimers, trimers, tetramers), secondary structures (single or multiple stackings) and conglomerates (mixed structures).

Primary structures are formed via direct connection between the magnets and secondary structures via the weaker magnetic interactions where the magnets are shielded by the surrounding polymer (the larger surfaces of the pentagon). The stability of the primary structures decreased with increasing number of plates (from tetramer to trimer to dimer). Linear tetramers or trimers were not observed. This suggests that the stability increase as the number of connections per pentagon increases (as predicted by Endres et al. (2005)).

The secondary structures could be largely eliminated by increasing the turbulence, however, at the cost of primary structure formation. At medium turbulence a tetramer was observed which was the most complex structure in this study.

We did not observe kinetic trapping (the self-assembly process comes to an halt due to formation of stable local minima energy structures) possibly due to the limited duration of experiment. We did observe correction processes of a wrongly connected straight dimer where individual pentagons rearranged into the desired tilted structure. The presence of spontaneous correction represents a similarity between macroscopic and microscopic self-assembly supporting the idea of analogy between the macro and microscale self-assembly.

To the best of our knowledge this was the first time the dynamical process of self-assembly a dodecahedral structure was visualized under controlled conditions. Even though self-assembly of an entire dodecahedron was not achieved, these preliminary results hold the promise that this approach is suitable to study the self-assembly dynamic process of spherical virusses.

5.6 Future work

Future investigations should include alteration of cone and pentagon design in order to utilize the flow and turbulence gradient even further to accomplish and study self-assembly. By altering the dimensions of the cone one can make the flow and turbulence gradient in the cone finer.

Undesired structures may only after a long time de-assemble and subsequently self-assemble into higher primary structures and the final desired geometry. Long

experiments elucidate the influence of time on self-assembly of a dodecahedron and if the structures shown in this study are kinetically trapped or not.

Adding an excess of monomers may lead to faster and/or more complete self-assembly. By using a number of macroscopic pentagonal platelets large enough to self-assemble multiple viruses in parallel, the probability of parallel self-assembly in the cell can be evaluated. The *yield* of the self-assembly process, as defined by the number of complete self-assembled structures with respect to the total number of structures, can be evaluated. A constant monomer influx can identify an equilibrium between structure formation and rate of monomer addition. Parameters such as monomer addition or altered disturbing energy that lead to or away from kinetical trapping can be identified. The probability of parallel self-assembly can be evaluated as well as the time for parallel self-assembly can help answer the question if a large number of pentagons rather hinders of supports the self-assembly process.

Analogous subcomponents of the pentagon i.e. five regular triangles can be studied in future experiments. Polymeric triangular plates with various number of magnets and polarities can help to describe post-self-assembly processes.

Even though simple primary structures such as the dimer can rearrange at high turbulence there were no primary structures of higher complexity observed. This indicates that there might not be one distinct level of disturbing energy necessary for succesful self-assembly but rather a range or a regime of changing disturbing energy. The conical insert provides a gradient of turbulence due to its shape and ideally self-assembly should take place at different heigths in the cone depending on the size and complexity of the structure. One can also vary the turbulence with time by gradually opening and closing the inlet valves. Kinetically trapped structures can be broken up again by increasing the disturbing energy so that the self-assembly can continue. If the kinetically trapped structures are being self-assembled for extended times at different degrees of disturbing energies they might break up and rearrange.

Hierarchial self-assembly can be carried out with dodecahedrons that connect to each other after succesful individual self-assembly forming a super-structure consisting of regularly connected dodecahedrons. The connection between the dodecahedrons may be “turned on” only after each individual dodecahedron has been succesfully self-assembled.

Data from described investigations reveal further insights into viral self-assembly which can be used in the design of experiments with biological viruses. It may contribute to the development of antiviral therapies, (bionano-)materials, encapsulation of drugs, reactive intermediates, nanoparticles or genes (gene therapy).

Chapter 6

Conclusion

Spontaneous organisation of matter into novel materials and microdevices in synthesis, manufacturing or fabrication requires an understanding of the underlying self-assembly mechanisms. It is equally demanding to understand how the molecular building blocks of life such as proteins or DNA self-assemble. Regrettably micro- and nanoscale processes proceed so rapidly that they cannot be observed and evaluated directly. But valuable insights about how to self-assemble matter would be won if we could analogously mimic the smaller scale and slow down the self-assembly process. If we scale up microscopic self-assembly, the process would slow down and be readily observable. Therefore the motivating research question for this thesis was:

> What can we learn about the microscale by studying the macroscopic scale?

Macroscopic self-assembly may serve as an analogous physical simulation of processes on the microscale. We characterized our 'macroscopic self-assembly reactor' via trajectory analysis of a single centimeter-sized sphere. Its average square displacement over time, or the 'diffusion' profile fit to a confined random walk model. The velocities of a single sphere are Maxwell-Boltzmann distributed and together with the random walk it is an analogy to Brownian motion on the microscale. The diffusion coefficient and the most probable velocity do not depend on sphere size with an average value of 20(1) $\mathrm{cm}^2\,\mathrm{s}^{-1}$ and 16.6(2) $\mathrm{cm\,s}^{-1}$ respectively.

Self-assembly dynamics were studied in the simplest system possible consisting of two magnetic spheres. Connections and disconnections and the cumulative distribution of the distance between the centers of the two spheres fits to a Maxwell-Boltzmann distribution. The disturbing energy was determined from both kinetic behaviour of a single sphere (kinetic energy) and from the interaction between two spheres (Einstein relation). The disturbing energy determined from a two-sphere interaction is an order of magnitude lower (approximately 6.5 μJ compared to 80 μJ)

than the single sphere experiments. Obviously the disturbing energy cannot be determined solely from single sphere experiments.

The disturbing energy increases with increasing sphere diameter, from 1.7 cm to 2.0 cm. For the single sphere experiment, this increase is more prominent (43 % via diffusion analysis (Einstein relation), 61 % via velocity analysis (kinetic energy)) than for the two-sphere experiment (17 %). This discrepancy might be due to the fact that only a part of the energy spectra of the turbulent flow is transferred to the sphere and that this part is dependent on the sphere diameter.

Naturally, in microscopic environments a temperature increase causes particles to move more rapidly and randomly conducting Brownian motion. At the macroscale we use turbulent flow as a temperature analog in order to make centimeter-sized macroscopic particles move rapidly, similar to a temperature increase at the microscale. Turbulence is created via four inlet valves which in addition are opened asymmetrically so that higher scale flow can be established. Three of four bottom inlet valves were closed step-wise to the same degree, while the fourth was kept open and the inlet flow becomes more asymmetric and turbulence increases which results in increasing velocity, diffusion coefficient and disturbing energy. The disturbing energy (equivalent to the thermal energy) can be increased by a factor of eight when determined via single sphere, and a factor of six when determined via two-sphere, interactions. There is a directional dependency for the velocity, diffusion and disturbing energy. The horizontal components are similar but the vertical component deviates to a greater extend with increasing turbulence and asymmetry.

Just as temperature, turbulence affects particle related parameters. Increasing turbulence results in a six fold increase in disturbing energy, a three fold increase in the most probable particle velocity and a sixfold increase in diffusion. The absolute values are a magnitude lower for the disturbing energy when evaluated from the two-sphere experiments than from single sphere experiments. The vertical flow velocity component is increasingly lower as turbulence decreases whereas the two horizontal components remain essentially equal.

The thermodynamical conclusions achieved in this investigation have consequences for the study of microscale self-assembly. Our results indicate that macroscale self-assembly can be used as an analog system in order to study microscale self-assembly since we can change turbulence and the disturbing energy in a similar manner as we can change temperature for microscale systems. Processes such as crystallization or quenching are likely to be studied analogously at the macroscopic scale provided that an ideal directional homogeneous turbulent flow field can be decreased rapidly in order to achieve quenching. One can take advantage of the possibility of inhomogeneous design which may open up novel venues of investigation. An inhomogeneous turbulent flow field may be interpreted as a temperature gradient. A precisely designed three-dimensional inhomogeneous turbulent flow field may be used for macroscopic mimicking of several processes in for example microscopic mammal or bacterial cells, organelles or organs which for the moment resembles solely a future vision, but simultaneously a most probable achievable target.

We showed how turbulence can be used as a "macroscopic temperature" and its influence on separation of two spheres from which we can determine the disturbing energy. The minimum number of particles needed for self-assembly is two, but in natural systems the number of particles is much higher. Structures of dipolar particles exceeding two members can be chains and rings of magnetic spheres. We decided to study multiple magnetic spheres, more precisely, which structures 3-6 magnetic spheres form at increasing level of turbulence. This would mimic how a microscopic multiple particle system behaves at increasing or decreasing temperature. The occurance of the structures "chains", "rings" and "others", was determined manually and the probability of occurance related to the existing microscopic theory.

Four spheres was a clear transition point above which rings are more probable than chains which is expected according to theory. Three spheres form exclusively lines. The observed occurences of states deviate considerably from the theoretical values even though our system is in agreement with thermodynamic theory. The measured data scatters greatly and the chance of finding a line amongst the connected structures is much higher than what theory predicts.

The occurance of "others" increase with disturbing energy as well as the decreasing number of spheres. At maximum turbulence there are almost exclusively single spheres present which suggests that a macroscopic multiple sphere system would lend itself perfectly for the study of quenching, heating and possibly glass formation. Our systems tries to realize minimum energy states which resembles the microscopic scale since actually the mimimum energy structures assemble.

Multiple magnetic polymeric spheres represent an important step towards analogous study of real self-assembly systems. In the course of our investigations in macroscopic self-assembly we gained the tentative insight that macroscopic self-assembly can be used in a twofold manner: one can study either a representation of natural occuring phenomena (crystallisation, glass formation) or test hypotheses in physics or existing physical laws, theories or theorems (eqipartitioning theorem).

We moved from multiple spheres to a much higher level of complexity by studying the self-assembly of a deodecahodron. A dodecahedron consists of twelve pentagonal plates and its hollow geometry represents a higher degree of complexity compared to multiple spheres. It is an example of both cases of macroscopic self-assembly. On the one hand it represents a natural occuring phenomena since spherical viruses self-assembly via twelve pentagonal protein plates during virus replication. On the other hand it represents a physical study since self-assembly of hollow structures in a turbulent flow is largely underresearched.

In addition to turbulence-regulation via four inlets, a conical insert in the self-assembly reactor was used in order to create a flow and turbulence gradient in the upward directed water flow. In this way it was possible to present a gradient disturbing energy to the self-assembling platelets and possibly support the more complex self-assembly of a hollow structure.

At different degrees of turbulent flow primary structures (dimers, trimers, tetramers), secondary structures (single or multiple stackings) and conglomerates (mixed structures) were observed. Primary structures are formed via direct con-

nection between the magnets and secondary structures via the weaker magnetic interactions where the magnets are shielded by the surrounding polymer (the larger surfaces of the pentagon). The stability of the primary structures decreased in the following order; tetramer, trimer, dimer. Linear tetramers or trimers were not observed. Stability seem to increase as the number of connections per pentagon increase just as predicted by theory. High turbulence eliminated secondary structures but only simple primary structures were observed at the same degree of turbulence. The most complex structure was a tetramer which was observed at medium turbulence.

The self-assembly of the entire dodecahedron was not achieved. Kinetic trapping where the self-assembly process comes to an halt due to formation of stable local minima energy structures was not observed either. A wrongly connected straight dimer rearranged into the desired tilted structure was observed and it is possibly a rare example of the direct observation of self-assembly dynamics. Spontaneous correction represents a similarity between macroscopic and microscopic self-assembly supporting the idea of analogy between the macro and microscale self-assembly.

Two horizontally and one vertically mounted cameras were used to observe the dynamical process of self-assembly of twelve pentagons into dodecahedral intermediate structures. The dynamical process of macroscopic magnetic self-assembly was for the first time visualized under controlled conditions. The results indicate that the macroscopic self-assembly is a suitable tool for studying natural occuring phenomena such as virus self-assembly. The first steps has succesfully been taken towards self-assembly of a dodecahedron representing a spherical virus.

6.1 Suggestions for future work

Future work may include technical development, continuation of the presented work in this thesis as well as as well as extended investigations into novel fields. The self-assembly reactor design can be altered on order to achieve more accurate experimentation. Cone design can be improved in order to utilize the flow and turbulence gradient to a greater extent. Introduction of turbulence may have other or additional sources other than the simple but well functioning valves used in this study. The number of valves and inlets into the reactor and combinations with ultrasound or other means. The pressure over the valve might be a suitable additional measure for the incoming flow. The assembling energy, i.e. the magnetic attraction may be fine tuned by implementing materials that change their attractive magnetic force with temperature (low Curie point materials). In addition to the size of the magnet and its surrounding material also a slight change in temperature may help to fine tune the assembling energy. Fine tuning of assembling and disturbing energies may broaden the way even further for fruitful investigations.

The thermodynamic similarity with the microscale as illustrated in the two first chapters is essential to investigate further. By applying the springs as probes at different positions of the rector and measure frequency, amplitude etc. as a function

of turbulence would reveal insight into which wavelengths are involved in which part of the self-assembly. For example if there are preferred wavelengths for the separation of two spheres and others for the motion of the spheres and how this relates to sphere size and strength of magnet. The energy spectrum of the provided turbulent flow can then be compared with its counterpart of the microscale thermal energy. Here an experimental description of the equipartitioning theorem may be envisaged. The dipolar magnetic self-assembly of spheres can be carried out further and also with a large number of spheres with different aspect ratios.

Self-assembly of a dodecahedron can be carried out by adding an excess of monomers which may lead to faster and complete self-assembly. A constant monomer influx can identify an equilibrium between structure formation and rate of monomer addition. Parallel self-assembly of more than one dodecahedron may also be of interest and hierarchial self-assembly is an additional option. After several dodecahedrons self-assembled they can via an additional mechanism connect to each other and form a super-structure consisting of regularly connected dodecahedrons. Subcomponents of the pentagonal buildingblocks, five regular triangles, can be studied in future experiments and thereby elucidate the post-self-assembly processes. Data from described investigations should be complemented with experiments of the biological counterpart. Enhanced understanding of the viral self-assembly proccess may contribute to the development of antiviral therapies as well as encapsulating (bionano-)materials.

In the context of scaling, one shoud not forget that the macroscopic scale can also be used to analogously simulate much bigger systems such as the universe, planetary motion or a galaxy. There are several reasons for establishing macroscopic self-assembly as a valid way of experimentation. To study hard and difficult phenomena in various disciplines (almost all thinkable disciplines can be valid) that can be studied in a representative manner. Also physical laws or phenomena that are just as valid on the macroscale can be studied easily such as the equipartition theorem or enthalpy.

The thermodynamic theory on the macroscopic scale has proven to be valid also when microscopic entities was replaced with macroscopic counterparts. Turbulence can be used instead of heat. Multiparticle systems seek the lowest energy state and the first step of mimicing natural occuring phenomena was taken. With this we paved the way for future macroscopic studies of the microscale.

Bibliography

Abelmann L, Tas N, Berenschot E, Elwenspoek M, 2010
"Self-assembled three-dimensional non-volatile memories"
Micromachines **1**, pp. 1–18, doi: 10.3390/mi1010001

Avila K, Moxey D, De Lozar A, Avila M, Barkley D, Hof B, 2011
"The onset of turbulence in pipe flow"
Science **333**, pp. 192–196, doi: 10.1126/science.1203223

Bennewitz R, Crain J N, Kirakosian A, Lin J L, McChesney J L, Petrovykh D Y, Himpsel F J, 2002
"Atomic scale memory at a silicon surface"
Nanotechnol. **13**, pp. 499–502, doi: 10.1088/0957-4484/13/4/312

Boncheva M, Gracias D, Jacobs H, Whitesides G, 2002
"Biomimetic self-assembly of a functional asymmetrical electronic device"
Proceedings of the National Academy of Sciences of the United States of America **99**, pp. 4937–4940, doi: 10.1073/pnas.032667599

Boncheva M, Andreev S A, Mahadevan L, Winkleman A, Reichman D R, Prentiss M G, Whitesides S, Whitesides G M, 2005
"Magnetic self-assembly of three-dimensional surfaces from planar sheets"
Proceedings of the National Academy of Sciences **102**, pp. 3924–3929, doi: 10.1073/pnas.0500807102

Bowden N, Terfort A, Carbeck J, Whitesides G, 1997
"Assembly of mesoscale objects into ordered two-dimensional arrays"
Science **276**, pp. 233–235, doi: 10.1126/science.276.5310.233

Brown P P, Lawler D F, 2003
"Sphere drag and settling velocity revisited"
J. Environ. Eng. **129**, pp. 222–231, doi: 10.1061/(ASCE)0733-9372(2003)129:3(222)

Caspar DL K A, 1962
"Physical principles in the construction of regular viruses"
Cold Spring Harb Symp Quant Biol. **27**, pp. 1–24

Chang E, Maxey M, 1994
"Unsteady flow about a sphere at low to moderate reynolds number. part 1. oscillatory motion"
Journal of Fluid Mechanics **277**, pp. 347–379, doi: 10.1017/S002211209400279X

Chang E, Maxey M, 1995
"Unsteady flow about a sphere at low to moderate reynolds number. part 2. accelerated motion"
Journal of Fluid Mechanics **303**, pp. 133–153, doi: 10.1017/S0022112095004204

Darras A, Fiscina J, Pakpour M, Vandewalle N, Lumay G, 2016
"Ribbons of superparamagnetic colloids in magnetic field"
The European Physical Journal E **39**, p. 47, doi: 10.1140/epje/i2016-16047-0

Dellutri M, Pulici P, Guarnaccia D, Stoppino P, Vanalli G, Lessio T, Vassallo F, Di Stefano R, Labriola G, Tenerello A, Lo Iacono F, Campardo G, 2006
"1 Gb stacked solution of multilevel NOR flash memory packaged in a LFBGA 8 mm by 10 mm by 1.4 mm of thickness"
Thermal, Mechanical and Multi-Physics Simulation and Experiments in Micro-Electronics and Micro-Systems. Proceedings of EuroSimE 2006 (IEEE Cat. No.06EX1341) pp. 5 pp. –

Dimitrov D S, 2004
"Virus entry: molecular mechanisms and biomedical applications"
Nature Reviews Microbiology **2**, pp. 109–122, doi: 10.1038/nrmicro817

Dinner A R, Sali A, Smith L J, Dobson C M, Karplus M, 2000
"Understanding protein folding via free-energy surfaces from theory and experiment"
Trends in Biochemical Sciences **25**, pp. 331– 339, doi: https://doi.org/10.1016/S0968-0004(00)01610-8

Elwenspoek M, Abelmann L, Berenschot E, van Honschoten J, Jansen H, Tas N, 2010
"Self-assembly of (sub-)micron particles into supermaterials"
J. Micromech. Microeng. **20**, p. 064001, doi: 10.1088/0960-1317/20/6/064001

Endres D, Miyahara M, Moisant P, Zlotnick A, 2005
"A reaction landscape identifies the intermediates critical for self-assembly of virus capsids and other polyhedral structures"
Protein Science **14**, pp. 1518–1525, doi: 10.1110/ps.041314405

Erb R, Son H, Samanta B, Rotello V, Yellen B, 2009
"Magnetic assembly of colloidal superstructures with multipole symmetry"
Nature **457**, pp. 999–1002, doi: 10.1038/nature07766

de la Escosura A, R J M N, Cornelissen J J L M, 2009
"Viruses and protein cages as nanocontainers and nanoreactors" **19**, pp. 2274–2278

Feynman R P, Leighton R B, Sands M, 1970
The Feynman Lectures on Physics, Vol I.,
Addison Wesley

Friedrich T, Rehberg I, Richter R, 2015
"Comment on "self-assembly of magnetic balls: From chains to tubes""
Physical Review E - Statistical, Nonlinear, and Soft Matter Physics **91**, doi: 10.1103/PhysRevE.91.057201

Gracias D H, Tien J, Breen T L, Hsu C, Whitesides G M, 2000
"Forming electrical networks in three dimensions by self-assembly"
Science **289**, pp. 1170–1172, doi: 10.1126/science.289.5482.1170

Grant J, Jack R, Whitelam S, 2011
"Analyzing mechanisms and microscopic reversibility of self-assembly"
Journal of Chemical Physics **135**, doi: 10.1063/1.3662140

Gross R, Dorigo M, Sept 2008
"Self-assembly at the macroscopic scale"
Proceedings of the IEEE **96**, pp. 1490–1508, doi: 10.1109/JPROC.2008.927352

Guo H, Wen W, Tao R, 2005
"Dynamics and statistics study of rings formed by magnetic balls"
Physics Letters A **340**, pp. 427 – 433, doi: http://dx.doi.org/10.1016/j.physleta.2005.04.037

Hacohen A, Hanniel I, Nikulshin Y, Wolfus S, Abu-Horowitz A, Bachelet I, 2015
"Meshing complex macro-scale objects into self-assembling bricks"
Scientific Reports **5**, doi: 10.1038/srep12257

Hartley R I, Zisserman A, 2004
Multiple View Geometry in Computer Vision,
Cambridge University Press, ISBN: 0521540518, second edition

Hwang H, Irons G, 2012
"A water model study of impinging gas jets on liquid surfaces"
Metallurgical and Materials Transactions B: Process Metallurgy and Materials Processing Science **43**, pp. 302–315, doi: 10.1007/s11663-011-9613-3

Ilievski F, Mirica K A, Ellerbee A K, Whitesides G M, 2011a
"Templated self-assembly in three dimensions using magnetic levitation"
Soft Matter **7**, pp. 9113–9118, doi: 10.1039/C1SM05962A

Ilievski F, Mani M, Whitesides G, Brenner M, 2011b
"Self-assembly of magnetically interacting cubes by a turbulent fluid flow"
Phys. Rev. E Stat. Nonlinear Soft Matter Phys. **83**, pp. –, doi: 10.1103/PhysRevE.83.017301

Ipparthi D, Winslow A, Sitti M, Dorigo M, Mastrangeli M, 2017
"Yield prediction in parallel homogeneous assembly"
Soft Matter **13**, pp. 7595–7608, doi: 10.1039/C7SM01189J

Iwase E, Shimoyama I, 2005
"Multistep sequential batch assembly of three-dimensional ferromagnetic microstructures with elastic hinges"
Journal of Microelectromechanical Systems **14**, pp. 1265–1271, doi: 10.1109/JMEMS.2005.851814

Jacobs H, Tao A, Schwartz A, Gracias D, Whitesides G, 2002
"Fabrication of a cylindrical display by patterned assembly"
Science **296**, pp. 323–325, doi: 10.1126/science.1069153

Katen S, Zlotnick A, 2009
"The thermodynamics of virus capsid self-assembly"
Methods Enzymol. **455**, pp. 395–417, doi: 10.1016/S0076-6879(08)04214-6

Kolmogorov A, 1941
"Local structure of turbulence in an incompressible viscous fluid at very high reynolds numbers"
C. R. Acad. Sci. URSS **30**

Kostiainen M, Kasyutich O, Cornelissen J J L M, J M R N, 2010
"Self-assembly and optically triggered disassembly of hierarchical dendron–virus complexes"
NATURE CHEMISTRY **2**, pp. 394–399

Landau L, Lifshitz E M, 1987
Fluid Mechanics,
PERGAMON PRESS, doi: 10.1016/B978-0-08-033933-7.50003-9

Langevin P, 1908
"Sur la théorie du mouvement brownien"
C. R. Acad. Sci. (Paris) **146**, pp. 530–533

Lash M, Fedorchak M, Little S, McCarthy J, 2015
"Fabrication and characterization of non-brownian particle-based crystals"
Langmuir **31**, pp. 898–905, doi: 10.1021/la501511s

Lemons D, Gythiel A, 1997
"Paul langevin's 1908 paper "on the theory of brownian motion" ["sur la théorie du mouvement brownien," c. r. acad. sci. (paris) 146, 530-533 (1908)]"
American Journal of Physics **65**, pp. 1079–1080, doi: 10.1119/1.18725

Li T, Kheifets S, Medellin D, Raizen M G, 2010
"Measurement of the instantaneous velocity of a brownian particle"
Science **328**, pp. 1673–1675, doi: 10.1126/science.1189403

Love J, Urbach A, Prentiss M, Whitesides G, 2003
"Three-dimensional self-assembly of metallic rods with submicron diameters using magnetic interactions"
J. Am. Chem. Soc. **125**, pp. 12696–12697, doi: 10.1021/ja037642h

Magono L, 1966
"Meteorological classification of natural snow crystals"
Journal of the Faculty of Science ,Hokkaido University, Japan **II**, pp. 321–335

Manoharan V N, Elsesser M T, Pine D J D, 2003
"Dense packing and symmetry in small clusters of microspheres"
Science **301**, pp. 483–487, doi: 10.1126/science.1086189

Mastrangeli M, Abbasi S, Varel C, van Hoof C, Celis J P, Böhringer K F, 2009
"Self-assembly from milli- to nanoscales: methods and applications"
Journal of Micromechanics and Microengineering **19**, pp. 1–37, doi: 10.1088/0960-1317/19/8/083001

Mateu M M, 2013
"Assembly, stability and dynamics of virus capsids"
Archives of Biochemistry and Biophysics **531**, pp. 65–79, doi: 10.1016/j.abb.2012.10.015

Messina R, Stankovic I, 2015*a*
"Reply to "comment on 'self-assembly of magnetic balls: From chains to tubes' ""
Physical Review E - Statistical, Nonlinear, and Soft Matter Physics **91**, doi: 10.1103/PhysRevE.91.057202

Messina R, Stankovic I, 2015*b*
"Self-assembly of magnetic spheres in two dimensions: The relevance of onion-like structures"
EPL (Europhysics Letters) **110**, p. 46003, doi: 10.1209/0295-5075/110/46003

Messina R, Stankovic I, 2017
"Assembly of magnetic spheres in strong homogeneous magnetic field"
Physica A: Statistical Mechanics and its Applications **466**, pp. 10–20, doi: 10.1016/j.physa.2016.08.079

Messina R, Khalil L, Stankovic I, 2014
"Self-assembly of magnetic balls: From chains to tubes"
Physical Review E - Statistical, Nonlinear, and Soft Matter Physics **89**, doi: 10.1103/PhysRevE.89.011202

Mora P, Mitsuhiro M, Madariaga R, Minster J B, 2013
Microscopic and Macroscopic Simulation: Towards Predictive Modelling of the Earthquake Process,
Birkhauser

Murugesan Y, Pasini D, Rey A, 2015
"Self-assembly mechanisms in plant cell wall components"
Journal of Renewable Materials **3**, pp. 56–72, doi: 10.7569/JRM.2014.634124

Nakamura H, Cartwright J, 2016
"De nive sexangula -a history of ice and snow- part 1"
Weather **71**, pp. 291–294, doi: 10.1002/wea.2912

Odar F, Hamilton W, 1964
"Forces on a sphere accelerating in a viscous fluid"
Journal of Fluid Mechanics **18**, pp. 302–314, doi: 10.1017/S0022112064000210

Olson A J, 2015
"Self-assembly gets physical"
Nature Nanotechnology **10**, p. 728, doi: 10.1038/nnano.2015.172

Olson A J, Hu Y H E, Keinan E, 2007
"Chemical mimicry of viral capsid self-assembly"
PNAS **104**, pp. 20731–20736, doi: 10.1073/pnas.0709489104

Pantaleone J, Messer J, 2011
"The added mass of a spherical projectile"
American Journal of Physics **79**, pp. 1202–1210, doi: 10.1119/1.3644334

Penrose L S, 1959
"Self-reproducing machines"
Scientific American **200**, pp. 105–114

Penrose L S, Penrose R, 1957
"A self-reproducing analog"
Nature **179**, p. 1183, doi: 10.1038/1791183a0

Philipse A, 1989
"Solid opaline packings of colloidal silica spheres"
J. Mater. Sci. Lett. **8**, pp. 1371–1373, doi: 10.1007/BF00720190

Press W H, Teukolsky S A, Vetterling W T, Flannery B P, 1992
Numerical Recipes in C (2nd Ed.): The Art of Scientific Computing,
Cambridge University Press
ISBN 0-521-43108-5

Richardson L, 1922
Weather prediction by numerical process,
Cambridge University Press

Richardson L F, 1926
"Atmospheric diffusion shown on a distance-neighbour graph"
Proceedings of the Royal Society of London. Series A, Containing Papers of a Mathematical and Physical Character **110**, pp. 709–737, doi: 10.1098/rspa.1926.0043

Roland J C, Reis D, Vian B, 1992
"Liquid crystal order and turbulence in the planar twist of the growing plant cell walls"
Tissue and Cell **24**, pp. 335–345, doi: 10.1016/0040-8166(92)90050-H

Rothemund P W K, 2006
"Folding DNA to create nanoscale shapes and patterns"
Nature **440**, pp. 297–302, doi: doi:10.1038/nature04586

Rycenga M, McLellan J M, Xia Y, 2008
"Controlling the assembly of silver nanocubes through selective functionalization of their faces"
Advanced Materials **20**, pp. 2416–2420, doi: 10.1002/adma.200800360

Shetye S, Eskinazi I, Arnold D, 2008
"Self-assembly of millimeter-scale components using integrated micromagnets"
IEEE Transactions on Magnetics **44**, pp. 4293–4296, doi: 10.1109/TMAG.2008.2001344

Shetye S, Eskinazi I, Arnold D, 2010
"Magnetic self-assembly of millimeter-scale components with angular orientation"
Journal of Microelectromechanical Systems **19**, pp. 599–609, doi: 10.1109/JMEMS.2010.2042681

Stambaugh J, Lathrop D, Ott E, Losert W, 2003
"Pattern formation in a monolayer of magnetic spheres"
Physical Review E - Statistical, Nonlinear, and Soft Matter Physics **68**, pp. 026207/1–026207/5

Taheri S M, Michaelis M, Friedrich T, Fürster B, Drechsler M, Römer F M, Bösecke P, Narayanane T, Weber B, Rehberg I, Rosenfeldt S, Förster S, 2015
"Self-assembly of smallest magnetic particles"
PNAS **112**, pp. 14484–14489, doi: 10.1073/pnas.1511443112

Tanaka H, Kido M, Yahashi K, Oomura M, Katsumata R, Kito M, Fukuzumi Y, Sato M, Nagata Y, Matsuoka Y, Iwata Y, Aochi H, Nitayama A, 2007
"Bit cost scalable technology with and plug process for ultra high density flash memory"
Digest of Technical Papers - Symposium on VLSI Technology pp. 14–15, doi: 10.1109/VLSIT.2007.4339708

Terfort A, Bowden N, Whitesides G, 1997
"Three-dimensional self-assembly of millimetre-scale components"
Nature **386**, pp. 162–164, doi: 10.1038/386162a0

Tibbits S, 2011
"A model for intelligence of large-scale self-assembly"
In: *ACADIA 2011: Integration Through Computation*, ACADIA

Tibbits S, Tomas A F, 2013
"Biomolecular, chiral and irregular self-assemblies"
In: *ACADIA 2013 Adaptive Architecture*,

Wang S, Wolynes P, 2011
"Communication: Effective temperature and glassy dynamics of active matter"
Journal of Chemical Physics **135**, doi: 10.1063/1.3624753

Wen W, Kun F, Pál K F, Zheng D W, Tu K N, May 1999
"Aggregation kinetics and stability of structures formed by magnetic microspheres"
Phys. Rev. E **59**, pp. R4758–R4761, doi: 10.1103/PhysRevE.59.R4758

Whitelam S, Aug 2010
"Control of pathways and yields of protein crystallization through the interplay of nonspecific and specific attractions"
Phys. Rev. Lett. **105**, p. 088102, doi: 10.1103/PhysRevLett.105.088102

Whitelam S, Jack R, 2015
"The statistical mechanics of dynamic pathways to self-assembly"
Annual Review of Physical Chemistry **66**, pp. 143–163, doi: 10.1146/annurev-physchem-040214-121215

Whitesides G M, Grzybowski B, 2002
"Self-assembly at all scales"
Science **295**, pp. 2418–2421, doi: 10.1126/science.1070821

Woldering L A, Been A J, Alink L, Abelmann L, 2016
"Using magnetic levitation for 2D and 3D self-assembly of cubic silicon macroparticles"
Physica status solidi RRL **10**, pp. 176–184, doi: 10.1002/pssr.201510298

Yang Y, Meyer R B, Hagan M F, Jun 2010
"Self-limited self-assembly of chiral filaments"
Phys. Rev. Lett. **104**, p. 258102, doi: 10.1103/PhysRevLett.104.258102

Yener A, Klapp S, 2016
"Self-assembly of three-dimensional ensembles of magnetic particles with laterally shifted dipoles"
Soft Matter **12**, pp. 2066–2075, doi: 10.1039/c5sm02648b

Zhang Z, Keys A, Chen T, Glotzer S, 2005
"Self-assembly of patchy particles into diamond structures through molecular mimicry"
Langmuir **21**, pp. 11547–11551, doi: 10.1021/la0513611

Zheng W, Buhlmann P, Jacobs H, 2004
"Sequential shape-and-solder-directed self-assembly of functional microsystems"
Proceedings of the National Academy of Sciences of the United States of America **101**, pp. 12814–12817, doi: 10.1073/pnas.0404437101

Zlotnick A, 2005
"Theoretical aspects of virus capsid assembly"
J. Mol. Recognit. **18**, pp. 479–490

Abstract

Exploring the macroscopic scale's similarities to the microscale is part and parcel of this thesis as reflected in the research question: *what can we learn about the microscopic scale by studying the macroscale?* Investigations of the *environment* in which the self-assembly takes place, and the *self-assembly* itself helps to answer this question.

We mimicked the microscale and identified several analogue parameters. Instead of heat we use turbulence, instead of microscopic we use centimeter-sized particles. Gravity was counteracted by an upward directed water flow since its influence on macroscopic particles is considerable but has only a minor influence on microscopic particles. Likewise heat has a great influence on the microscopic scale but a minor influence on macroscopic particles. Turbulence proved to be an accurate representation for heat and was modelled as if on a microscopic scale, applying thermodynamical concepts such as Brownian motion, diffusion, kinetics and the Einstein relation. Those concepts proved suitable also on the macroscopic scale. Particle velocity is Maxwell-Boltzmann distributed and the average squared displacement is in agreement with a confined random walk. The diffusion coefficient and velocity is independent on particle size. This leads to the interpretation that the motion of a single centimeter-size sphere resembles the motion of a microscopic particle in that it conducts a random walk and Brownian motion.

To visualize micro- or nanoscopic particles electron- or light-microscopy is often used. Instead of microscopes we used video cameras to record the experiments with centimeter sized particles. A swimmingpool pump and asymmetric inflow is used to create upward flow and turbulence. The asymmetric inflow causes large macroscopic swirls representing the applied heat level at the microscale. In the microscopic case the Brownian motion of particles is result of propagating heat originating at its source whereas at the macroscopic scale the vortice propagation originating in the asymmetry of flow cause the Brownian motion of large particles. Despite of those analogies between heat and turbulence the values for the disturbing energy varies considerably depending on if they were determined via single sphere diffusion (Einstein relation) and velocity (kinetic energy) or via two sphere interactions over distance. The latter case is an order of magnitude lower, approximately 6.5 µJ compared to 80 µJ. This suggests that the heat or turbulence energy spectra may differ with respect to its action on the particle(s). There is a

directional dependency of particle velocity, diffusion and disturbing energy. The horizontal dimensions are similar but the vertical component show a stronger dependency with respect to flow asymmetry and turbulence. The directional dependency can most likely be counteracted via future technical adjustments. It can also be interpreted as a temperature gradient.

Self-assembly was studied via structure formation of multiple magnetic spheres or twelve heptagonal magnetic platelets by systematic variation of turbulence and asymmetry. The multiple magnetic spheres form lines and rings and their occurance were in accordance with theory, however the absolute energies of the structures deviated from theory. For experiments with increasing number of spheres, four spheres represents a transition between lines and rings. The system proved to seak for the minimum energy structure which again makes the our macroscopic system behave similar to the microscale. Turbulence acted in a similar way as heat since almost only individual particles were observed at high turbulence whereas lines and rings formed as turbulence decreased which resembles a phase transition between a liquid and a solid or a gas and a liquid.

Self-assembly of twelve centimeter-sized pentagonal platelets showed the same energy minimum seaking behavior. A complete self-assembly of the dodecahedron was not achieved. Predominantley intermediate structures with maximum contacts to each particle formed (trimer and tetramer etc.) which is the minimum energy structure. Also in this more complex case the system prove to behave similar to the microscale.

The two examples of self-assembly represent on the one hand formation of simple structures (rings and lines) and on the other hand a more complex case of self-assembly (a hollow dodecahedron). The later example can be interpreted as self-assembly of geometrical construct or as a representation of self-assembly of a spherical virus. This underlines the potential of macroscopic self-assembly; it can be used in the investigation of general largely scale-independent problems or as an analogue representation in the investigations of natural occuring phenomena.

Zusammenfassung

Die Untersuchung der Ähnlichkeiten zwischen der mikroskopischen und makroskopischen Größenordnung ist Teil dieser Arbeit, die sich in der Forschungsfrage widerspiegelt: *Was können wir über die mikroskopische Skala durch Untersuchung der Makroskala erfahren?* Untersuchungen der *Umgebung*, in der das Selbst-assembly stattfindet, und das *Selbst-assembly* an sich helfen diese Frage zu beantworten.

Wir imitierten die Mikroskala und identifizierten mehrere analoge Parameter. Anstelle von Hitze verwenden wir Turbulenz, statt mikroskopisch kleine Partikel kommen zentimetergroße Partikel zum Einsatz. Der Schwerkraft wurde durch einen nach oben gerichteten Wasserstrom entgegengewirkt, da ihr Einfluss auf makroskopische Partikel beträchtlich ist. Auf mikroskopische Partikel hat sie dagegen nur einen geringen Einfluss. Auf die gleiche Art und Weise hat Wärme einen großen Einfluss auf die mikroskopische Skala, aber einen geringen Einfluss auf die makroskopische Partikel. Die Turbulenz erwies sich als geeignetes Analogon für Wärme und wurde wie im mikroskopischen Maßstab modelliert. Dabei kamen thermodynamische Konzepte wie Brownsche Bewegung, Diffusion, Kinetik und die Einstein-Relation zum Einsatz. Diese Konzepte erwiesen sich auch im makroskopischen Maßstab als geeignet.

Die Teilchengeschwindigkeit ist Maxwell-Boltzmann verteilt und die durchschnittliche quadratische Verschiebung ist in Übereinstimmung mit einer begrenzten Zufallsverschiebung. Der Diffusionskoeffizient und die Geschwindigkeit sind unabhängig von der Partikelgröße. Dies führt zu der Interpretation, dass die Bewegung einer einzelnen zentimetergroßen Kugel der Bewegung eines mikroskopischen Teilchens ähnelt, indem sie eine Zufallsverschiebung und eine Brownsche Bewegung ausführt. Um mikro- oder nanoskopische Partikel sichtbar zu machen, werden häufig Rasterelektronen- oder Lichtmikroskopie verwendet. Anstelle von Mikroskopen verwendeten wir Videokameras, um die Experimente mit zentimetergroßen Partikeln aufzuzeichnen. Eine Schwimmbadpumpe und asymmetrische Einströmung (eines von vier Einlassventilen ist immer geschlossen) wurden eingesetzt, um Turbulenzen und asymmetrische Strömung zu erzeugen. Dieser asymmetrische Zufluss kann große makroskopische Wirbel verursachen, die die Eingangswärme im Mikromaßstab darstellen. Im mikroskopischen Fall ist die Brownsche Bewegung

der Teilchen das Ergebnis der Ausbreitung von Wärme, die von ihrer Quelle ausgeht, während im makroskopischen Maßstab die von der Asymmetrie der Strömung herrührende Vermehrung die Brownsche Bewegung großer Teilchen verursacht. Trotz dieser Ähnlichkeiten zwischen Wärme und Turbulenz variieren die Werte für die Perturbationsenergie erheblich, je nachdem, ob sie über eine Einzelkugel-Diffusion (Einstein-Beziehung) und Geschwindigkeit (kinetische Energie) oder über Wechselwirkungen zwischen zwei magnetische Kugeln über die Entfernung bestimmt wurden. Der letztere Fall ist um eine Größenordnung niedriger, etwa 6.5 μJ verglichen mit 80 μJ. Dies legt nahe, dass die Wärme- oder Turbulenzenergie-Spektren in Bezug auf ihre Wirkung auf die Partikel unterschiedlich sein können. Es besteht eine gerichtete Abhängigkeit von Teilchengeschwindigkeit, Diffusion und Perturbationsenergie. Die horizontalen Dimensionen sind ähnlich, aber die vertikale Komponente zeigt eine stärkere Abhängigkeit in Bezug auf Strömungsasymmetrie und Turbulenz. Der Richtungsabhängigkeit kann voraussichtlich über zukünftige technische Anpassungen entgegengewirkt werden. Die gerichtete Abhängigkeit kann auch als Temperaturgradient interpretiert werden.
Das Self-assembly wurde durch Strukturbildung mehrerer magnetischer Kugeln oder eines Dodekaheders aus zwölf heptagonalen magnetischen Plättchen durch systematische Variation von Turbulenz und Asymmetrie untersucht. Die multiplen magnetischen Kugeln bilden Linien und Ringe, und ihr Auftreten entsprach der Theorie, jedoch wichen die absoluten Energien der Strukturen von der Theorie ab. Für Experimente mit zunehmender Anzahl von Kugeln stellen vier Kugeln einen Übergang zwischen Linien und Ringen dar. Das System erwies sich als geeignet um die minimale Energiestruktur anzustreben, was wiederum zeigt, dass sich unser makroskopisches System ähnlich wie die Mikroskala verhält. Die Turbulenz wirkte ähnlich wie die Wärme, da fast nur einzelne Teilchen bei hoher Turbulenz beobachtet wurden, während sich Linien und Ringe, bei abnehmender Turbulenz bildeten, was einem Phasenübergang zwischen einer Flüssigkeit und einem Feststoff oder einem Gas und einer Flüssigkeit ähnelt.

Das Self-assembly von zwölf Zentimeter großen pentagonalen Plättchen zeigte das gleiche Energieminimierungsverhalten wie die Kugelstrukturen. Ein vollständiges Self-assembly des Dodekaeders wurde nicht erreicht. Vorherrschend waren intermediäre Strukturen mit maximalen Kontakten zwischen jedem Partikel (Trimer und Tetramer etc.), was der minimalen Energiestruktur entspricht. Auch in diesem komplexeren Fall verhält sich das System ähnlich wie im Mikromaßstab.

Die beiden Beispiele des Self-assembly repräsentieren zum einen die Bildung einfacher Strukturen (Ringe und Linien) und zum anderen einen komplexeren Fall des Self-assembly (ein hohles Dodekaeder). Das letztere Beispiel kann als Self-assembly eines geometrischen Konstrukts oder als Modell f ür das Selbst-assembly eines sphärischen Virus interpretiert werden. Dies unterstreicht das Potenzial des makroskopischen Self-assembly; es kann bei der Untersuchung von allgemein weitgehend größenunabhängigen Problemen oder als analoge Darstellung bei der Untersuchung von natürlich vorkommenden Phänomenen eingesetzt werden.

Samenvatting

Onze wereld bestaat uit atomen. Die atomen organiseren zichzelf in moleculen. Kleintjes, zoals water, en grote, zoals virussen, zonder dat iemand regelt hoe die atomen dat moeten doen. Dit proces noemen we self-assembly. Veel onderzoekers proberen dit proces uit te voeren op micrometer schaal, om materialen te maken met bijzondere eigenschappen. Self-assembly is een moeilijk proces om te bestuderen, omdat de onderdelen zo klein zijn en alles erg snel gaat. In dit proefschrift wordt self-assembly op de centimeter schaal onderzocht, waar de relevante tijdsconstanten in de tienden van seconden zijn. Een eenvoudig webcam volstaat. De onderzoeksvraag in dit proefschrift is daarom "wat kunnen we leren over self-assembly op de microschaal door observatie op de macro-schaal".

Om drie-dimensionale self-assembly op de macroschaal mogelijk te maken, moeten twee belangrijke problemen worden opgelost. Omdat de massa van de onderdelen groot is, speelt zwaartekracht een grote rol. Om te voorkomen dat de onderdelen op de bodem van een vat vallen zonder voldoende tijd om te assembleren, laten we ze in een opwaartse stroom van water "vallen". Daardoor blijven ze zweven voor de camera. Op de nano- en microschaal bewegen deeltjes door thermische energie: de Brownse beweging. Op de macro-schaal is de thermische energie onvoldoende. Daarom schudden we de onderdelen door elkaar door middel van turbulentie in het water. In dit proefschrift wordt aangetoond dat turbulentie dezelfde thermodynamische eigenschappen heeft als thermische energie.

We kunnen een diffusie-constante definiëren, de snelheid van een object in het water volgt een Maxwell-Boltzman verdeling en de onderdelen voldoen aan de Einstein relatie tussen wrijving en diffusieconstante. Omdat we de turbulentie kunnen vergroten door het water aysymmetrisch in te laten stromen, hebben we een eenvoudige manier om de verstorende energie (de "temperatuur") van het systeem te regelen.

Niet alle eigenschappen voldoen aan de thermodyamische wetten. Zo is bijvoorbeeld de absolute grootte van de verstorende energie afhankelijk van de lengteschaal waarop we kijken. De Brownse beweging van een enkel deeltje heeft bijna tien keer zoveel energie als die beschikbaar is om twee deeltjes met magneten uit elkaar te trekken. Ook is de energie die in de Brownse beweging zit afhankelijk van de richting waarin we kijken, en die afhankelijkheid varieert zelfs met de mate van turbulentie.

Rekening houdend met deze tekortkomingen, kunnen we veel leren van macroscopische experimenten. Bollen met geintegreerde magneten, als voorbeeld van dipool-interactie tussen bolvormige objecten, vormen kettingen. Die kettingen vormen bij voorkeur ringen als het aantal bollen groter is dan vier, met een statische waarschijnlijkheid die kwalitatief in overeenstemmig is met de thermodynamische voorspelling.

Als een sprong in het diepe, is in dit proefschrift geprobeerd de self-assembly van een bolvormig virus te bestuderen. Twaalf vijfhoekige onderdelen werden in een speciale conus bij elkaar gebracht om interactie met de wand van het systeem te verminderen. Door het juiste ontwerp van magnetische interacties tussen de vijfhoeken, zouden de twaalf in principe zichzelf in een dodecahedron kunnen assembleren. Dit hebben we echter niet kunnen observeren. Ten hoogste kwamen vier vijfhoeken bij elkaar. Een van de problemen was de vorming van ongewenste structuren. Het ontbrak ons aan de tijd om verder te experimenteren. Dit experiment is echter een prachtig voorbeeld van de kracht van het bestuderen self-assembly processen op de macro-schaal, en wat we daarvan kunnen leren over soortelijke processen op de micro- en nano-schaal.

Sammanfattning

Denna avhandling handlar om att undersöka den makroskopiska skalans likheter med den mikroskopiska och återspeglas i forsknings frågan: *vad kan vi lära oss om den mikroskopiska skalan genom att studera den makroskopiska?* Undersökningar av *omgivningen* där självassociation äger rum, och själva *självassociationen* i sig kan besvara den frågan. Vi imiterade mikroskalan och identifierade flera analoga parametrar. I stället för värme använder vi turbulens, istället för mikroskopiska partiklar använder vi centimeterstora partiklar. Gravitationens inflytande kompenserades av ett uppåtriktat vattenflöde. Den påverkar makroskopiska partiklar avsevärt men har endast ett litet inflytande på mikroskopiska partiklar. På samma sätt har värme ett stort inflytande på den mikroskopiska skalan men ett litet inflytande på den makroskopiska. Turbulens visade sig vara en en bra analog för värme och modellerades på den mikroskopiska skalan, med hjälp av termodynamiska koncept som Brownsk rörelse, diffusion, kinetik och Einstein-relationen. Det visade sig att dessa kan användas även på den makroskopiska skalan. Partikelhastigheten är Maxwell-Boltzmann distribuerad och den genomsnittliga sträckan i kvadrat av en partikel i rörelse överensstämmer med en slumpvandring. Diffusionskoefficienten och hastigheten är oberoende av partikelstorleken. De makroskopiska partiklarnas rörelse liknar de mikroskopiska eftersom de utför en slumpvandring och Brownsk rörelse.

För att visualisera mikro- eller nanoskopiska partiklar används ofta elektron- eller ljusmikroskopi. I stället för mikroskop använde vi videokameror för att spela in experimenten med centimeterstora partiklar. En pump och asymmetrisk tillflöde (en av fyra inloppsventiler är alltid stängd) användes för att skapa turbulens och asymmetri. Det asymmetriska inflödet kan orsaka makroskopiska virvlar som motsvarar mikroskalans ingångsvärme. För mikroskopiska sfäriska Brownska partiklar är rörelse resultatet av värme, medan på den makroskopiska skalan är det turbulent virvelfortplantning vilket härrör från asymmetrin och turbulens i inflödet som orsakar den Brownska rörelsen av de centimeterstora partiklarna. Trots dessa analogier mellan värme och turbulens varierar värdena för perturbationssenergin, kraftigt beroende på om de beräknades med hjälp av diffusion av en sfär (Einstein-relationen) och dess hastighet (kinetisk energi) eller via växelverkan mellan två magnetiska, sfäriska partiklar. Det senare fallet är en storleksordning mindre, ungefär 6.5 μJ jämfört med 80 μJ, i det första fallet. Detta visar att värme- eller turbulensenergispektrumen kan variera med avseende på dess verkan på partikeln

eller partiklarna. Det finns ett riktningsberoende av partikelhastighet, diffusion och perturbationsenergi. De horisontella dimensionerna är likartade men den vertikala komponenten visar ett starkare beroende med avseende på flödesasymmetri och turbulens. Riktningsberoendet kan sannolikt motverkas genom framtida tekniska justeringar. Det kan också tolkas som en temperaturgradient.

Självassociationen studerades via strukturbildning av flera magnetiska sfärer eller en dodecahedron bestående av tolv heptagonala magnetiska plattor genom systematisk variation av turbulens och asymmetri. De magnetiska kulorna bildar linjer och ringar vilkas förekomst var i överensstämmelse med teorin, men de absoluta energierna hos strukturerna avviker från teorin. Experiment med olika antal sfärer visade att fyra sfärer representerar en övergång mellan linjer och ringar. Strukturen med den lägsta energin bildades, vilket återigen visar att, vårt makroskopiska system beter sig som ett mikroskopiskt. Turbulens agerade på liknande sätt som värme eftersom nästan endast enskilda partiklar observerades vid hög turbulens medan linjer och ringar bildades när turbulensen minskades vilket liknar en fasövergång mellan en vätska och ett fast ämne eller en gas och en vätska. Självassociationen av de tolv pentagonala plattorna strävade efter en strukturell energiminimering precis som de magnetiska sfärerna. En fullständig självassociation av en dodecahedron uppnåddes dock inte. Framförallt intermediära strukturer med maximalt antal kontakter mellan varje partikel bildades (trimer och tetramer etc.). Dessa strukturer har den lägsta energin. Även i detta mer komplicerade fall visar det sig att det makroskopiska systemet uppträder som ett mikroskopiskt. Dessa två exempel på självassociation representerar å ena sidan bildandet av enkla strukturer (ringar och linjer) och å andra sidan ett mer komplicerat fall av självassociation (en ihålig dodekaedron). Det senare exemplet kan tolkas som självassociation av en geometrisk form eller som en representation av självassociation av ett sfäriskt virus. Detta visar potentialen för makroskopisk självassociation; Den kan användas för att studera generella frågeställningar som är till någon grad oberoende av storleksordningen eller som en analog representation av naturligt förekommande fenomen.

요약

거시규모와 미소규모의 유사성을 탐구하는 것은 다음 연구 질문에 반영되어 있듯이 이 논문의 한 부분이다. *우리는 과연 거시규모를 연구함으로써 미소규모에 대해서 무엇을 배울 수 있을까?* 자가조립이 일어나는 *배경*에 대한 연구와 *자가조립* 그 자체가 이 질문에 대하여 대답을 하는 데 도움을 준다.

우리는 미소규모를 모방하였고 몇 가지 아날로그 매개변수들을 설정하였다. 열 대신 난기류를 사용하였으며, 미소 규모 대신 센티미터 크기의 입자를 사용하였다. 중력은 위 방향으로 향하는 물의 흐름에 의해서 상쇄되는데 거시 입자들에 미치는 이것의 영향은 상당하지만 미소 입자들에 미치는 영향은 미미하기 때문이다.

이와 마찬가지로, 열은 미소 규모에는 상당한 영향을 미치지만 거시 규모의 입자에는 미미한 영향을 미친다. 난기류는 열을 비교적 정확하게 모사한다고 밝혀졌고 브라운운동, 확산작용, 운동학, 아인슈타인 관계 등의 열역학적인 개념을 적용하면서 미소 규모로서 모델링 되었다.

이러한 개념들은 거시 규모에서도 적절하다고 밝혀졌다. 입자의 속도는 Maxwell-Boltzmann 분포를 따르며 제곱평균변위는 제한된 랜덤 워크에 대응된다. 확산작용 변수와 속도는 입자의 크기에 대해 독립적이다. 고로 센티미터 크기의 단일 구 입자의 운동은 랜덤 워크와 브라운 운동을 수행한다는 점에서 미소 입자와의 유사성을 가진다고 할 수 있다.

마이크로/나노 입자들을 가시화 하기 위해서는 전자/광학 현미경이 종종 이용된다. 현미경을 이용하는 대신 우리는 센티미터 크기의 입자들의 실험을 기록하기 위해 비디오 카메라를 이용하였다. 수영장 펌프와 비대칭 유입수는 위 방향의 물의 흐름과 난기류 발생에 이용된다. 비대칭 유입수는 큰 거시규모의 소용돌이를 이끌어내는데 이는 미소 규모에서의 적용 열량에 해당된다. 미소 규모의 경우 입자들의 브라운 운동은 열원에서 전파되는 열의 결과인 반면에 거시규모에서는 비대칭 유입수로부터 발생되는 소용돌이들이 거시 입자들의 브라운 운동을 일으킨다.

이러한 열과 난기류의 상사성에도 불구하고, 방해 에너지 (disturbing energy) 값은 단일입자 확산(아인슈타인 관계) 과 속도(운동에너지)에 기반하여 결정될 것인지, 혹은 떨어진 두 구 입자들의 상호작용으로 인해서 결정될 것인지에 따라 상당히 의존적으로 달라진다. 후자의 경우는 크기가 낮은 것부터, 대략 6.5 μJ 에서 80 μJ 정도이다. 이는 열 혹은 난기류 에너지의 스펙트럼은 이것이 입자들의 움직임에 영향을 주는 정도에 따라 달라질 수 있다는 것을 암시한다.

입자 속도, 확산, 방해 에너지에는 방향 의존성이 있다. 수평 방향의 차원은 비슷하지만 수직 방향의 성분들은 흐름의 비대칭성과 난기류에 상당히 의존적

이다. 방향 의존성은 장차 기술적 조정에 의해서 제어될 수 있을 것이다. 이것은 또한 온도의 구배(gradient)로 해석될 수 있다.

자가조립은 여러 개의 자성 구 입자들 혹은 7각형의 자성 혈소판들이 난기류와 비대칭성의 체계적인 변화에 의해서 구조를 형성하는 과정에서 연구되었다. 여러 개의 자성 구들은 선/고리모양을 형성하며 이론과 부합하였지만, 구조의 절대 에너지 값은 이론으로부터 다소 벗어난 결과를 보였다. 구의 개수를 늘리며 수행했던 실험에서는, 4개의 구는 선과 고리 사이의 전이단계를 나타낸다.

계(system)는 최소 에너지를 갖는 구조를 찾아간다고 밝혀졌고 이는 우리의 거시 계가 미소 계와 비슷하게 행동한다는 것을 보여준다. 난기류는 열과 비슷한 방식으로 작용하였다. 높은 난기류 상태에서는 주로 각각의 입자들이 관찰되었지만 난기류가 감소함에 따라서 입자들이 선과 고리들을 형성하였다. 이는 액체와 고체 혹은 기체와 액체 간의 상 변화와 유사하다.

12센치 크기의 오각형의 자성 혈소판들의 자가조립 또한 같은 방식으로 최소 에너지를 찾아가는 거동을 보였다. 12면체의 완전한 자가조립은 이루어지지 않았다. 주로 입자들 사이에서 최대 접촉을 하는 중간 단계의 구조들은 (삼량체 및 테트라머 등을) 형성하였는데 이는 에너지를 최소화하는 구조이다. 또한 이러한 더욱더 복잡한 경우에도 계(system)는 미소 규모와 비슷하게 거동을 보인다고 밝혀졌다.

자가조립의 두 가지 예시는 각각 간단한 구조(선 및 고리) 형성과 더 복잡한 형태의 자가조립 (중공 12면체)를 보여준다. 이후의 예시는 기하학적 구조의 자가조립 혹은 구형 바이러스의 자가조립으로서 해석될 수 있다. 이는 거시 자가조립이 일반적인 거시 규모의 독립적인 문제들 혹은 자연에서 발생하는 아날로그적인 문제들에 대한 탐구에 쓰일 수 있는.

Acknowledgments

The author of this thesis would like to cordially extend thanks to his family and friends, most and foremost my mother Anna and my father Stig. My father as well as my uncles Per, Sture and Bosse and my aunt Ingrid are not alive today to experience that I accomplished my doctorate. Needless to point out how I feel about this unavoidable fact. I thank my brother Peter and his family and the extended family Löthman and Andersson which I for so many years have been unable to keep contact to on a regular basis. A word of thank to all of you and a word of regret on my side since I was so very absent for many years; Klas, Dag, Anders, Stina, Åsa, Helena, Christer, Elisabeth, Olle, Lasse, Lena, Monika, Monika, Bitte, Karin, Patric, Fia, Anders.

Some wonderful people I would like to cordially thank, are those still at KIST Europe and those who moved on to new adventures as well as former colleauges and freinds at previous institutes, first and foremost my magnetics team friends; Marc Pichel, Tijmen Hageman, Thomas Jansson, Nuriye Korkmaz, Bohyun Ryu, André-René Blaudzun. Also at KIST in other research grops: Ruth Eggers, Jaeho Lee, Felix Löser, Dr. Chang-Hoon Nam, Ana Vanessa Jobling Almeida, Levent Yobas, Pavel Neuzil, Jang Mi, Xian Ping Li, Kai Sauer, Agu Vahtrik, Jingeum Lee, Himani Sharma, Seung Jae Lee, Eric Castro, Oliver Weiß, Neha Agarwal, Mark Tarn, Yukjung Park, Galina Skorikova, Camila Campos, Daniela Vanni-Strassner, Jong-Ok Arnhold, Dr. Kuiwon Choi, Sabrina Lehnert, Melanie Schneider, Susanne Schäfer, Anja Philippi, Kilian Smith, Michael Müller, Carsten Brill, Rüdiger Lauer, Matthias Altmeyer, Jean-Philippe Saarbach, Holger Krause, Rosanne Guijt, Gaiyoung Kim, Dong Hoon Kim, Minyoung Kim, Yannick Klein, Nicodemia Bienia, Helen Schneider, Varun Sridar, Tim Melhorn, Jooyoung Im, Angela Damian, Franziska Emmerich, Alveena Mir. And affiliated or from other places: Michael Dirnberger (Max Planck Institute for Informatics), Caspar Abelmann (computer animation expert). A special thanks to my excellent paranymphs Kilian Smith and Tijmen Hageman.

My dear and numerous friends I made during my time in Twente and Saarbrücken are more than worthy a special thank for lighting up my day; Erika Maizi, Christine Mahdi, Dorothee Wendel, Mercedes Mertinez Martinez, Andreas Neuner, Dorothee Wiebe, Thomas Karwoth, Karin Konz, Eugen Voigt, Corinna Markmann. Friends, former colleagues and beloved ones who are not from Sarbrücken nor from Twente; Hartmut and Verena Göhler, Francoise Lapointe and Lisanne Leb,

Matthias Schmidt (Green Sugar), Petra Tumova, Pavel Tuma, Marit Schulte, Sigrid Gaadt-Klössler, , Annette Swiergiel, Genevieve Neuville, Gina Moncada and the Moncada family, Isabelle Legault, Elyse Adam, Marie Denise Fagnan, Marion Kittel, Owinch Asuaje, Mario Alberto Gomez, Mayeli Alvarez Silva, Paula Proa Flores, Yaneth Aguilar, Delphine Bouilly, Lydia Aguirre, Issam Telahigue, Zippora Nochasak, Maxime Lafrance, Gilberte Fortuné, Mert Clk, Richard Martel, Patric Desjardin, Eric Anglaret, Vincent Jourdain, Alain Pignacault, Camilo Zamora-Ledezma, Vincent Leon, Anders Dannvik, Lotta Nyman, Kerstin Ottosson, Monica Wikehult, Anders Ottosson, Gunnar Lundin, Oskar Lundin, Dina Goldbaum, Eva Pisana, Annett Bellack, David Prangishvili, Patric Forterre, Jonas Ekblom, Eric Cimmini, Jacek Koziorowski, Leila Ekman, Erik Ronne, Gustav Magnusson.

A special thank to the wonderful Argentinian artist Pablo Carlos Budassi for letting me use his picture "Orders of magnitude" (2012). Muchas gracias, conpatriota. Our collaborators at the German University of Cairo Mohammad Elwi, Islam S. M. Khalil, Heba Ali Mohamed Mostafa, Osama Mosleh and many more students, interns and professors from the same prestigious university. Thank you to all the members of the RAM and Bionano groups at the university of Twente, especially; Gijs Krijnen, Miko Elwenspoek, Henk van Wolferen, Susan Janse, Kodai Hatakeyama, Laurens Remco Sanders, Léon Woldering for initial work on the project. Massimo Mastrangeli form University of Delft and Dhananjay Ipparthi of Universiteé libre de Bruxelles.

My excellent, exquisite supervisor Leon Abelmann can not be praised enough and so cannot my co-supervisor Gijs Krijnen as well as Andreas Manz and the always creative and two-steps-ahead-thinking Miko Elwenspoek who were always eager to make the best out of my thesis. Thank you for struggling together on the exciting topic of self-assembly as well as other neighbouring exciting topics for so many years. The numerous questions and ideas that came up during my thesis are not forgotten but are work in progress, so our research just begun. And we are looking forward to many more endeavors in the future also after my thesis has been accomplished. The equipartition theorem, frequency dependence of turbulence with respect to the various self-assembly processes, archaea viruses, bacteriophages and so on are topics that still need to be tackled. And I happily do it with my supervisor involved, one way or another. The very best is yet to come!

I am grateful to all the members of the committee, for taking my thesis into consideration and making this defence possible: Leon Abelmann, Gijs Krijnen, Uwe Hartmann, M. Vielhaber, Hajo Broersma, Jeroen J.L.M. Cornelissen, Jost Kok, Miko Elwenspoek and Massimo Mastrangeli. A sincere and friendly, thank you.

Publications

The research presented in this thesis has lead to some of the following publications:

Journal articles

Arenal R, Löthman P, Picher M, Jourdain V, 2012
"Atomic structural studies of ultralong carbon nanotubes"
Microscopy and Microanalysis **18**, pp. 1518–1519, doi: 10.1017/S1431927612009440

Arenal R, Löthman P, Picher M, Than T, Paillet M, Jourdain V, 2012
"Direct evidence of atomic structure conservation along ultra-long carbon nanotubes"
The Journal of Physical Chemistry C **116**, pp. 14103–14107, doi: 10.1021/jp212540n, arXiv:http://dx.doi.org/10.1021/jp212540n

Löthman P, Janson T, Klein Y, Blaudszun A R, Ledwig M, Abelmann L, 2017
"Magnetic particle spectrometry of microfabricated magnetic particles"
International Journal on Magnetic Particle Imaging **3**
URL `https://journal.iwmpi.org/index.php/iwmpi/article/view/76`

Löthman P A, Hageman T A G, Dirnberger M, Elwenspoek A M C Manz, Abelmann L, 2018
"Macroscopic equivalence for microscopic motion in a turbulence driven threedimensional self-assembly reactor"
Journal of Applied Physics **123**, p. 024091

Mueller J, Löthman P, Meyer D C, 2005
"Small angle X-ray transmission characterisation of nanometer-sized Pt-clusters in a ceramic thin film on metal substrate"
Crystal Research and Technology **40**, pp. 177 – 181, doi: 10.1002/crat.200410321

Per Arvid Löthman O A, Gründer J, Landgraf G, 2000
"Mechanische eigenschaften metallischer hohlkugelformkörper und charakterisierung ihrer zellwandeigenschaften"
Materialwissenschaft und Werkstofftechnik **31**, doi: 10.1002/1521-4052(200006)31:6<529::AID-MAWE529>3.0.CO;2-C

Conference contributions

Abelmann L, Löthman P, Hageman T, Manz A, 2015
"3d self-assembly of magnetic memory crystals"
In: *International Workshop on Magnetic Nanowires and Nanotubes 2015 (IWMNN), From 3D Nanostructuring Towards Novel Magnetic Data Storage, Meersburg/Lake Constance, Germany, Volume:* 2,

Abelmann L, Löthman P, Hageman T, Pichel M, Manz A, 2016
"Magnetically assisted three-dimensional self-assembly"
In: *Joint MMM-Intermag Conference*,

Arenal R, Löthman P A, Picher M, Jourdain V, 2013
"Atomic structure of ultra-long carbon nanotubes"
In: *HeteroNanoCarb 2013*,

Bargel H, Löthman P A, Neinhuis C, 2006
"The skin of plants: multifunctional interface and inspiration for biomimetic engineering"
In: *5th World Congress of Biomechanics, Volume: 5*,

Göhler H, Löthman P A, Waag U, Schneidereit H, Bernard E, 2001
"Manufacture and properties of hollow sphere structures in sound absorption applications"
In: *Proceedings of the Cellular Metalls and Metall Foaming Technology Metfoam Conference, Bremen*,

Gründer J, Landgraf G, Andersen O, Löthman P A, 2001
"Modelling and simulation of the meso- and macro-mechanical properties of hollow sphere structures"
In: *Cellular metals and metal foaming technology: International Conference on Cellular Metals and Metal Foaming Technology, Volume: 5*,

Hageman T A G, Löthman P A, Janson T G, Manz A, Abelmann L, 2015
"Characterization of a macroscopic self-assembly reactor"
In: *Micromechanics and microsystems Europe workshop*,

Hageman T A G, Löthman P A, Woldering L, Bienia N, Manz A, Abelmann L, 2015
"Disturbing energy in a macroscopic self-assembly reactor"
In: *FNANO15 - Conference on foundations of nanoscience: self-assembled structures and devices*,

Hageman T A G, Löthman P A, Manz A, Abelmann L, 2016
"Characterization of a macroscopic self-assembly reactor"
In: *Micromechanics and microsystems Europe workshop*,

Hageman T A G, Dirnberger M, Elwenspoek M, Krijnen G, Löthman P A, Manz A, Pichel M P, Abelmann L, 2017
"Turbulence-driven macroscopic magnetic self-assembly with adjustable level of agitation"
In: *Intermag2017*,

Hageman T A G, Löthman P A, Manz A, Abelmann L, 2017a
"Analysis of dipolar chain and ring formation in a macroscopic self assembly reactor"
In: *Micromechanics and microsystems Europe workshop*,

Illerhaus B, Jasiuniene E, Goebbels J, Löthman P A, 2002
"Investigation and image processing of cellular metals with highly resolving 3d microtomography (uct)"
In: *Proceedings of SPIE - The International Society for Optical Engineering*,

Kieback B, Stephani G, Waag U, Schneider L, Löthman P A, 2000
"Powder metallurgy of ultralight materials"
In: *International Workshop on Advanced Powder Metallurgy, Japan Society of Powder and Powder Metallurgy, Kyoto November 17th 2000*,

Löthman P, Hageman T, Manz A, Abelmann L, 2015
"Biomimetic macroscopic 3d self-assembly, how viral infection may lead to magnetic memory"
In: *International Workshop on Magnetic Nanowires and Nanotubes (IWMNN), From 3D Nanostructuring Towards Novel Magnetic Data Storage, Meersburg/Lake Constance, Germany, Volume: 2*,

Löthman P A, 2013
"Nanotechnology in the archaeal virosphere"
In: *Workshop Institute of Microbiology, University of Regensburg, Regensburg, Germany, At University of Regensburg, Institute of Microbiology, Regensburg, Germany*,

Löthman P A, 2014
"Viral self-assembly - small & big"
In: *MESA+ MEETING, Twente, The Netherlands*,

Löthman P A, Favret E, 2013
"Seeing surface architecture by novel optical and digital methods - a study of biological and technological surfaces by uloi, rimaps and variogram analysis"
In: *Euromat 2013, September, Sevilla, Spain*,

Löthman P A, Stephani G, 2003
"A novel implant material with adjustable youngs modulus"
In: *Proceedings of the Annual meeting of the European Biomaterial Society, EBS 2003, Stuttgart, Germany, 2003*,

Löthman P A, Andersen O, Gründer J, Landgraf G, 2000
"Cell wall mechanics of ifam-dresden hollow sphere structures-derivation of testing methods and computersimulation"
In: *Proceedings of Materials week 2000, München, September 2000*,

Löthman P A, L U Waag, Schneider L, Stephani G, 2001
"Metallic hollow spheres and hollow sphere structures for automotive applications"
In: *International Conference on Materials Engineering, New Materials Technology and Biomaterials, Liberec, Czech Republic, Volume: 1*,

Löthman P A, Neinhuis C, Rothe U, 2005
"Nanostructuring of monomolecular tetraetherlipid surfaces"
In: *Euromat 2005, Prague Czech Republic*,

Löthman P A, Martel R, Desjardins P, Picher M, Jourdain V, 2009
"Ccvd synthesis of individual, ultra-long carbon nanotubes"
In: *RQMP Réuniion annuelle, Centre Mont-Royal, Montréal, Quebec, Canada, Lundi 1er juin 2009*,

Löthman P A, Manz A, Prangishvili D, 2013
"Bionanotechnological applicationsof the archaea-virus afv1"
In: *THERMOPHILES 2013, 12th International Conference, 8-12 Sept., 2013, Regensburg, Germany*,

Löthman P A, Woldering L, Hageman T, Abelmann L, Manz A, 2014
"Towards biomimetic microfabrication via three-dimensional macroscopic magnetic self-assembly"
In: *Micromechanics and microsystems Europe workshop*,

Löthman P A, Hageman T A G, Manz A, Abelmann L, 2015
"Crossing the point - architectures for novel magnetic memories via 3d macroscopic self-assembly"
In: *26th Micromechanics and Microsystems Europe Workshop, Toledo, Spain, Volume: 26*,

Löthman P A, Hageman T A G, Woldering L, Bienia N J, Elwenspoek M, Manz A, Abelmann L, 2015
"Macroscopic self-assembly via turbulent flow and magnetic interaction"
In: *FNANO15 - Conference on foundations of nanoscience: self-assembled structures and devices*,

Löthman P A, Hageman T A G, Manz A, Abelmann L, 2016
"Turbulence as the disturbing force in macroscopic self-assembly"
In: *Micromechanics and microsystems Europe workshop*,

Perez Garza H H, Ghatkesar M K, Löthman P A, Hageman T A G, Manz A, Staufer U, 2014
"Enabling local deposition and controlled synthesis of au-nanoparticles using a femtopipette"
In: *IEEE-NEMS International conference on nano/micro-engineered and molecular systems, At At Waikiki Beach, Hawai, USA, Volume: 9*,

Pichel M, Hageman T, Löthman P A, Manz A, Abelmann L, 2016
"Magnetic response of magentospirillum gryphiwaldense"
In: *MTB2016, At Marseille, France, Volume: 5*,

Schneider L, Waag U, Löthman P A, 2000
"Steel hollow spheres made from iron oxides"
In: *Proceedings of PM 2000, Powder Metallurgy World Congress & Exhibition 2000, Japan Society of Powder and Powder Metallurgy, 12. -16. November 2000, Kyoto, Japan, 2000*,

Stephani G, Waag U, Löthman P, Andersen O, Schneider L, Bretschneider F, Schneidereit H, 2000
"New light weight structurs based on low-cost metallic hollow sphere structures"
In: *Proceedings of International Conference on Powder Metallurgy & Particulate Materials (PM2TEC) 2000, Vol. 6, 2000, New York, USA*,

van Tiem J, Westeriek P, Löthman P, Hageman T, Pichel M, Groenstejn J, Manz A, Abelmann L, Krijnen G, 2014
"B-o inspired fabrication and devices"
In: *MESA+ MEETING, At Twente, The Netherlands, Volume: 8*,

Waag U, Schneider L, Löthman P, Stephani G, Kieback B, 2000
"Metallic hollow spheres - a new pm product"
In: *Proceedings of PM 2000 - Powder Metallurgy World Congress & Exhibition 2000, Japan Society of Powder and Powder Metallurgy, 12. -16. November 2000, Kyoto, Japan*,

Biography

Per Löthman was born in Enköping, Sweden and studied Materials Science and Engineering at the Friedrich-Alexander-Universität Erlangen-Nürnberg in Erlangen, Germany as well as at Alfred University, New York, USA. After working several years in industry, research institutes and universities in Germany and abroad he joined the RAM research Group at Universiteit Twente and Systems Engineering at Universität des Saarlandes. In the Magnetics group at KIST Europe (Korean Institute of Science and technology) he conducted interdisciplinary research leading to a joint PhD at Universiteit Twente and Universität des Saarlandes. He supervised several students and taught several courses at the Saarland University and initiated a fruitful collaboration at Institute Pasteur, Paris, France on archaea viruses.

About the cover

The three cover images are works of Leonardo da Vinci (1452-1519, "Studies of water passing obstacles and falling" (1508), frontcover), Johannes Kepler (1571-1630, "Harmonices mundi libri quinque" (1619), "Harmony of the Universe", back side right) and Pablo Carlos Budassi ("Orders of magnitude" (2012), back side left) which are all related to the topic of my thesis. The work of Budassi illustrates the scale of everything. Starting at the bottom with spacetime and ends at the end the Universe. Leonardo da Vinci saw earth as an organism similar to the human body which was one of Leonardo's concepts both for paintings and scientific works. He describes the effects of flowing water such as turbulence in all its transparency, with waves and bubbles. It is observed painted in all its details suggesting that he spent an enormous amount of time watching the way in which water moved. Leonardo da Vinci's studies of water flowing past obstacles, dated around 1507, in its artistic beauty of the water patterns is also a masterpiece in accuracy of observation. Water pouring into the pool, with natural patterns of the forms of the swirling waves is an early depiction of turbulence. Early seventeenth century thinkers placed a high value on universal harmony as indicated also in the in Johannes Kepler's publication "Harmonices mundi libri quinque" ("Harmony of the Universe"). Kepler tried to link the six planets and their relative distances from the sun with the relationships between the five so-called Platonic solids. According to Euclidean geometry, there are only five polyhedra that have identical polygons for each face: tetrahedron, cube, octahedron, dodecahedron, and icosahedron. The images were chosen since they relate to the content of this thesis. The dodecahedron is the geometry of self-assembled viral capsids and plays a role in the harmony of the universe according to Kepler. The turbulent flow as depicted by Leonardo da Vinci is the macroscopic analogy of heat and the various scales in Buddassi's work reminds us of the research question "what can I learn about the microscale by studying the macroscopic scale".

The precise description of Buddasi's beautiful work is borrowed from the website of the QR code in the margin which also shows an impressive video of "Orders of Magnitude": Objects of sizes in different order of magnitude. At 10^{-32}m is thought to exist a foam of twisted spacetime (Quantum foam). 10^{-24}m cross section radius of 1 MeV neutrinos. 10^{-22}m Top Quark, the smallest quark. 10^{-20}m Bottom and Charm quarks. 10^{-18}m Up and Down quarks. 10^{-16}m Protons and Neutrons. 10^{-14}m Electrons and nuclei. 10^{-12}m Longest wavelength

of gamma rays. 10^{-11}m Radius of hydrogen and helium atom. 10^{-10}m Radius of carbon atoms. 10^{-9}m Diameter of the DNA helix. 10^{-8}m Smallest virus (Porcine circovirus). 10^{-7}m Largest virus (Megavirus). 10^{-6}m X Chromosome. 10^{-5}m Typical size of a red blood cell. 0.1mm width of human hair. 10mm width of an adult human finger. 1m height of an infant human being. 10m Argentinosaurus is the biggest dinosaur discovered yet (30 to 35 meters). Human figure is for comparison. In reality humans and dinosaurs didn't live at the same time. 1km Diameter of Barringer Crater in the northern Arizona desert (1186m). 100km Jamaica Island (235km long). 10000km Diameter of planet Earth (12,742 km). 10^{8}m Moon's orbit (770,000km). 10^{9}m Diameter of the Sun (1391400km). 10^{11}m Diameter of the inner Solar System. (600,000,000 km). 10^{13}m Diameter of the Solar System. 10^{15}m Outer limit of the Oort Cloud. 10^{16}m Distance to Alpha Centauri. 10^{18}m Messier 13 globular cluster. 10^{20}m Diameter of the Milky Way Galaxy. 10^{22}m Local Group of galaxies including Milky Way, M31(Andromeda), M33, SMC, LMC and smaller galaxies. 10^{23}m Typical galaxy cluster. 10^{24}m Laniakea Supercluster of galaxies. (160 Mpc). 10^{25}m End of Greatness ("Cosmic web" structure). 10^{26}m Diameter of the observable universe sphere. The entire Universe is larger than 10^{27}m and possibly infinite.

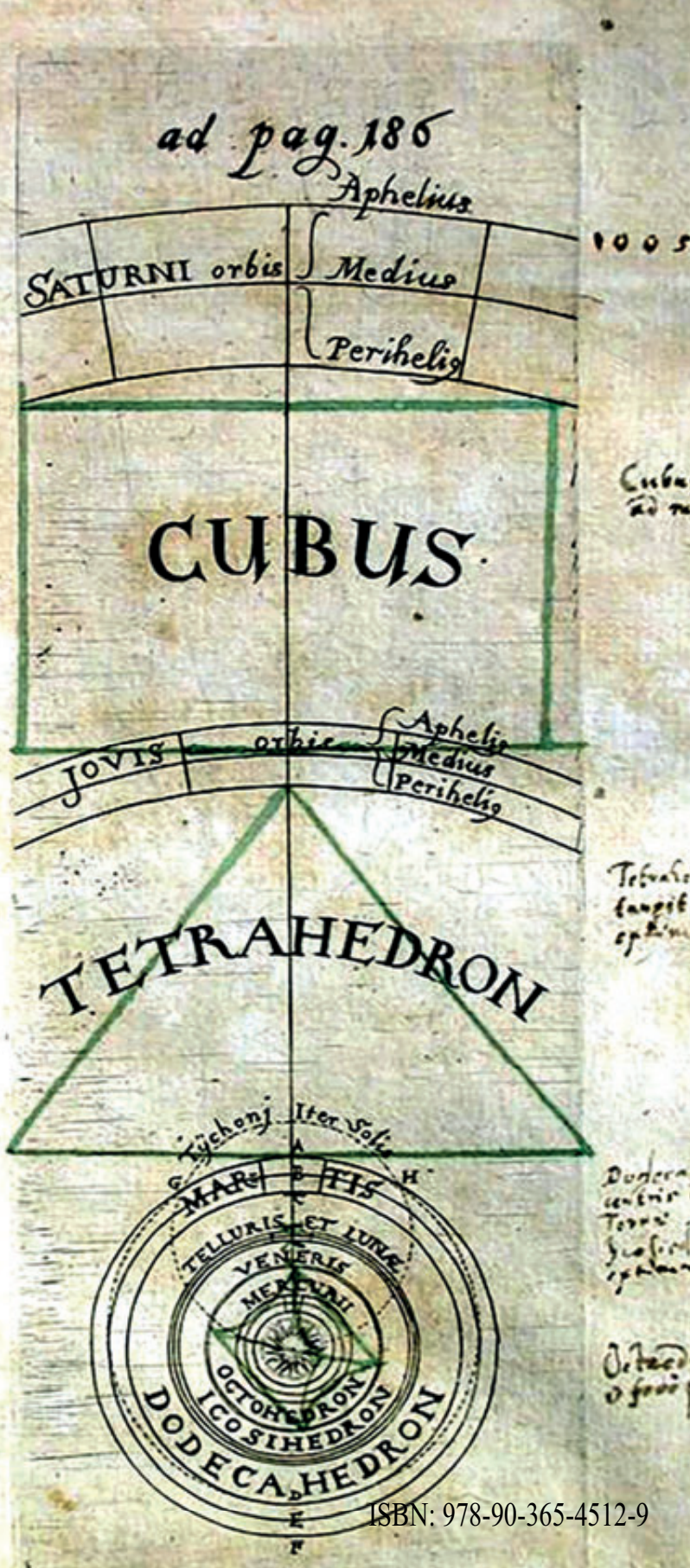

ISBN: 978-90-365-4512-9